Encoding of Coordinating Information in a Network of Coupled Oscillators

Inaugural-Dissertation

zur

Erlangung des Doktorgrades

der Mathematisch-Naturwissenschaftlichen Fakultät

der Universität zu Köln

vorgelegt von

Anna Caren Schneider

aus Herne

Köln

März 2017

Berichterstatter/in: Dr. Carmen Wellmann

Prof. Dr. Ansgar Büschges

Tag der mündlichen Prüfung: 03. Mai 2017

Index

Zusammenfassung vii
Abstract ix
1 Introduction 1
1.1 The Crayfish Swimmeret System 2
1.2 The Coordinating Circuit 4
1.3 Activation and Modulation of the Swimmeret System 7
Coordination of the Swimmeret System at Different Excitation Levels 7
1.4 Aim of Study 9
2 Materials and Methods 11
2.1 Dissection 11
2.2 Electrophysiological Setup 11
2.3 Electrophysiological Protocols 13
2.4 Analysis 15
Statistics and Data Presentation 17
2.5 Histology 17
2.6 Microscopy 18
2.7 MALDI-TOF Mass Spectrometry 18
3 Results 20
PART I: Cellular Properties 20
3.1 Isolating Neurons 20
3.2 Different Mechanisms Shaped ASC_E and DSC bursts 22
Hysteresis in Coordinating Neurons 26
Network Effect Masked Rebound Properties 28
3.3 Setting the Excitation Level with Carbachol and EdCI 29
Effect on Membrane Potential 32
Effect on Tuning Curves 35
Effect on Input Resistance 37
PART II: Neurotransmitters 41
3.4 Antibody Labeling Against Serotonin 41
3.5 MALDI-TOF Mass Spectrometry 44
4 Discussion 47
4.1 Isolating Neurons 47
4.2 Burst Shaping Mechanisms 48

Burst Shaping in ASC_E 48
Burst Shaping in DSC 51
Post-inhibitory Rebound in ASC_E and DSC 52
Burst Shaping in Other Neurons and Systems 53
Burst Shaping: Conclusions 54
4.3 Hysteresis of Coordinating Neurons 56
Spike-Frequency Adaptation 56
Intraburst Hysteresis 57
Interburst Hysteresis 59
Hysteresis: Conclusions 60
4.4 Effect of Carbachol and EdCl on the Swimmeret System's Excitation Level 61
No Dose-Dependent Effect on Burst Strength 61
Dose-Dependent Effect on Period 63
Excitation Level: Conclusions 64
Differences in the Number of ASC_E and DSC Spikes 65
4.5 Encoding Coordinating Information at Different Excitation Levels 66
Changes in Membrane Potential 66
Shift of Tuning Curves 68
Differential Effect on Input Resistance 70
Encoding Coordinating Information: Conclusions 72
4.6 Transmitters of Coordinating Neurons 73
Intracellular Staining and Immunohistochemistry 73
MALDI-TOF Mass Spectrometry 74
4.7 Comparison to Coordination in Other Systems 75
5 Conclusions and Outlook 79
Bibliography 83
Abbreviations 95
Appendix 96
Acknowledgements 110
Eigentständigkeitserklärung 111

Zusammenfassung

Bewegung von Tieren erfolgt meist durch zyklische Bewegungen des Körpers oder der Gliedmaßen. Diese Bewegungen werden von neuronalen Netzwerken gesteuert, die durch zentrale Mustergeneratoren (CPG) angetrieben werden. In der Regel wird jedes Körpersegment, jede Extremität oder sogar jedes Gelenk durch einen eigenen CPG gesteuert. Um zielgerichtetes Verhalten auszuführen, müssen die verschiedenen CPGs koordiniert werden.

Das Netzwerk zur Bewegungskontrolle der Schwimmbeine eignet sich als Modell um die Koordination dezentralisierter CPGs zu untersuchen. Die Schwimmbeine sind vier paarige abdominale Pleopoden. Neben dem Schwimmen werden sie benutzt, um die Körperposition zu halten oder Eier zu belüften. Jedes der Schwimmbeine bewegt sich in alternierender Retraktion (PS), die den Antrieb erzeugt, und Protraktion (RS), die das Schwimmbein zurück in die Ausgangsstellung bringt. Die beiden Schwimmbeine desselben Segments bewegen sich in Phase. Die vier ipsilateralen Schwimmbeinpaare bewegen sich in einer metachronalen Welle. Das posteriore Paar beginnt jeden Bewegungszyklus. Die anterioren Paare folgen dem jeweils posterioren Paar mit einem Phasenversatz von ungefähr 25%. Dieser Phasenversatz ist unabhängig von der Periodendauer eines Schwimmzyklus.

Auf neuronaler Ebene wird jedes Schwimmbein von einem eigenen Netzwerk im jeweiligen abdominalen Hemiganglion kontrolliert. Der CPG besteht aus Inhibitoren des PS (IPS) und Inhibitoren des RS (IRS), die sich gegenseitig inhibieren. Weiterhin inhibieren sie jeweils die PS und RS Motoneurone, was zur alternierenden Protraktion und Retraktion eines Schwimmbeins führt. In jedem Hemiganglion sind drei weitere Neurone notwendig und hinreichend für den spezifischen Phasenversatz zwischen den Segmenten. Das Ascending Coordinating Neuron (ASC_E) erhält denselben synaptischen Eingang vom CPG wie die PS Motoneurone. Es codiert Timing, Dauer und Stärke jedes PS und leitet die Information als Aktionspotentialburst zu den anterioren Ganglien. Das Descending Coordinating Neuron (DSC) erhält denselben synaptischen Eingang vom CPG wie die RS Motoneurone. Es codiert Timing, Dauer und Stärke jedes RS und leitet die Information als Aktionspotentialburst zu den posterioren Ganglien. Das Kommissurale Interneuron 1 (ComInt 1) erhält die koordinierenden Informationen der anterioren und posterioren Ganglien und integriert sie über eine elektrische Synapse in eins der IRS Neurone.

Die isolierte abdominale Ganglienkette generiert dieselbe (fiktive) motorische Aktivität wie das intakte Tier. Sie kann für mehrere Stunden in Ringer gehalten werden, um die neuronale Aktivität durch intra- und extrazelluläre Ableitungen zu untersuchen. Die

Burststärke wird durch die Anzahl an Aktionspotentialen (AP) in jedem ASC_E und DSC Burst codiert. Wenn sich die Burststärke spontan ändert, folgt die Anzahl der APs in einem linearen Zusammenhang. Cholinerge Agonisten, wie z.B. Carbachol, können die mittlere absolute Burststärke konzentrationsabhängig zu hohen oder niedrigen Werten verschieben, indem sie die Erregung des Systems ändern. In diesem Fall wird die absolute Burststärke nicht mehr linear von den koordinierenden Neuronen codiert. Dieses paradoxe Ergebnis kann durch die Adaptive Encoding Hypothese erklärt werden: Das koordinierende Netzwerk besteht aus aufeinander abgestimmten Encodern (ASC_E und DSC) und Decoder (ComInt 1), und das Erregungslevel gleicht die neuronalen Eigenschaften zum Codieren und Decodieren an. Daher kann die gleiche Anzahl an APs einen absoluten starken Burst bei einem hohen oder einen absoluten schwachen Burst bei einem niedrigen Erregungslevel bedeuten. ComInt 1 interpretiert die Anzahl an ankommenden APs im Kontext der Erregung um die Burststärke zu decodieren.

Ein Ziel dieser Studie war es, in elektrophysiologischen Experimenten das mögliche adaptive Codieren durch koordinierende Neurone zu untersuchen. Das zeigte, dass der Erregungslevel sowohl das ganze Netzwerk als auch die einzelnen koordinierenden Neurone beeinflusste. Wenn die koordinierenden Neurone chemisch isoliert waren, steigerte Carbachol ihre Erregbarkeit durch Depolarisation des Membranpotentials, Steigerung des Eingangswiderstands und Verringern der AP Schwelle. Gleichzeitig führte diese gesteigerte Erregung dazu, dass weniger APs als Antwort auf einen Stimulus generiert werden konnten, wahrscheinlich durch die Inaktivierung von Natriumkanälen. Im synaptisch verbundenen Netzwerk wurden die koordinierenden Neurone stärker durch den CPG inhibiert, wenn die Erregung des Systems gesteigert wurde. Diese ausgleichenden Mechanismen zur Steigerung und Verringerung der neuronalen Erregbarkeit ermöglichten es den koordinierenden Neuronen sich dem Umfang der auftretenden Burststärken bei jedem Erregungslevel anzupassen, so dass die relativen Burststärken codiert wurden.

Das zweite Ziel dieser Arbeit war es, die neuronalen Transmitter von ASC_E und DSC an der Synapse zu ComInt 1 zu identifizieren. Obwohl die Konnektivität des Netzwerks zur Bewegungskontrolle der Schwimmbeine sehr gut untersucht ist, ist das Wissen über die vorhandenen Transmitter gering. Mit immunohistochemischen Versuchen konnte Serotonin als Transmitter ausgeschlossen werden, weil koordinierende Neurone nicht mit serotonin-immunoreaktiven Neuronen kolokalisiert waren. Durch MALDI-TOF Massenspektrometrie wurde Acetylcholin als wahrscheinlicher Transmitter identifiziert.

Abstract

Animal locomotion is driven by cyclic movements of the body or body appendages. These movements are under the control of neural networks that are driven by central pattern generators (CPG). Usually, each body segment, appendage, or even individual joints of an appendage, is driven by its own CPG. In order to produce meaningful behavior, CPGs need to be coordinated.

The crayfish swimmeret system is a model for investigating the coordination of distributed CPGs. Swimmerets are four pairs of limbs that are located on the animal's abdomen. They are used for forward swimming, controlling body posture or ventilating eggs. Each swimmeret moves in cycles of alternating power-strokes (PS), which generate the driving force, and return-strokes (RS), which bring the limb back to its protracted resting position. The swimmerets on one body segment move in phase. Along the abdomen, the swimmeret pairs are coordinated in a metachronal wave. The most posterior pair starts each cycle. Each anterior pair follows its posterior pair with a phase lag of approximately 25%. This phase lag is independent of the cycle period.

On the neuronal level, each swimmeret is controlled by its own microcircuit that is located in the body segment's hemiganglion. The CPG consist of two reciprocally inhibiting pools of Inhibitors of PS (IPS) and inhibitors of RS (IRS). They inhibit the pools of PS and RS motor neurons, driving the alternating PS-RS activity of the limb. Three neurons per hemiganglion are necessary and sufficient for the 25% phase lag between segments. The Ascending Coordinating Neuron (ASC_E) receives the same input from the CPG as the PS motor neurons. It encodes timing, duration, and strength of each PS and sends this information as burst of spikes to the anterior ganglia. The Descending Coordinating Neuron (DSC) receives the same input from the CPG as the RS motor neurons. It encodes timing, duration, and strength of each RS and sends this information as burst of spikes to the posterior ganglia. Coordinating information is received by the Commissural Interneuron 1 (ComInt 1), which integrates it via an electrical synapse into one of the IRS neurons.

The isolated abdominal ganglia chain reliably produces the same motor output as in the intact animal, i.e. fictive swimming. It can be kept in a Petri dish covered with saline for several hours to investigate the neural activity by intra- and extracellular recordings. Motor burst strength is encoded by the number of spikes per ASC_E and DSC burst. If burst strength varies spontaneously, the coordinating neurons accurately track these changes linearly. Cholinergic agonists, e.g. carbachol, can balance the mean absolute burst strength towards high or low values, depending on concentration, i.e. change the system's excitation level. In this case, the absolute burst strength across excitation levels is no longer tracked by the

coordinating neurons. This paradox result can be explained by the Adaptive Encoding Hypothesis: The coordinating circuit consists of matched encoders (ASC_E and DSC) and decoder (ComInt 1), and the excitation level tunes their encoding and decoding properties. Hence, the same number of coordinating spikes can encode an absolute strong burst at a high excitation level and absolute weak burst at a low excitation level. ComInt 1 interprets the arriving number of spikes in the context of excitation to decode the burst strength.

One aim of this study was to investigate the putative adaptive encoding of the coordinating neurons in electrophysiological experiments. This revealed that the excitation level influenced both the whole system and the individual coordinating neurons. When chemically isolated, carbachol increased the coordinating neurons' excitability by depolarizing their membrane potential, increasing input resistance, and lowering spike threshold. Concomitantly, this increased excitability diminished the amount of spikes generated as response to stimulation, presumably caused by sodium channel inactivation. In the synaptically connected network, the coordinating neurons received stronger inhibition from the CPG when the system's excitation increased. These mechanisms allowed the coordinating neurons to adapt to the range of burst strengths at any given excitation level by encoding relative burst strengths.

The second aim of this study was to identify the transmitters that the coordinating neurons use at the synapse to ComInt 1. Although the connectivity of the swimmeret system is well understood, knowledge about the transmitters of the individual neurons is sparse. Immunohistochemical experiments ruled out serotonin as transmitter because coordinating neurons were not co-localized with serotonin-immunoreactive positive neurons. MALDI-TOF mass spectrometry suggested acetylcholine as presumable transmitter.

1 Introduction

One of the fundamental goals in neuroscience is to explain how nervous systems generate behavior. More than 100 years ago, Brown (1911) concluded from his experiments on spinalized and deafferented cats that sections of the spinal cord are able to produce alternating motor activity by alternating activation of motor neurons. Nowadays, neural oscillators to govern rhythmic behavioral output are found in all investigated animals. To name just a few, those identified in locomotion drive leech swimming (Kristan and Calabrese, 1976), insect walking (Pearson and Iles, 1970), locust flying (Wilson, 1961), dragonfly flying (Simmons, 1977), lamprey swimming (Cohen and Wallén, 1980), or mouse walking (Smith and Feldman, 1987). Non-locomotor CPGs are for example governing leech heartbeat (Thompson and Stent, 1976a, 1976b), or breathing in the mammalian preBötzinger complex (Smith et al., 1991). On the cognitive side, oscillations have been linked for example to perception, as in honeybee odor discrimination (Stopfer et al., 1997), or memory, as seen in human hippocampal theta oscillations (Backus et al., 2016).

Perhaps the most thoroughly investigated neural oscillators are the central pattern generators (CPGs) involved in locomotion. A CPG's most distinguishing feature is its ability to generate rhythmic recurrent activity even in the absence of sensory input or other external timing cues. One way to achieve this rhythmicity is by singular pacemaker neurons that are oscillating on their own because of the interplay of their ionic conductances. Examples of pacemaker neurons are AB in the stomatogastric nervous system (STNS) of crustaceans (Miller and Selverston, 1982) or R15 in *Aplysia* (Alving, 1968). Another way for rhythmogenesis is via the interconnection of neurons in a network, which do not necessarily have pacemaker properties. Such examples are seen in the swim networks in leech (reviewed in Brodfuehrer et al., 1995) or *Tritonia* (Getting et al., 1980). In networks that produce oscillations, the most commonly found motif in invertebrates is reciprocal inhibition of two neurons, or two neuronal populations, to produce alternating activity.

Body segments, limbs, or limb joints are under the control of individual CPGs. For example in the crayfish swimmeret system each swimmeret is controlled by its own CPG (Murchison et al., 1993). In the stick insect, even each individual leg joint is driven by its own CPG (Büschges et al., 1995). In these examples, only the precise execution of limb movements allows for goal-directed locomotion. In addition, interacting rhythms can operate on different time scales, e.g. pyloric and gastric mill rhythm in the STNS (Bartos et al., 1999) or swimming and breathing in lamprey (Gariépy et al., 2012). Recently, it has been shown in humans that natural nasal respiration, but not oral respiration, is able to entrain

cortical and subcortical brain oscillations (Zelano et al., 2016). Hence, in order to produce a meaningful (motor) output, CPGs have to be coordinated.

In most systems, it is still not well understood how the individual oscillators are coordinated. Several examples exist for the varying importance of coordination through sensory feedback on the one hand, or central mechanisms, like direct interaction of CPGs or via coordinating interneurons and pathways, on the other hand. Examples demonstrating the different weighting and interplay of those mechanisms are for example insect walking (Borgmann et al., 2009; Berendes et al., 2016) or leech swimming (Yu et al., 1999). One system in which the central coordinating mechanism is understood on a cellular level is the crayfish swimmeret system. This was one of the first preparations in which fictive locomotion in the isolated central nervous system (CNS) was demonstrated (Hughes and Wiersma, 1960). Here, coordinating circuits consisting of identified neurons coordinate the CPGs (Namba and Mulloney, 1999; Tschuluun et al., 2001; Mulloney et al., 2006; Smarandache et al., 2009). Therefore, the swimmeret system can serve as a model to understand the coupling of distributed neural oscillators because the relatively small number of necessary and sufficient neurons to generate and coordinate the swimmeret motor output is identified. Since the coordination is independent of sensory feedback (Ikeda and Wiersma, 1964) it can be studied in the isolated CNS, allowing easy access for multiple recording electrodes.

1.1 The Crayfish Swimmeret System

The swimmerets are four pairs of limbs on the crayfish's abdomen that can be activated during a wide range of behaviors. They are used for propelling the animal forward during swimming, burrowing, egg ventilation in females (Huxley, 1880), supporting walking (Cattaert and Clarac, 1983), or righting of the body if rolled along the longitudinal axis (Davis, 1969; Neil and Miyan, 1986). Each swimmeret is active in alternating power-stroke (PS; generating the driving force) and return-stroke (RS) movements. The two swimmerets of each segment move in phase and all pairs of swimmerets move in a metachronal wave from posterior to anterior with a phase lag of approximately 25% between segments (Hughes and Wiersma, 1960; Ikeda and Wiersma, 1964). This phase lag is independent of swimming frequency (Braun and Mulloney, 1993; Mulloney, 1997) and optimized for fluid-mechanical efficiency (Zhang et al., 2014).

Each hemiganglion in the abdominal ganglia (A) chain A2 to A5 contains a microcircuit (Figure 1) that controls the respective swimmeret (Murchison et al., 1993). The microcircuit's neurons synapse in the Lateral Neuropil (LN) of their home ganglion (Sherff

and Mulloney, 1997; Mulloney and Hall, 2003; Smarandache-Wellmann et al., 2013). The approximately 70 motor neurons project through the first nerve root (N1). The anterior branch carries axons from RS motor neurons (MN), the Return-Stroke Exciters (RSE) and Return-Stroke Inhibitors (RSI). The posterior branch carries axons from PS MNs, the Power-Stroke Exciters (PSE) and Power-Stroke Inhibitors (PSI) (Mulloney and Hall, 2000). Non-spiking Inhibitors of the Power-Stroke (IPS; three types) and Inhibitors of the Return-Stroke (IRS; two types) form the pattern-generating kernel. They inhibit the pools of PS and RS MNs, leading to alternating RS and PS of the swimmeret (Paul and Mulloney, 1985a, 1985b; Mulloney, 2003; Smarandache-Wellmann et al., 2013).

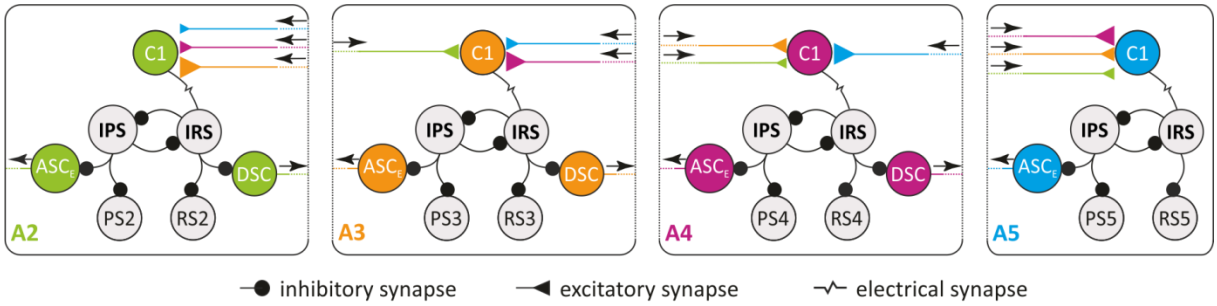

Figure 1: Connectivity diagram of four coupled local microcircuits controlling the ipsilateral swimmerets. A2, A3, A4, A5: Abdominal ganglion 2, 3, 4, 5; ASC$_E$: Ascending Coordinating Neuron (early); C1: Commissural Interneuron 1; DSC: Descending Coordinating Neuron; IPS: Inhibitor of Power-Stroke; IRS: Inhibitor of Return-Stroke; PS: Power-stroke; RS: Return-stroke. Size of the excitatory connections corresponds to synaptic strength. Modified after Smarandache-Wellmann and Grätsch 2014.

The Ascending Coordinating Neuron (ASC$_E$) and Descending Coordinating Neuron (DSC) are necessary and sufficient to coordinate the microcircuits across segments and maintain the 25% phase lag (Namba and Mulloney, 1999; Tschuluun et al., 2001). ASC$_E$ and DSC encode information about timing, duration, and strength of their microcircuit's PS and RS bursts, respectively (Mulloney et al., 2006). ASC$_E$ sends this information to anterior ganglia, DSC to posterior ganglia (Namba and Mulloney, 1999). Their activity is driven by the same non-spiking pattern generating neurons (IPS and IRS) that also drive MN activity (Smarandache-Wellmann and Grätsch, 2014).

Coordinating information from the other ganglia's ASC$_E$s and DSCs arrives with a gradient of synaptic strength at the non-spiking Commissural Interneuron 1 (ComInt 1, in figures abbreviated with C1) (Smarandache et al., 2009). ComInt 1 receives the coordinating information at the midline of its home ganglion (Mulloney and Hall, 2003). This neuron decodes the coordinating information and integrates it into the pattern-generating kernel via an electrical synapse to one of the two IRS (Smarandache-Wellmann et al., 2014).

1.2 The Coordinating Circuit

One presynaptic ASC_E and DSC of their home module and one postsynaptic ComInt 1 in a target module form the coordinating circuit. ASC_E is present in every ganglion from A2 to A5 (Figure 2). Its soma is located ventrally and posterior to N1 in the pool of PS motor neurons. Dendrites branch in the LN, the primary neurite traverses in the anterior Minuscule Tract (MnT) dorsally towards the midline and projects anterior along the midline (Namba and Mulloney, 1999; Mulloney and Hall, 2003). The anterior termination site of ASC_E is unknown; it presumably reaches further than the fifth thoracic ganglion (Tschuluun et al., 2001). DSC is present in A2 to A4 (Figure 2). Its soma is located ventrally and anterior to N1 in the pool of RS motor neurons. Dendrites branch in the LN, the primary neurite traverses in the posterior MnT dorsally towards the midline and projects posterior along the midline to A6 (Namba and Mulloney, 1999; Tschuluun et al., 2001; Mulloney and Hall, 2003). Coordinating neurons synapse at the midline of each abdominal target ganglion with *en passent* synapses onto one of the bilaterally symmetrical ComInt 1 (Mulloney and Hall, 2003). Hence, input to the coordinating neurons affects timing and strength of their target's motor output (Namba and Mulloney, 1999; Jones et al., 2003; Mulloney and Hall, 2007a).

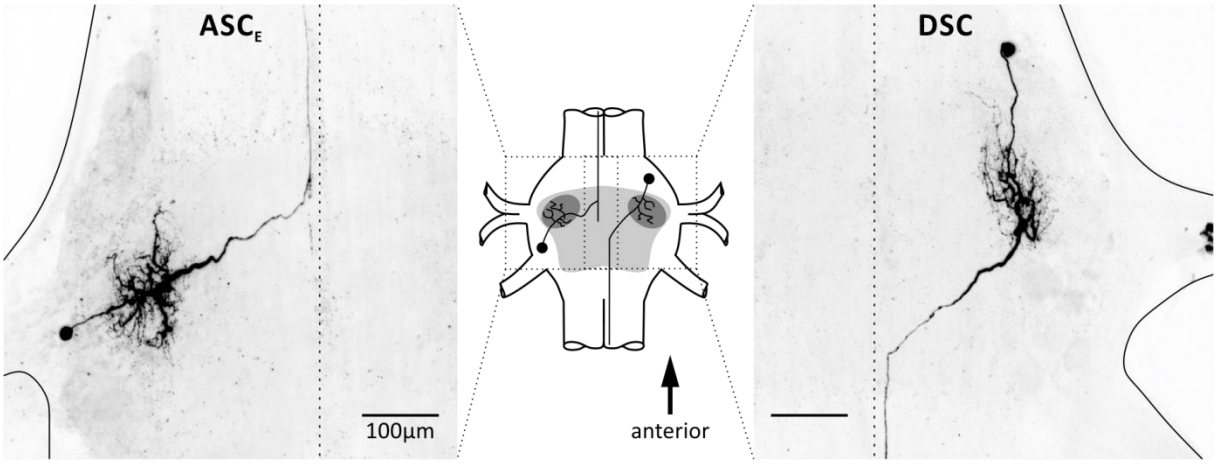

Figure 2: Morphology of ASC_E and DSC. Schematic shows location of the neurons in a ganglion with the core region containing the neuropils shaded in light grey and the lateral neuropil in dark grey. Lines indicate ganglion outline and midline.

ASC_E is active in phase with the PS of its home ganglion and sends coordinating information to the anterior ganglia (Figure 3 A). Extracellular recordings may contain activity from two neurons (ASC_E and ASC_L) and is therefore labeled ASC, but only ASC_E coordinates the oscillators (Mulloney et al., 2006). Depolarization of ASC_E results in an increase of the anterior ipsilateral PS bursts strength; hyperpolarization results in a decrease (Figure 3 B).

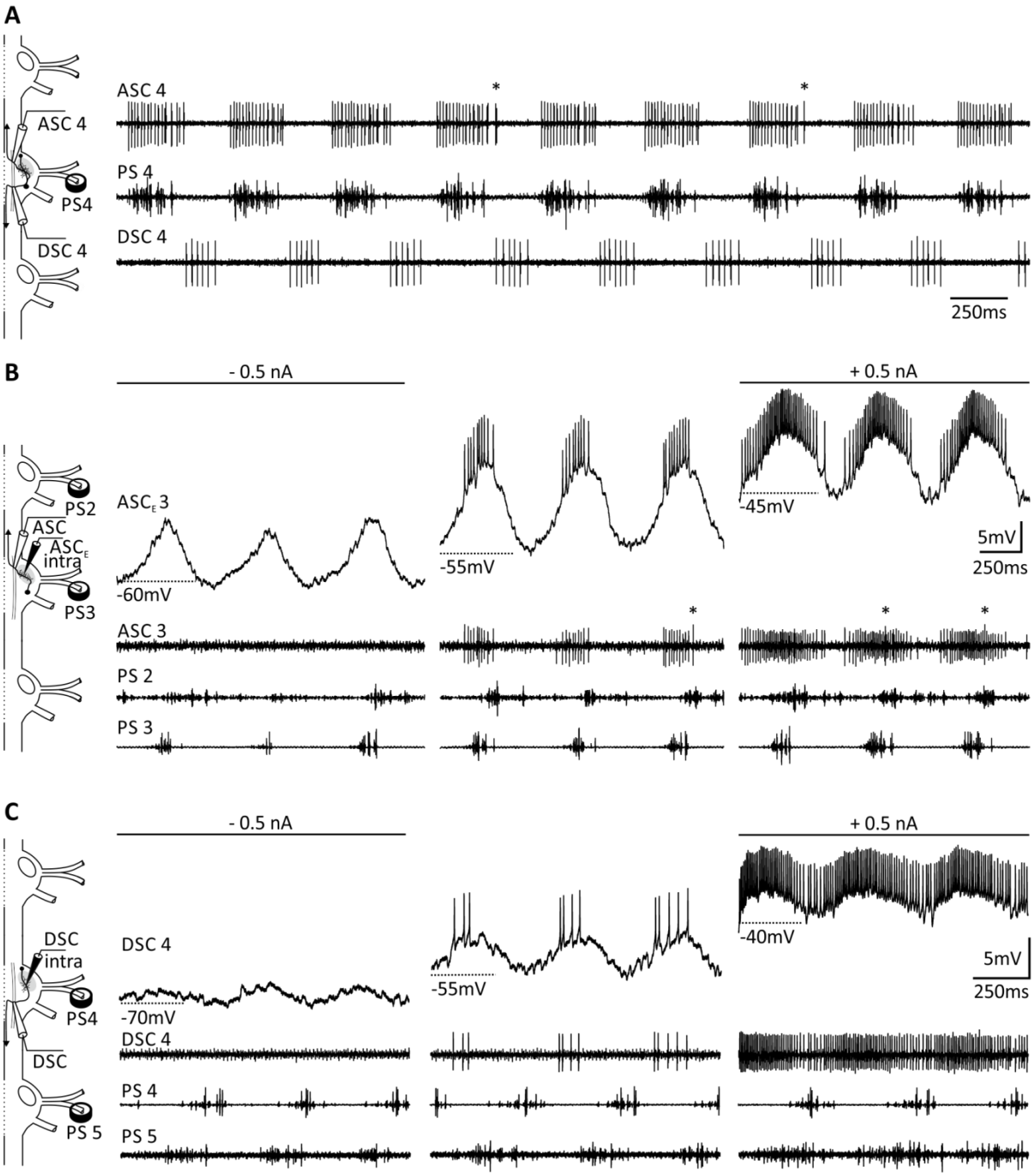

Figure 3: Extracellular and intracellular recordings of ASC_E's and DSC's activity and their influence on the ongoing rhythm. A: ASC is active in phase with the PS of its home ganglion; DSC is active in antiphase with the PS of its home ganglion. Asterisks mark ASC_L spikes. B: Hyperpolarization of ASC_E decreased the anterior PS burst strength; depolarization increased the anterior PS burst strength. Asterisks mark ASC_L spikes. C: Hyperpolarization of DSC decreased the posterior PS burst strength; depolarization increased the posterior PS burst strength. ASC: Ascending Coordinating Neurons (this trace may contain spikes of two ascending coordinating neurons: ASC_E and ASC_L (asterisks), see text for description); ASC_E: Ascending Coordinating Neuron, early; DSC: Descending Coordinating Neuron; PS: Power-stroke; 2, 3, 4, 5: Number of the recorded abdominal ganglion. Recordings in C by Swantje Grätsch.

DSC is active in antiphase with the PS of its home ganglion and sends coordinating information to the posterior ganglia (Figure 3 A). Depolarization of DSC results in an increase of the posterior ipsilateral PS burst strength; hyperpolarization results in a decrease (Figure 3 C). Generally, DSC stimulation seems to have a weaker effect on its target ganglion than ASC_E stimulation (Namba and Mulloney, 1999). Furthermore, posterior coordinating neurons fire more spikes per burst in longer bursts and at a higher frequency than anterior ones (Mulloney et al., 2006).

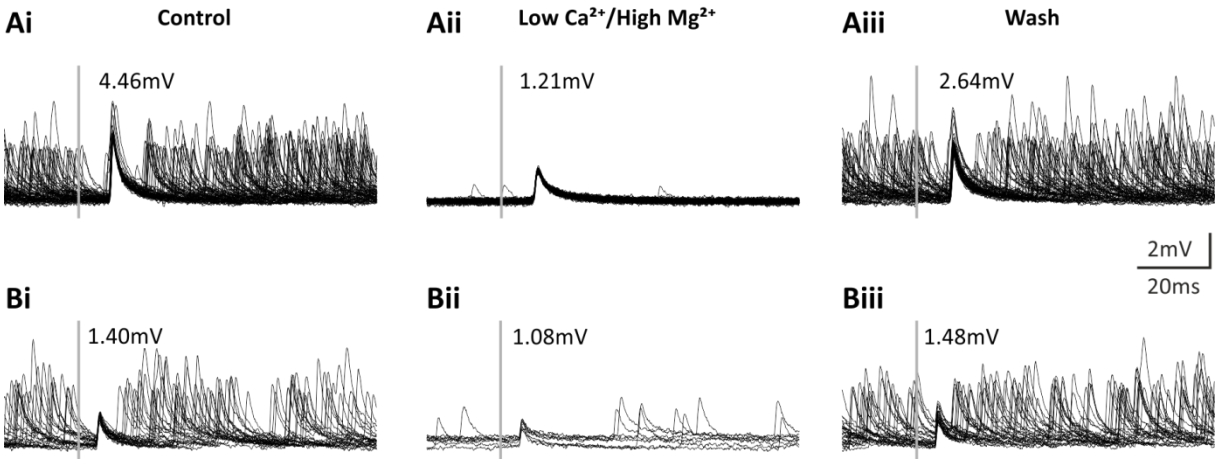

Figure 4: Multisweeps of ComInt 1 in normal saline (i and iii) and LowCa^{2+} saline (ii). A: Triggered on ASC_E spike. B: Triggered on DSC spike. Grey bar indicates time of trigger. Voltages are amplitudes of the average waveform. Recordings by Carmen Wellmann.

It has been shown that the excitatory connections of coordinating neurons to ComInt 1 have a gradient of synaptic strength (Mulloney and Hall, 2003; Smarandache et al., 2009). In preliminary experiments to determine if these synapses are chemical or electrical, ComInt 1's EPSP amplitude was measured in normal saline and low Ca^{2+} / high Mg^{2+} saline, which blocks transmission at chemical synapses. Average EPSP amplitude was reduced in 4 of 4 experiments and recovered after washing with normal saline (Figure 4). This was similar for EPSPs elicited by ASC_E and DSC. Since transmitter release via vesicle fusion is directly dependent on intracellular Ca^{2+} concentration (reviewed in Zucker, 1993; Südhof, 2012) this indicated a mainly chemical connection between the neurons with the possibility of an electrical component. Because of the EPSP's short rise times, we hypothesized that the coordinating neurons use low molecular weight transmitters like glutamate or GABA. Bath application of glutamate and GABA antagonists did not change EPSP shape, excluding them as transmitters (pers. comm. Henriette Seichter).

1.3 Activation and Modulation of the Swimmeret System

In the early experiments on the swimmeret system, interganglionic fiber bundles containing excitatory 'command neurons' were tonically stimulated to induce rhythmic activity from quiescent preparations (Hughes and Wiersma, 1960; Wiersma and Ikeda, 1964). Atwood and Wiersma (1967) found out that swimmeret rhythm frequency depended on the command neurons' stimulation frequency. In addition, Davis and Kennedy (1972a) demonstrated that the simultaneous stimulation of two command neurons led to stronger PS bursts than stimulation of single command neurons.

Three of five excitatory command neurons release proctolin when activated (Acevedo et al., 1994). Similarly, bath application of proctolin is also activating the swimmeret system and modulating its activity in a dose-dependent manner (Mulloney et al., 1987). In the same study, the authors report that they elicited rhythmic activity by application of the muscarinic agonist pilocarpine as well. Later, Braun and Mulloney (1993) extended these findings by demonstrating that pilocarpine can also modulate the activity in a dose-dependent manner. Furthermore, they described that nicotine does not induce rhythmic activity but can modulate ongoing activity. This dose-dependent modulation covers wider frequency ranges than proctolin or pilocarpine. The cholinergic agonist carbachol combines the effect of pilocarpine and nicotine. Bath application activates the swimmeret system and higher doses increase burst strength and shorten cycle periods (Braun and Mulloney, 1993, 1995; Mulloney, 1997; Mulloney and Hall, 2007b).

Braun and Mulloney (1993) concluded that separate pathways exist for activation and modulation of the swimmeret system because cholinergic antagonists do not interrupt the proctolin-induced rhythm. Hence, one pathway is activated by proctolin, the other by cholinergic agonists. The cholinergic pathway can be further subdivided in one predominantly activating (muscarinic) and one predominantly modulating (nicotinic) pathway. Even if the period of the motor output changes, the phase lag between segments remains stable (Mulloney et al., 2006).

Coordination of the Swimmeret System at Different Excitation Levels

The activity of coordinating neurons in the swimmeret system of *Procambarus clarkii* was first observed by Hughes and Wiersma (1960) who speculated that they could transmit an efference copy of the motor output from their home ganglion to other ganglia. This was corroborated by experiments from Stein (1971), who could delimit coordinating activity from the activity of command neurons, and by Mulloney (1997), who uncoupled swimmeret circuits by blocking spike transmission through the connectives. Namba and Mulloney

(1999) identified the individual coordinating neurons in *Pacifastacus leniusculus* on the cellular level. They noted that if PS frequency increases because of increased excitation, the spike frequency of ASC_E and DSC would increase as well. In addition, the instantaneous spike frequency within a burst decreases over time. On a cycle-to-cycle basis, the beginning of a coordinating neuron's burst signals the beginning of a PS or RS, respectively. The burst duration correlates to the duration of PS or RS activity, and the number of spikes correlates to PS or RS burst strength (Figure 5 A) (Mulloney et al., 2006). Apparently, DSC's fidelity is lower than ASC_E's. Smarandache-Wellmann and Grätsch (2014) could finally demonstrate that the coordinating neurons are indeed directly driven by the CPG, reinforcing the efference copy hypothesis.

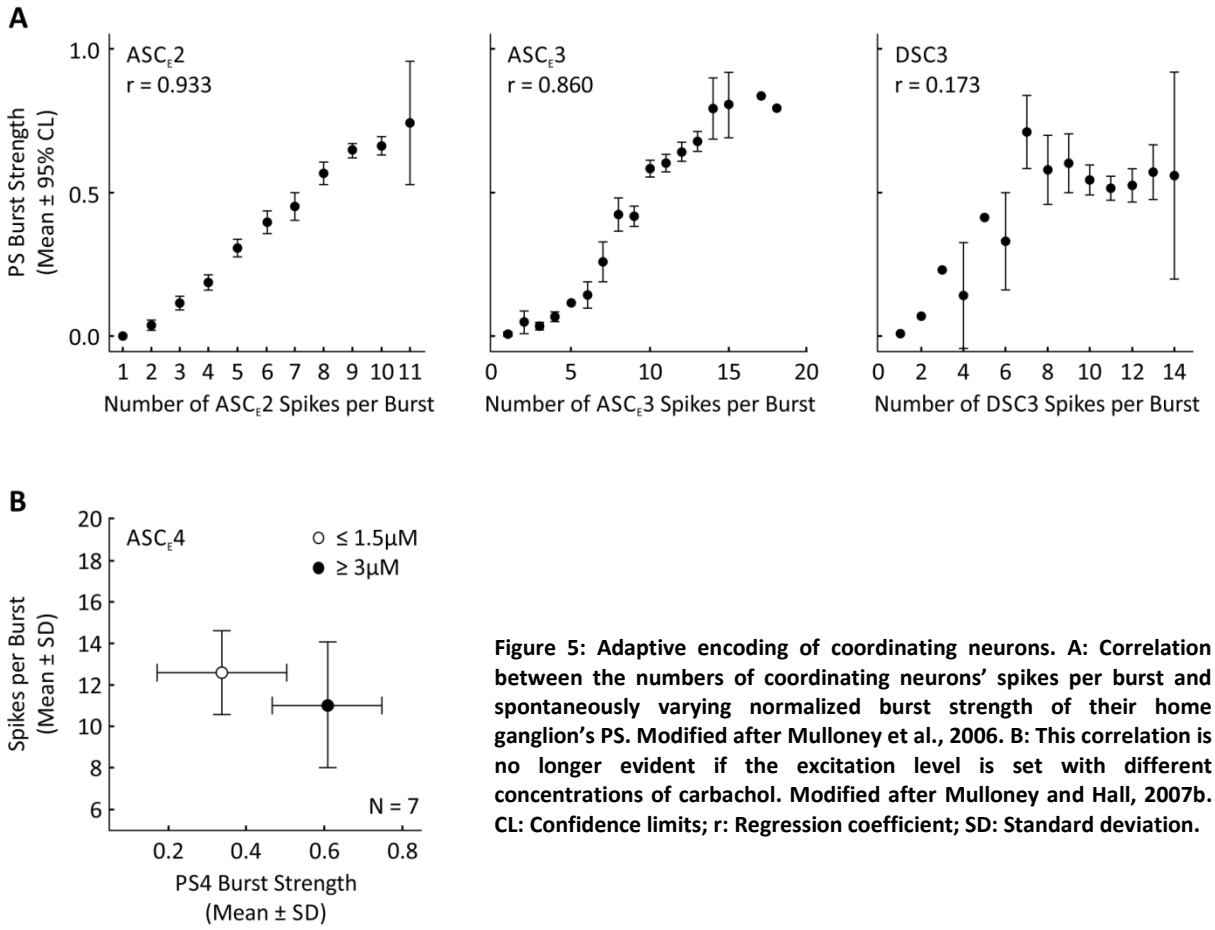

Figure 5: Adaptive encoding of coordinating neurons. A: Correlation between the numbers of coordinating neurons' spikes per burst and spontaneously varying normalized burst strength of their home ganglion's PS. Modified after Mulloney et al., 2006. B: This correlation is no longer evident if the excitation level is set with different concentrations of carbachol. Modified after Mulloney and Hall, 2007b. CL: Confidence limits; r: Regression coefficient; SD: Standard deviation.

Braun and Mulloney (1995) conducted split-bath experiments in which the anterior and posterior parts of the abdominal ganglia chain were independently excited to different levels by selective application of pilocarpine or carbachol. They found out that the active phase of anterior PS is advanced, and duty cycle shortened in the posterior PS, if the anterior ganglia are at a high excitation level. Anterior PS is delayed if anterior ganglia are at a low excitation level relative to the posterior ganglia. Mulloney and Hall (2007b) extended these

findings in further split-bath experiments. They observed that PS burst strength is higher in those ganglia that are bathed in high carbachol concentrations compared to application of low concentrations. Based on the results from Mulloney et al. (2006) they expected these stronger bursts to be encoded by more spikes in the coordinating neurons. Surprisingly this was not the case: Spike number did not correlate with the chemically induced change in burst strength (Figure 5 B).

These seemingly paradox results could be explained by the Adaptive Encoding Hypothesis. The encoders and decoder (ASC_E, DSC, and ComInt 1) are matched to each other (Mulloney et al., 2006), meaning that ComInt 1 interprets the number of arriving coordinating spikes in the context of excitation. The excitation level itself tunes the encoding and decoding properties of the encoders and decoder, so that large differences in burst strength are encoded in a narrow fixed range of spikes by adapting the spike range to the mean burst strength. ComInt 1 is able to match the same number of spikes to different burst strengths, depending on the system's excitation (pers. comm. Carmen Wellmann).

1.4 Aim of Study

One aim of this study was to characterize cellular properties of the coordinating neurons, especially those that allow the precise encoding of coordinating information at different excitation levels, in order to test the Adaptive Encoding Hypothesis. My working hypothesis was that different excitation levels acted on two stages: Influencing the network itself, which in turn affected ASC_E and DSC, and influencing the coordinating neurons directly, changing their excitability.

To set the system to different excitation levels I exploited the nicotinic pathway. It is known so far that the swimmeret system can be activated by stimulating command neurons (Wiersma and Ikeda, 1964), via a proctolinergic pathway, or via a muscarinic pathway (Braun and Mulloney, 1993). But the modulation of the system's output can be achieved effectively with nicotinic agonists in a dose-dependent manner (Mulloney, 1997; Mulloney et al., 1997).

Most of the knowledge about ASC_E and DSC is derived from extracellular recordings. While this is a non-invasive method of recording that causes no or only little damage to neurons, it is only possible to monitor a neuron's output. I used intracellular recordings to gain insights about the neurons' synaptic input and intrinsic properties, such as changes in membrane potential, input/output functions, and changes in conductances based on different excitation levels with the network intact or the neurons chemically isolated.

Just knowing the connectivity and characteristics of single neurons in a network is not enough to predict the output of such a network (reviewed in Harris-Warrick, 2011). Some networks are not functional without the presence of neuromodulators. Either they are not active at all or the activity is not coordinated. It has been demonstrated very clearly in the STNS that even if the network is active all kinds of neuromodulators can alter the motor output by influencing the efficacy of synaptic connections or change ionic conductances in single neurons (Flamm and Harris-Warrick, 1986a, 1986b; Johnson and Harris-Warrick, 1990). The same neuromodulator can activate distinct intracellular pathways in individual neurons, or different neuromodulators can converge onto the same intracellular pathway (Swensen and Marder, 2000).

In the swimmeret system, only little is known about the transmitters the neurons use. Because ComInt 1 receives information from two different types of coordinating neurons I asked which transmitters they used. As the transmitters are presumably of low molecular weight, and GABA and glutamate have already been excluded, I hypothesized them to be most likely serotonin (5-HT) or acetylcholine (ACh). To test this, I used immunohistochemistry and mass spectrometry.

2 Materials and Methods

All experiments were carried out in adult crayfish (*Pacifastacus leniusculus*, DANA, 1852) of both sexes. 421 crayfish were used in this study. Animals were fished from the Wupper at Müngstener Bückenpark, Solingen, by a local fisherman. They were kept in freshwater tanks at 14°C – 18°C until sacrificing. Once a week they were fed with carrots and monthly with additional shrimp pellets. Successful electrophysiological experiments were obtained from 40 animals, successful antibody labeling from 17 animals, and successful mass spectrometry from 11 animals.

2.1 Dissection

All experiments were conducted in the isolated abdominal nerve cord. The detailed dissection procedure is described in Seichter et al. (2014). Briefly, crayfish were anesthetized in ice for 20 minutes. Claws and uropods were removed for exsanguination with 50ml ice-cold crayfish saline (concentrations in mM: 195 NaCl, 5.4 KCl, 13.5 $CaCl_2$, 2.6 $MgCl_2$; buffered with 10mM Tris base and 4.7mM maleic acid at pH 7.4). After decapitation and cutting off the peraeopods, the sternal plate with the abdominal ganglia chain was removed. The ganglia chain from thoracic ganglion 4 (T4) to the last abdominal ganglion (A6) was dissected from the plate and pinned out dorsal side up in a small chamber in a Sylgard-coated (Dow Corning, Midland, MI, USA) Petri dish. The chamber in the Sylgard enabled faster wash-in and –out of substances because of the reduced volume. Special care was taken with the N1s from A2 to A5 because they were used to record extracellularly the fictive swimming pattern. All ganglia were desheathed dorsally with fine scissors to facilitate uptake of chemicals and electrode penetration.

2.2 Electrophysiological Setup

All experiments were carried out at room temperature (18°C – 21°C). In all experiments, I extracellularly recorded fictive motor and coordinating neuron activity, and intracellularly recorded from ASC_E or DSC (Figure 6 A).

I used custom-made differential stainless steel pin electrodes to record from the posterior N1 branches of A2 – A5, carrying PS motor neuron (MN) axons. The nerve was wrapped around the recording electrode and insulated with petroleum jelly, or nerve and recording electrode were placed in the same petroleum jelly wells. The reference electrode was placed nearby in the bath. Electrodes were connected to a custom-made 12-channel ‘switchbox’

which was connected to two 4-channel differential amplifiers (MA102, Electronics Lab, University of Cologne, Germany), thus allowing up to eight simultaneous extracellular recordings. Signals were band-pass filtered between 100Hz and 3kHz, and amplified 1000-fold.

I extracellularly recorded from coordinating neurons with suction electrodes (MWE-F15B, Warner Instruments, Hamden, CT, USA) mounted on a micromanipulator (M-3333, Narishige, Tokyo, Japan). Pipettes were pulled on a P-87 micropipette puller (Sutter Instruments, Novato, CA, USA) from borosilicate capillaries (O.D. 1.5mm, I.D. 0.86mm, Sutter) and broken down to a tip diameter slightly larger than the diameter of the Lateral Giant Axon (LG). For ASC recordings, I placed them dorsal to the LG on the anterior Minuscule Tract (MnT), for DSC recordings dorsal to the LG on the posterior MnT. Signals were preamplified 50-fold (MA103, Electronics Lab) and sent to the two differential amplifiers with the same settings as for pin electrode recordings.

I impaled ASC_E or DSC at the primary neurite in the area of its dendritic arborization in the LN (Figure 6 B). As those neurons are not visible in the ganglion, the following criteria had to be fulfilled for identification:

1. Membrane potential (V_m) oscillation in phase with PS (ASC_E) or in anti-phase (DSC).
2. Corresponding spikes on intra- and extracellular recordings.
3. Current injection modulated burst strength of the neuron's target ganglion.

Identity was confirmed afterwards by the dye-filled neuron's morphology.

Sharp intracellular electrodes (30MΩ – 40MΩ) were pulled from borosilicate capillaries with filament (O.D. 1.0mm, I.D. 0.5mm, Sutter) on a P-1000 micropipette puller (Sutter) and filled with 1% dextran Texas Red (dTR; Molecular Probes, Eugene, OR, USA) in 1M KAc + 0.1M KCl. The electrode was mounted on a micromanipulator (MM-3, Narishige) connected to a fine micromanipulator (Huxley Wall type MP-85, Sutter). To increase the chance of impaling ASC_E, I oriented the micromanipulator perpendicular to the ipsilateral ASC_E's primary neurite (Figure 6 C). To impale DSC, I oriented the micromanipulator perpendicular to the contralateral DSC's primary neurite (Figure 6 C). The intracellular electrode was connected to an amplifier (SEC-05X, npi, Tamm, Germany), which was used in discontinuous current clamp mode (1/4 duty cycle, 5kHz current filter) with switching frequencies between 28kHz to 32kHz. I also used this amplifier for constant current injections to hold V_m at a desired potential.

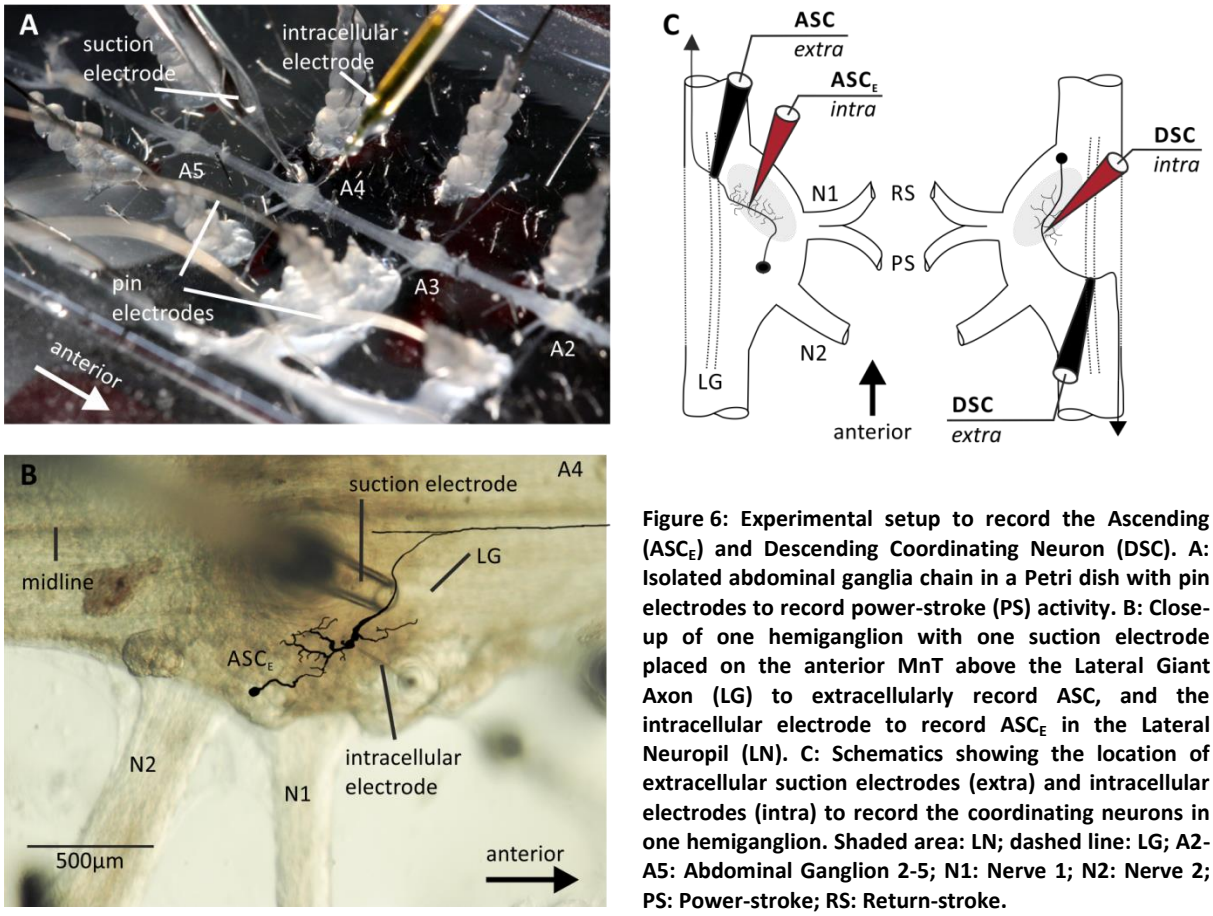

Figure 6: Experimental setup to record the Ascending (ASC_E) and Descending Coordinating Neuron (DSC). A: Isolated abdominal ganglia chain in a Petri dish with pin electrodes to record power-stroke (PS) activity. B: Close-up of one hemiganglion with one suction electrode placed on the anterior MnT above the Lateral Giant Axon (LG) to extracellularly record ASC, and the intracellular electrode to record ASC_E in the Lateral Neuropil (LN). C: Schematics showing the location of extracellular suction electrodes (extra) and intracellular electrodes (intra) to record the coordinating neurons in one hemiganglion. Shaded area: LN; dashed line: LG; A2-A5: Abdominal Ganglion 2-5; N1: Nerve 1; N2: Nerve 2; PS: Power-stroke; RS: Return-stroke.

Signals were digitized with either A/D converter Micro1401-3 with Expansion ACD12 (CED, Cambridge, UK) or Digidata 1440A (Molecular Devices, Sunnyvale, CA, USA) and recorded with Spike2 (CED) or Clampex (Molecular Devices), respectively. All signals were digitized at 10kHz, except extracellular recordings using Spike2, which were digitized at 5kHz. Depending on the setup, a stimulator (MS 501, Electronics Lab) was used to trigger execution of a stimulus protocol (with Spike2), or directly delivered the stimuli via the intracellular amplifier (with Clampex).

Saline and chemicals were delivered via a gravity-fed perfusion system and removed with a vacuum pump. Flow rate was 0.5-1ml/min when searching for neurons and 4-5ml/min during the experiments. Wash-in and wash-out was considered complete after 40ml (approx. 10min) because V_m had reached steady state by then. Initial wash-in of $LowCa^{2+}$ saline was at least 20min.

2.3 Electrophysiological Protocols

I conducted the experiments with the network either intact or the neurons chemically isolated. In the intact network I set the excitation level with different carbachol concentrations (in µM: 2, 3, 4) in normal saline, or edrophonium chloride (EdCl; Santa Cruz

Biotechnology, Dallas, TX, USA) concentrations (in µM: 50, 75, 100) in saline containing 50nM crustacean cardioactive peptide (CCAP; Bachem, Bubendorf, Switzerland).

Carbachol is a cholinergic agonist, acting both on muscarinic and nicotinic receptors. Therefore, it can both activate the swimmeret system and modulate its excitation level. The thereby induced fictive swimming is characterized by similar frequencies as reported for the intact crayfish swimmeret beating (Braun and Mulloney, 1993). EdCl is an acetylcholine esterase inhibitor and does not activate the swimmeret system on its own. Therefore, I used a combination of CCAP to activate the system (Mulloney et al., 1997) and different EdCl concentrations to modulate the output. Braun and Mulloney (1993) have shown that application of an ACh-esterase inhibitor increases burst frequency similar to application of carbachol. To chemically isolate the neurons, I used Low Ca^{2+}/High Mg^{2+} saline (LowCa^{2+} saline; in mM: 118.0 NaCl, 5.4 KCl, 52.0 $MgCl_2$, 2.4 $CaCl_2$, or 195.0 NaCl, 5.4 KCl, 16.4 $MgCl_2$, 0.6 $CaCl_2$) to block transmitter release at all chemical synapses (Tschuluun et al., 2001). In the synaptically isolated neurons, I set the excitation level with the above mentioned carbachol concentrations. Occasionally, I added low concentrations of tetrodotoxin (TTX; BioTrend, Cologne, Germany) to block any residual spike-driven modulations (TTX in µM: 0.1 – 0.5 without carbachol, 0.1 with carbachol). All experiments were conducted at the three different excitation levels mentioned above. Even with run-down of the preparations, recordings with good quality could be obtained for two hours.

When stimulus protocols were executed, the neurons were held at the same trough potential (most hyperpolarized membrane potential during an oscillatory cycle), usually sub-threshold at -55mV to -75mV. To measure input resistances (R_{in}), at least 100 brief hyperpolarizing currents (-1nA, 50ms – 100ms) were delivered every 5sec at each chemical concentration. R_{in} was measured in both intact network and isolated conditions.

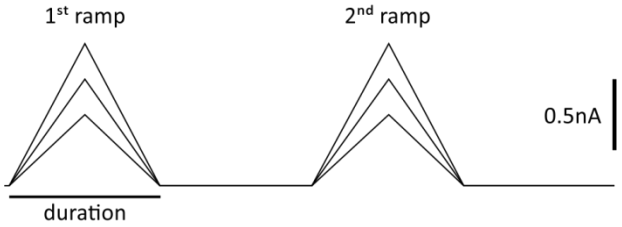

Figure 7: Schematic of paired ramp stimulus. Isolated neurons were stimulated with two consecutive ramps of three different amplitudes and three different durations. One stimulus sweep lasted ten seconds.

To reveal history effects, isolated neurons were held at -55mV and stimulated with paired triangular ramps every 10s (Figure 7). Ramps differed in amplitude (in nA: 0.5, 0.75, 0.1) and duration (in ms: 250, 500, 1000), giving 3 x 3 combinations for ramp stimuli. Except for two experiments, the ramps had 1/2 duty cycle. In two experiments the 1s ramps had 2/3 duty cycle. Periods and durations of ramp stimuli were in the same range as the observed motor

output (Mulloney et al., 2006). Ramp stimulation experiments were done in collaboration with T. Michael Wright (Mulloney Lab, UC Davis). V-I curves were obtained by injecting de- and hyperpolarizing currents (in nA: ±0.5, ±0.75, ±1) for at least 10 cycles. After the experiment, the neurons were filled with dTR for at least 10min and up to 2h (+1nA at 2Hz, 250ms pulse duration). Stained neurons were processed immediately if the axon and soma were clearly visible. If not, ganglia were kept at 4°C until dye diffusion was sufficient.

2.4 Analysis

I only analyzed experiments in which ASC_E or DSC were the only stained neurons and measurements were completed at two excitation levels minimum. Data were analyzed semi-automatically using Spike2 scripts or MATLAB (versions R2014b and R2016a, MathWorks, Natick, MA, USA). If voltage traces with different sampling frequencies (5kHz and 10kHz, see 2.2) were analyzed in MATLAB, I had to upscale the lower sampled data by duplicating each value. This may result in an error of 0.2ms in event detection that is negligible for this study and preferable over down sampling intracellular recordings. The following parameters were evaluated:

Membrane potential (V_m)

As oscillating neurons do not have a 'resting potential' I used the trough potential at the most hyperpolarized value during a cycle instead (Figure 8 A).

Spikes per burst

Number of ASC_E or DSC spikes during one burst.

Burst duration

Duration between a burst's first and last spike (Figure 8 A).

Cycle period

Duration between the beginning of a reference burst and the beginning of the consecutive burst (Figure 8 A).

Phase

First, I measured the latency from the beginning of a cycle to the occurrence of an event during that cycle. Second, I calculated phase by dividing the latency of an event (e.g. stimulus beginning, Figure 8 A) by cycle period.

Input resistance (R_{in})

Using Ohm's law, I calculated R_{in} by dividing V_m deflection by the injected current. R_{in} was calculated with respect to the phase of the stimulus.

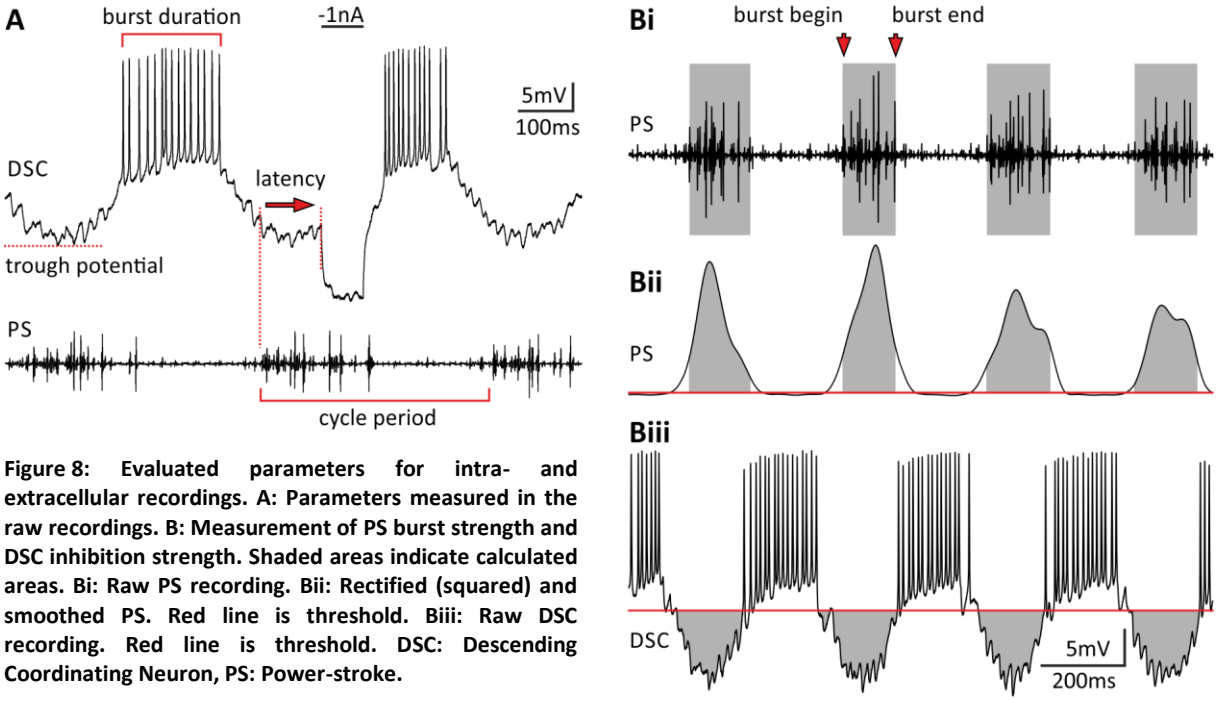

Figure 8: Evaluated parameters for intra- and extracellular recordings. A: Parameters measured in the raw recordings. B: Measurement of PS burst strength and DSC inhibition strength. Shaded areas indicate calculated areas. Bi: Raw PS recording. Bii: Rectified (squared) and smoothed PS. Red line is threshold. Biii: Raw DSC recording. Red line is threshold. DSC: Descending Coordinating Neuron, PS: Power-stroke.

Burst strength

During PS or RS bursts up to 30 MNs can be active at the same time (Mulloney, 1997; Mulloney and Hall, 2000), resulting in overlapping spikes in the extracellular recording (Figure 8 Bi). Burst strength is an approximation for unit amplitude and unit frequency: Higher activity of larger units results in a higher burst strength than lower activity of smaller units (Mulloney, 2005). Extracellular recordings were rectified by squaring the voltages and smoothed (Figure 8 Bii). The smoothing kernel was a Gaussian window (width = 1001) that was vertically shifted to zero and normalized to unity gain at DC. The area under the smoothed curve above noise threshold between burst beginning and burst end was calculated. Burst strength was calculated by dividing the area by burst duration. Because absolute burst strength depends on the signal-to-noise ratio of the recording, absolute values cannot be compared between experiments and were thus normalized to the maximum burst strength in each experiment across excitation levels. The bursts immediately before, after, and during stimulations were excluded from the dataset because coordinating neurons can influence the motor output of their home ganglion (Mulloney and Hall, 2007a).

Inhibition strength

DSC inhibition strength during PS was calculated analog to burst strength (Figure 8 Biii). The voltage trace was offset to the average voltage of the burst's first spike's afterhyperpolarization ('threshold' in Figure 8 Biii). The area's absolute value of the intracellular voltage trace between DSC burst end and burst begin below threshold was

calculated and divided by the interburst interval to get inhibition strength. Thus, not only the graded inhibition is taken into account but also the amount and amplitude of the inhibitory postsynaptic potentials (IPSP) in the interburst.

Statistics and Data Presentation

I used non-parametric tests in MATLAB for statistical analyses. Two data sets were compared with a rank-sum test if unpaired or Wilcoxon signed rank test if paired. Multiple data sets were compared with the Kruskal-Wallis test with Tukey's post-test for multiple comparisons. Significance level was $\alpha = 0.05$.

Linear regressions and their adjusted regression coefficients (R^2 - adj.) were calculated with MATLAB's built in linear model fit (fitlm). Nonlinear regression lines were calculated with MATLAB's built in polynomial curve fit (polyfit). Usually, median values are given in the text. Otherwise, means are notated with ± standard deviation.

All figures were prepared in MATLAB and Corel Draw X (Corel Corporation, Ottawa, Canada). Dot-density plots were created with Molly Rossow's Dot-Density-Plot script for MATLAB (Rossow, 2013).

In most figures, plots from one individual experiment illustrate representative results. The respective plots for all analyzed experiments are located as 'Supplementary Figures' in the Appendix. "N" denotes the number of animals used for an experiment, "n" denotes the measurements per animal.

2.5 Histology

After intracellular staining with fluorescent dyes, samples were protected from light in the following steps. I fixed whole ganglia with stained neurons for 2h in either Roti®-Histofix 4% (Carl Roth, Karlsruhe, Germany), 4% paraformaldehyde (Serva, Heidelberg, Germany) + 1.25% glutaraldehyde (Serva; not usable for antibody staining) in 0.1M phosphate buffered saline (PBS), or 4% paraformaldehyde + 0.5% glacial acetic acid in PBS. Afterwards, ganglia were rinsed 3x10min in PBS. If the fixative contained glutaraldehyde, autofluorescence was reduced by 10min incubation in 0.25% sodium borohydride in PBS with subsequent 3x10min washing in PBS.

For antibody staining, ganglia were first washed 3x10min in PBST-NGS (PBS with 1% Triton-X-100, 5% normal goat serum (Vector Laboratories, Burlingame, CA, USA), 0.1% NaAc). Second, they were incubated 36h in 1:400 rabbit anti-serotonin whole serum (Sigma-Aldrich, Munich, Germany) in PBST-NGS on a rotator at 4°C. Afterwards, ganglia were washed 3x2h in PBST and incubated on a rotator at 4°C overnight in 1:200 donkey anti-

rabbit conjugated to Alexa Fluor 488 (abcam, Cambridge, UK) in PBST-NGS. Ganglia were then washed 4x1h in PBS.

All ganglia were dehydrated in an ascending ethanol series (10min each: 30%, 50%, 70%, 90%, 96%, 2x100%) and mounted in methyl salicylate (Carl Roth) on microscope slides with a cavity.

2.6 Microscopy

Overview scans for neuron identification were obtained on a fluorescence microscope (BX61, Olympus, Hamburg, Germany). For 5-HT labeled neurons, I used a confocal microscope (LSM 500 Meta, Zeiss, Oberkochen, Germany) with 10x magnification for overview and 40x magnification (oil) for details in the axonal region. dTR excitation wavelength was 543nm, Alexa Fluor 488 excitation wavelength was 488nm, filtered by a primary dichroic beamsplitter (HFT 488/543). Emission of dTR was filtered by a 650nm long pass filter, emission of Alexa Fluor 488 by a 505-530nm band pass filter.

Scans were done in 5µm-10µm z-stacks at 10x magnification and 2µm z-stacks at 40x magnification. Maximum intensity projections were made with either Helicon Focus (Helicon Soft Ltd., Kharkov, Ukraine) or Zen 2011 black edition (Zeiss). Brightness and contrast were adjusted for each channel separately with Photoshop CS5 (Adobe Systems, San José, CA, USA).

2.7 MALDI-TOF Mass Spectrometry

This part of the study was done in collaboration with Susanne Neupert (University of Cologne). MALDI (Matrix-Assisted Laser Desorption/Ionization)-TOF (Time of Flight) mass spectrometry (MS) is a soft ionization technique used in mass spectrometry, allowing the analysis of biomolecules, such as proteins, peptides, lipids, and sugar, as well as large organic molecules such as polymers and other macromolecules. In total, three steps characterize the methodology of MALDI. In a first step, a suitable matrix is mixed to a sample onto a metal plate. Second, laser pulses are applied to the embedded sample mixture, triggering ablation and desorption of the matrix and embedded biomolecules. In a final step, the molecules are ionized by being protonated or deprotonated. During the TOF step, the ions are separated depending on the mass-to-charge ratio. Larger ionized molecules need more time to reach the detector than smaller ones.

Ganglia as well as the single cells were covered in *Lymnaea* saline (in mM: 46 NaCl, 4.0 KCl, 7.5 $CaCl_2$ at pH 7.4) containing 33% glycerol to stabilize the fluorescent dye. Stained somata of ASC_E, DSC, or motor neurons (control) were cleanly pulled out from the ganglion

with a glass capillary under a stereo fluorescence microscope (V12 Lumar, Carl Zeiss AG, Göttingen), and transferred to a stainless steel sample plate for MALDI-TOF MS analysis. After air-drying the samples at room temperature, 20nl - 30nl of α-cyano-4-hydroxycinnamic acid (CHCA) as matrix was applied using a glass capillary. An UltrafleXtreme TOF/TOF mass spectrometer (Bruker Daltonics, Bremen, Germany) was used to acquire mass spectra in positive ion mode. Settings were optimized for mass ranges of 0 – 300Da. MS/MS was performed with LIFT technology by an acceleration set at 1 kV. The number of laser shots used to obtain a spectrum varied from 1000 to 5000 depending on signal quality. Acetylcholine was verified using MS/MS fragmentation pattern and compared using fragmentation data provided by Scripps METLIN Center of Metabolomics (https://metlin.scripps.edu/index.php). Data were processed with FlexAnalysis (version 3.4, Bruker).

A principal component analysis (PCA) was performed on the mass spectra peaks from the individual neurons. With this method, extensive or high-dimensional datasets can be readily visualized by converting possibly correlated variables into new, linear uncorrelated variables (the principal components). This can reduce the dimensionality of a dataset and enhance differences across data. In our analysis, we projected the spectral data for the three classes of neurons into a three-dimensional subspace of the first three principal components. This allowed for a visual discrimination of coordinating and motor neurons. Single-cell MALDI-MS with subsequent PCA for example allows discrimination of metabolitic heterogeneity in unicellular organisms (Amantonico et al., 2010) or identification of three subspecies in the *Mycobacterium abscessus* complex (Kehrmann et al., 2016).

3 Results

In this study, I investigated the coordination of distributed neural oscillators. Two neurons in each hemiganglion of the crayfish swimmeret system serve this task. Both encode the activity state of their own module and send the information as bursts of spikes to the other ganglia where it is integrated and relayed to the CPG (Mulloney et al., 2006; Smarandache et al., 2009; Smarandache-Wellmann et al., 2014). The aims of this thesis were to unravel the cellular properties of ASC_E and DSC that allow the precise encoding of activity at different excitation levels, and to identify their transmitters at the synapse to ComInt 1. Because the general features how each ASC_E and DSC encodes information about its home ganglion's activity state are similar (Mulloney et al., 2006), and I observed no obvious differences for coordinating neurons from different ganglia, I assumed that tuning mechanisms are homolog across ganglia and did not differentiate between segments.

PART I: Cellular Properties

ASC_E and DSC encode information about timing, duration, and strength of their home ganglion's motor output as bursts of spikes (Mulloney et al., 2006). If PS burst strength varies spontaneously, ASC_E tracks this changes linearly by producing more spikes at higher PS burst strengths (Smarandache-Wellmann et al., 2014). Less is known about DSCs ability to track changes in burst strength. Paul and Mulloney (1986) report only a loose correlation between the amount of DSC spikes and PS and RS, respectively.

The focus of this chapter is on characterizing the electrophysiological properties of the coordinating neurons. I investigated the mechanisms shaping the bursts and the encoding of motor activity at different excitation levels. Subsequently, I asked which of these properties arise from the network activity and which are intrinsic to ASC_E and DSC.

Mulloney et al. (2006) stated that ASC_E tracks PS bursts. The authors also found correlations between DSC activity with both PS and RS. I never obtained RS recordings with a good enough signal-noise ratio for analysis; therefore, I also correlated DSC activity to PS.

3.1 Isolating Neurons

With bath application of chemicals, it remains elusive whether observed changes in neuronal activity and properties are a direct effect, or mediated by the network, or both. Therefore, I did my experiments in the intact (i.e. synaptically connected) network and in

neurons chemically isolated with LowCa^{2+} saline. When I applied LowCa^{2+} saline to suppress transmitter release, PS became tonically active with sporadic synchronized motor bursts (Figure 9). Coordinating neurons became tonically active in half of the experiments. Spike amplitude was reduced, most likely by sodium channel inactivation, because the membrane potential (V_m) depolarized compared to trough potential in normal saline.

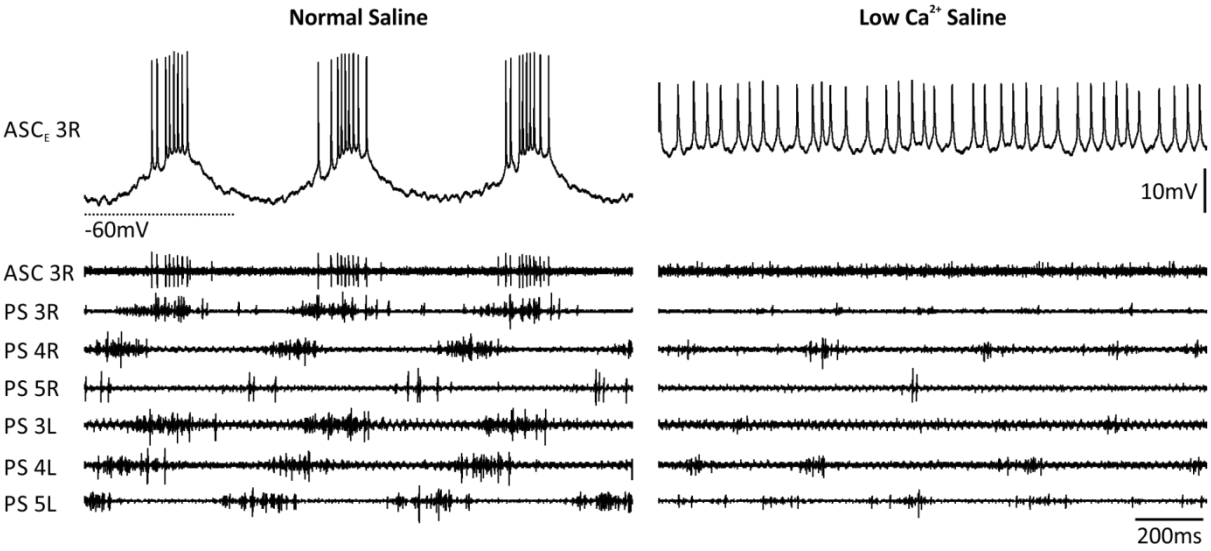

Figure 9: Activity of PS and ASC_E when the network was intact (left) or chemically isolated (right). Preparations became tonically active after application of LowCa^{2+} saline. Spike amplitude was reduced due to sodium channel inactivation.

In some isolation experiments, PS MNs occasionally synchronized to erratic PS bursts that correlated with V_m modulation in the coordinating neurons (Figure 10 A, 8 ASC_E experiments, 2 DSC experiments). This indicated an incomplete isolation or block of transmitter release. Because of the overall tonic activity, I assumed that the CPG was silenced or at least locked. With the addition of TTX to the LowCa^{2+} saline spiking was blocked and I never observed V_m modulations in the coordinating neurons (Figure 13 B).

In the following, I demonstrate that the response of the coordinating neurons to changes in excitation is different in the intact network compared to synaptic isolation, and that the network effect masked the direct effect of carbachol. Because of the similar effects of carbachol and EdCl on the motor output and the coordinating neurons, I combined those results when discussing the intact network in the following unless noted otherwise. For the same reasons I combined the results from LowCa^{2+} saline with and without TTX.

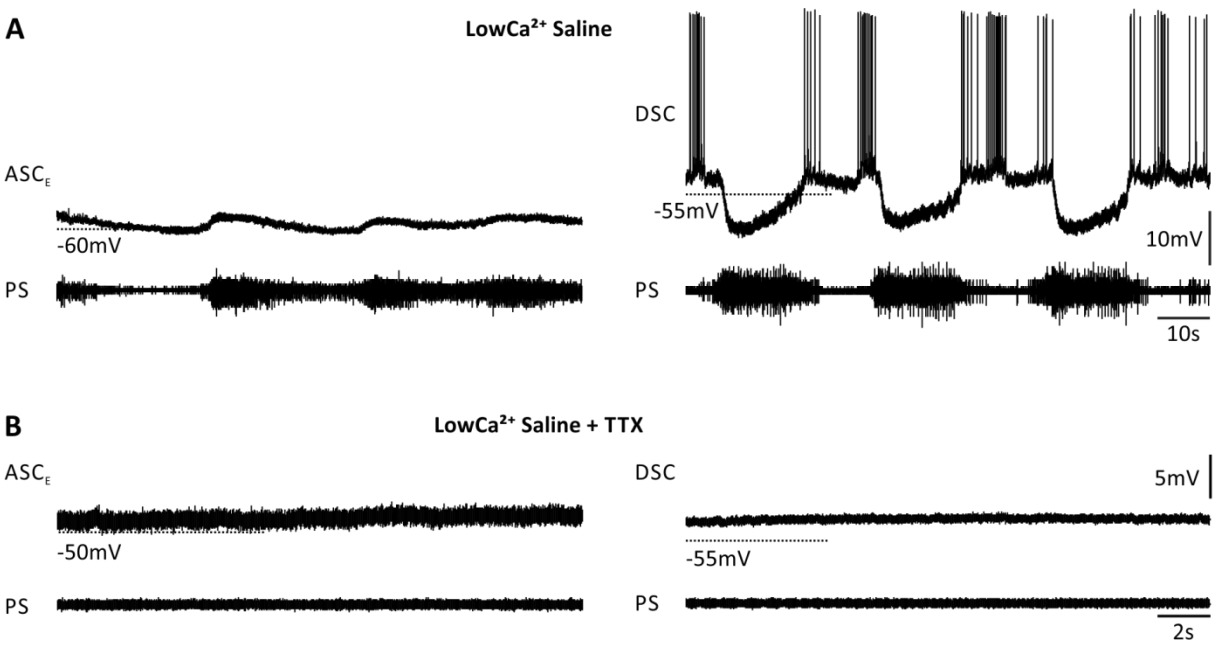

Figure 10: Recordings of the isolated coordinating neurons ASC_E and DSC, and power-stroke (PS) activity in their home ganglion in $LowCa^{2+}$ saline without (A) and with (B) TTX. Without TTX, the membrane potential of the coordinating neurons was modulated in phase with the PS.

3.2 Different Mechanisms Shaped ASC_E and DSC bursts

ASC_E and DSC are morphological mirror images (Figure 2). Their V_m oscillates phase-locked with PS and RS, respectively, and they fire bursts of spikes during their depolarized state. I used preparations that switched between an active and quiescent state to gain insight on the coordinating neurons' behavior during these transitions (Figure 11).

During the quiescent state, ASC_E was hyperpolarized and not spiking (Figure 11 A). Immediately before PS activity started, ASC_E depolarized. On top of this depolarization, V_m oscillated with bursts of spikes during peak oscillation in phase with PS. Very weak PS bursts were accompanied by V_m oscillations without spikes. After PS activity ceased, ASC_E's V_m hyperpolarized to its resting level (13 of 19 experiments). In the five remaining experiments resting level equaled trough potential. No tonic depolarization was obvious during the transition to the active state, and no hyperpolarization during the transition to the quiescent state.

In contrast, DSC was tonically firing if motor activity was quiescent (Figure 11 B). When the system is active, DSC oscillates in antiphase to the PS (Namba and Mulloney, 1999). Oscillations seemed to be mediated by strong inhibitory synaptic input during each PS burst (12 of 12 experiments). In this interburst interval, prominent postsynaptic potentials (PSPs) appeared in DSC but not ASC_E (Figure 11 insets). Inhibition during weak PS bursts did not hyperpolarize DSC as much as during strong PS bursts (Figure 11 B; see also Figure 13 C).

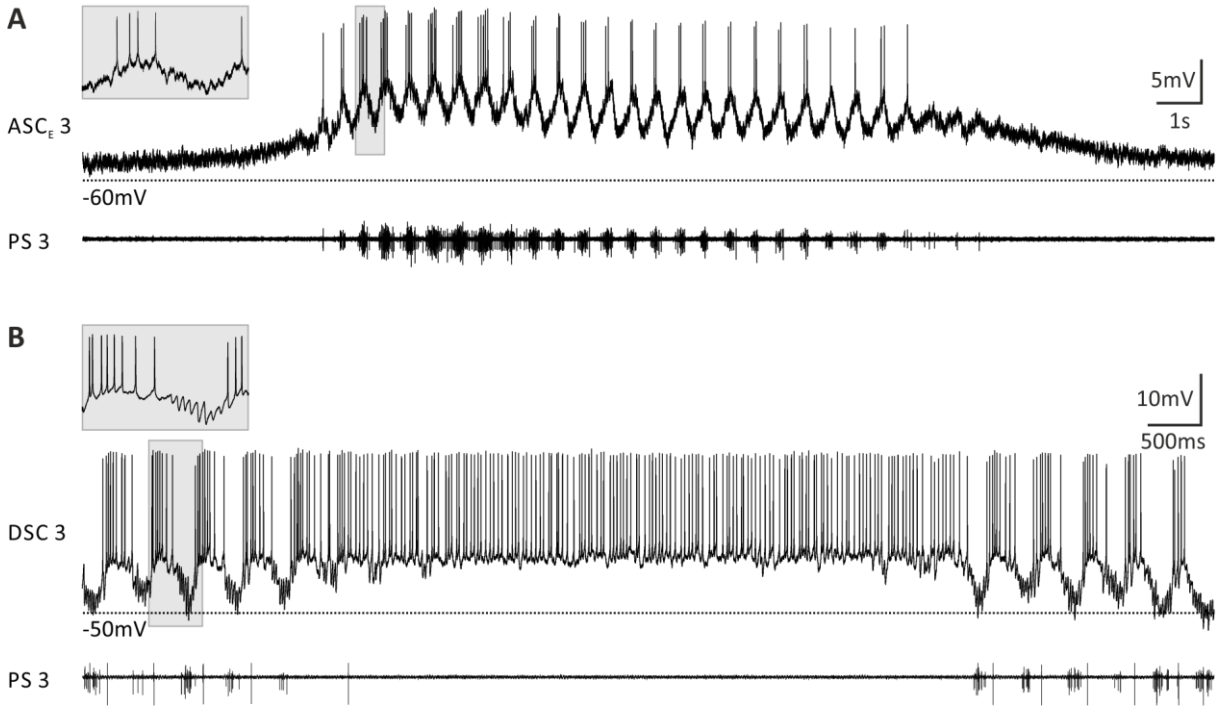

Figure 11: Activity of coordinating neurons in systems switching between active and quiescent states. A: Intracellular recording of ASC_E and respective PS. Inset shows one ASC_E cycle indicated by the grey box. B: Intracellular recording of DSC and respective PS. Inset shows one DSC cycle indicated by the grey box.

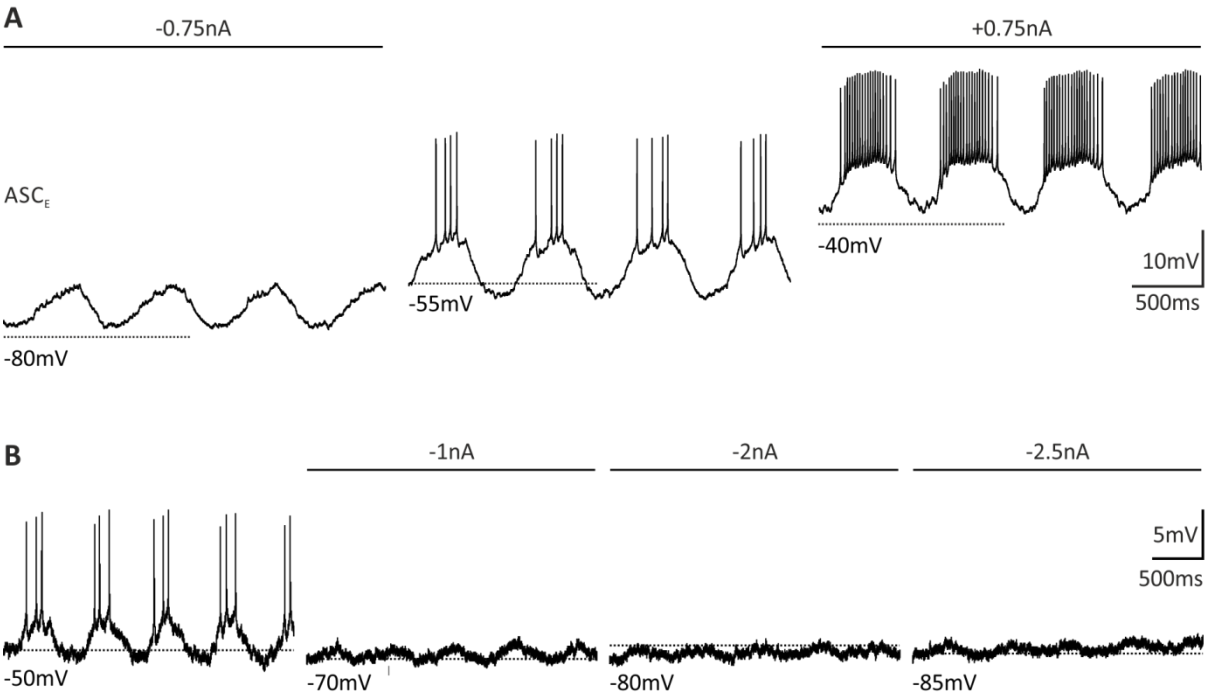

Figure 12: Shaping of ASC_E bursts. A: Intracellular ASC_E recording with hyperpolarizing (left), no, or depolarizing (right) current injection. B: Hyperpolarizing ASC_E reduced oscillation amplitude.

Compared to DSC, ASC_E's oscillations appeared rather smooth with only small PSPs in the interburst. When hyperpolarizing or depolarizing ASC_E, amplitudes of some interburst PSP decreased during hyperpolarization and increased during depolarization (7 of 7 experiments, Figure 12 A). Hyperpolarizing also reduced oscillation amplitude (Figure 12 B). This might be caused by a diminished driving force for K^+ ions, which means that the interburst is mediated by inhibition and that some of the PSPs in the interbursts are inhibitory postsynaptic potentials (IPSPs). In contrast to DSC, ASC_E seemed to receive a mix of excitatory postsynaptic potentials (EPSPs) and IPSPs, which were not as distinguished.

When I hyperpolarized DSC, amplitudes of oscillations and interburst PSPs decreased (5 of 5 experiments, Figure 13 A). Depolarizing increased interburst PSP amplitude. These IPSPs only occurred during PS activity (Figure 13 B). As soon as PS MNs were active in a burst-like manner in $LowCa^{2+}$ saline, DSC received a barrage of regularly spaced IPSPs. These IPSPs were not time-locked to any recorded PS motor unit (Figure 13 B inset) or ASC_E in DSC's home ganglion. Because of the regular interval between IPSP peaks, they were most likely caused by a single spiking neuron.

In regular carbachol-induced rhythms, I observed no obvious correlation between DSC's inhibition strength and PS burst strength (4 of 4 experiments. Figure 13 Ci, Supplementary Figure 1). In two experiments, PS burst strength was variable. In those cases, PS burst strength correlated with DSC inhibition burst strength (Figure 13 Cii, Supplementary Figure 1). Although oscillation amplitude of the coordinating neurons decreased with hyperpolarization, it never reached reversal potential in ASC_E, even if hyperpolarizing to -120mV. In DSC, oscillations reversed at -90mV (Figure 13 D, 1 of 5 experiments), which is approximately equilibrium potential for K^+ ions in nervous systems.

All this evidence suggests that ASC_E and DSC bursts were shaped by different mechanisms. ASC_E seemed to receive tonic excitatory input on top of which oscillations were shaped by inhibition. DSC bursts were shaped by inhibition only. If the coordinating neurons would receive additional phasic excitation, oscillation amplitude of that phasic excitation would increase when the neurons were hyperpolarized. I did not make that observation in my experiments.

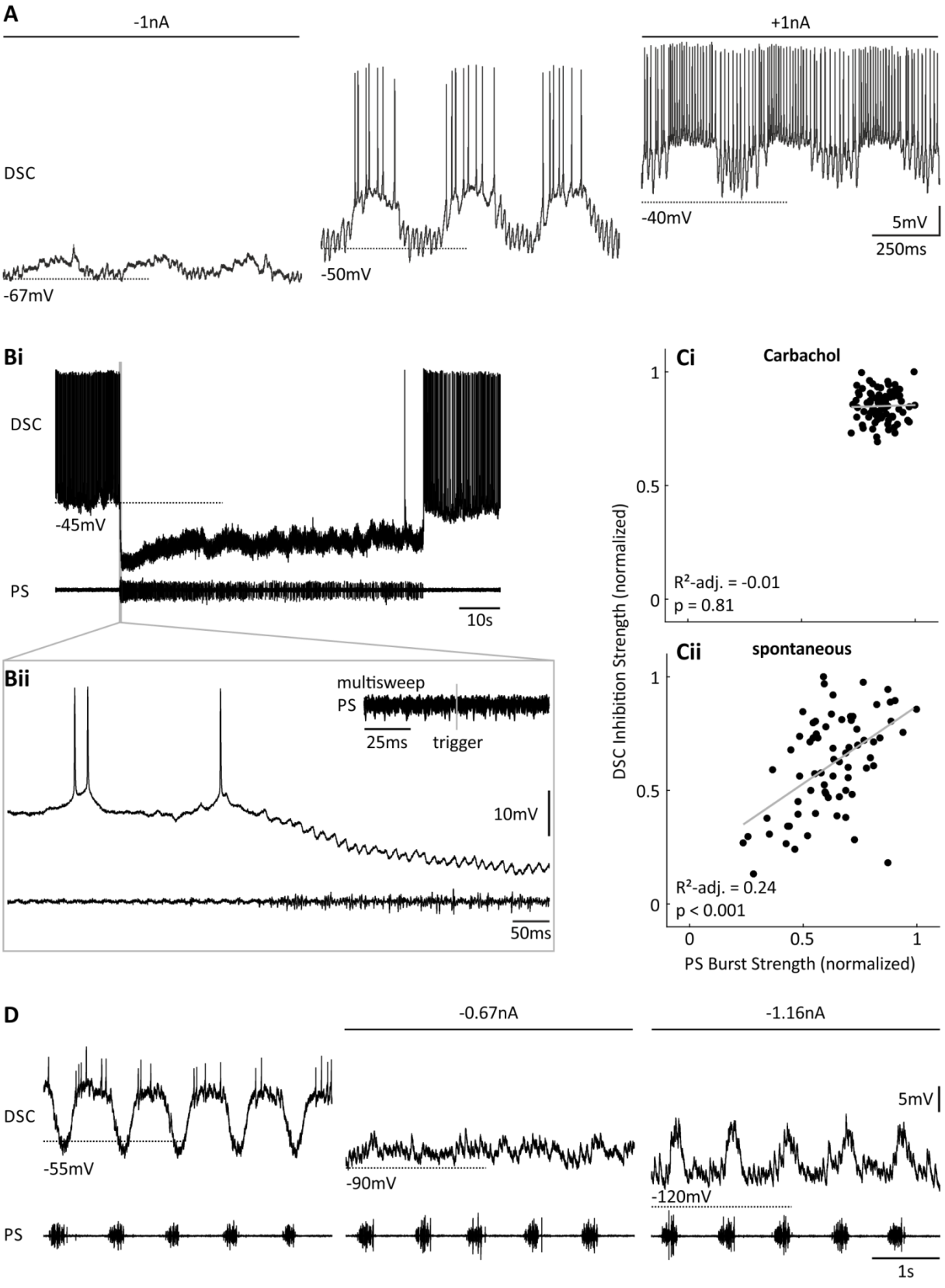

Figure 13: Shaping of DSC bursts. A: Intracellular DSC recording with hyperpolarizing (left), no, and depolarizing (right) current injection. B: Inhibition of DSC during tonic motor activity (in LowCa^{2+} saline). Bii: Expansion of time at the time indicated in Bi. Inset shows PS multisweep triggered by DSC IPSPs (42 sweeps); trigger time is indicated by the grey bar. C: Correlation between PS burst strength and DSC inhibition. Exemplary experiment in 2µM carbachol (Ci), and with spontaneous changes in activity (Cii). Regression line is grey. D: Reversal of DSC inhibition during PS.

Hysteresis in Coordinating Neurons

The swimmeret system is able to generate a regular rhythmic motor pattern. As shown in the previous chapter, the activity of the neurons, which are necessary and sufficient to maintain this stable motor output, was modulated similar to the motor activity. Hence, I asked if the coordinating neurons possess adaptive mechanisms that may influence the modulatory effects.

Upon constant current injection (≥ 10 cycles, ≥ 0.5nA), both ASC_E and DSC adapted to the stimulus (Figure 14 A). This caused the neurons to generate fewer spikes in consecutive bursts during the time of current injection (3 of 3 ASC_E, 4 of 4 DSC; Figure 14 B, Supplementary Figure 2) Injecting long hyperpolarizing current pulses (≥ 10 cycles, ≤ -0.5nA) led to subthreshold V_m oscillations.

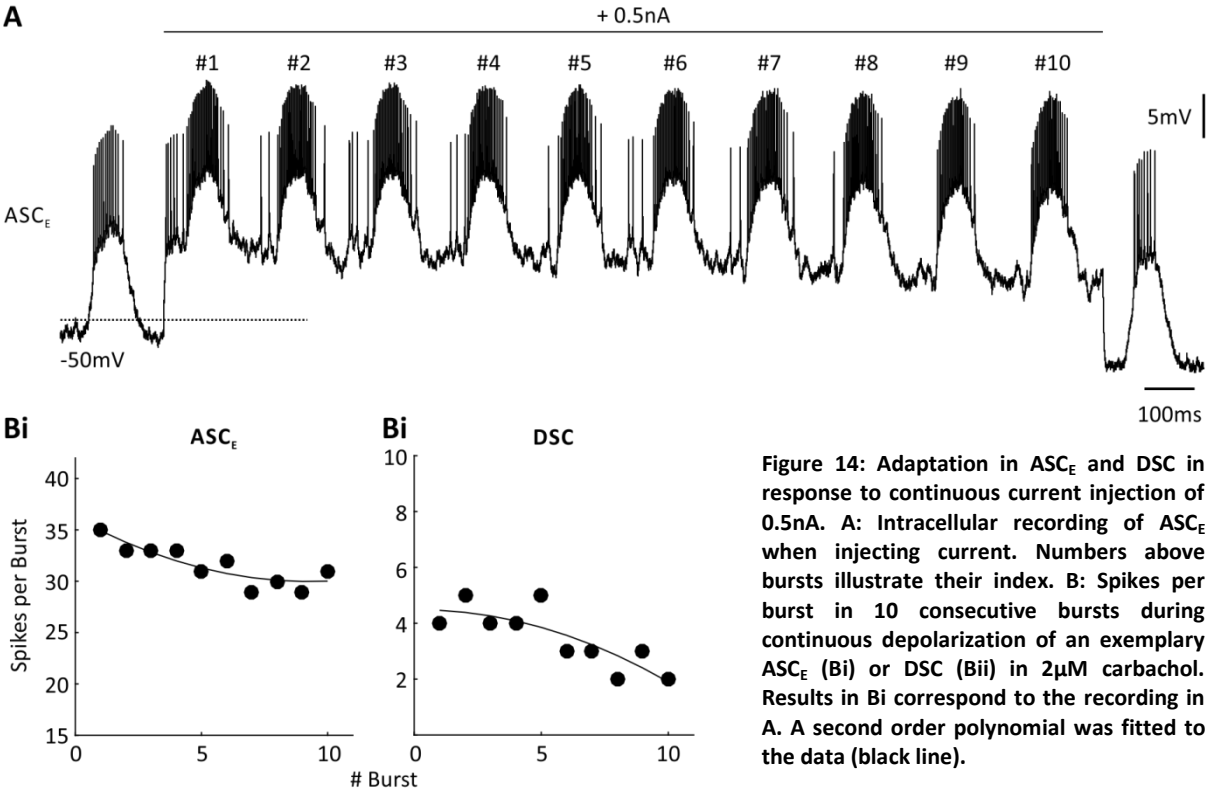

Figure 14: Adaptation in ASC_E and DSC in response to continuous current injection of 0.5nA. A: Intracellular recording of ASC_E when injecting current. Numbers above bursts illustrate their index. B: Spikes per burst in 10 consecutive bursts during continuous depolarization of an exemplary ASC_E (Bi) or DSC (Bii) in 2µM carbachol. Results in Bi correspond to the recording in A. A second order polynomial was fitted to the data (black line).

To investigate the adaptive mechanisms further, I first focused on changes in spike generation within a burst in ASC_E. The first spike in a burst was elicited at a more hyperpolarized V_m than the last spike (median -46.4mV vs. -41.9mV, Figure 15 A, Ci; 5 of 5 experiments; Wilcoxon $p < 0.001$). These results were obtained from synaptically connected ASC_Es that expressed a steady state rhythm. Thus, I chemically isolated ASC_E and stimulated it with triangular ramps to mimic their activity in the intact network (Figure 15 B). The spike trains elicited by the ramp currents represent input-output

functions that describe how the neuron encodes its input. Like in the intact network, the first spike was generated at a more hyperpolarized V_m than the last spike in response to ramp stimulation (median -50.6mV vs. -40.9mV, Figure 15 Cii; 4 of 4 experiments; Wilcoxon $p < 0.01$). Notably, spike threshold for the first spike was lower in the isolated ASC_E (Figure 15 C; difference between medians 4.2mV, rank sum $p = 0.034$). Additionally, more spikes were on the ramp's rising slope than the falling (median 13.5 vs. 6.5, Figure 15 D; 4 of 4 experiments; Wilcoxon $p < 0.01$).

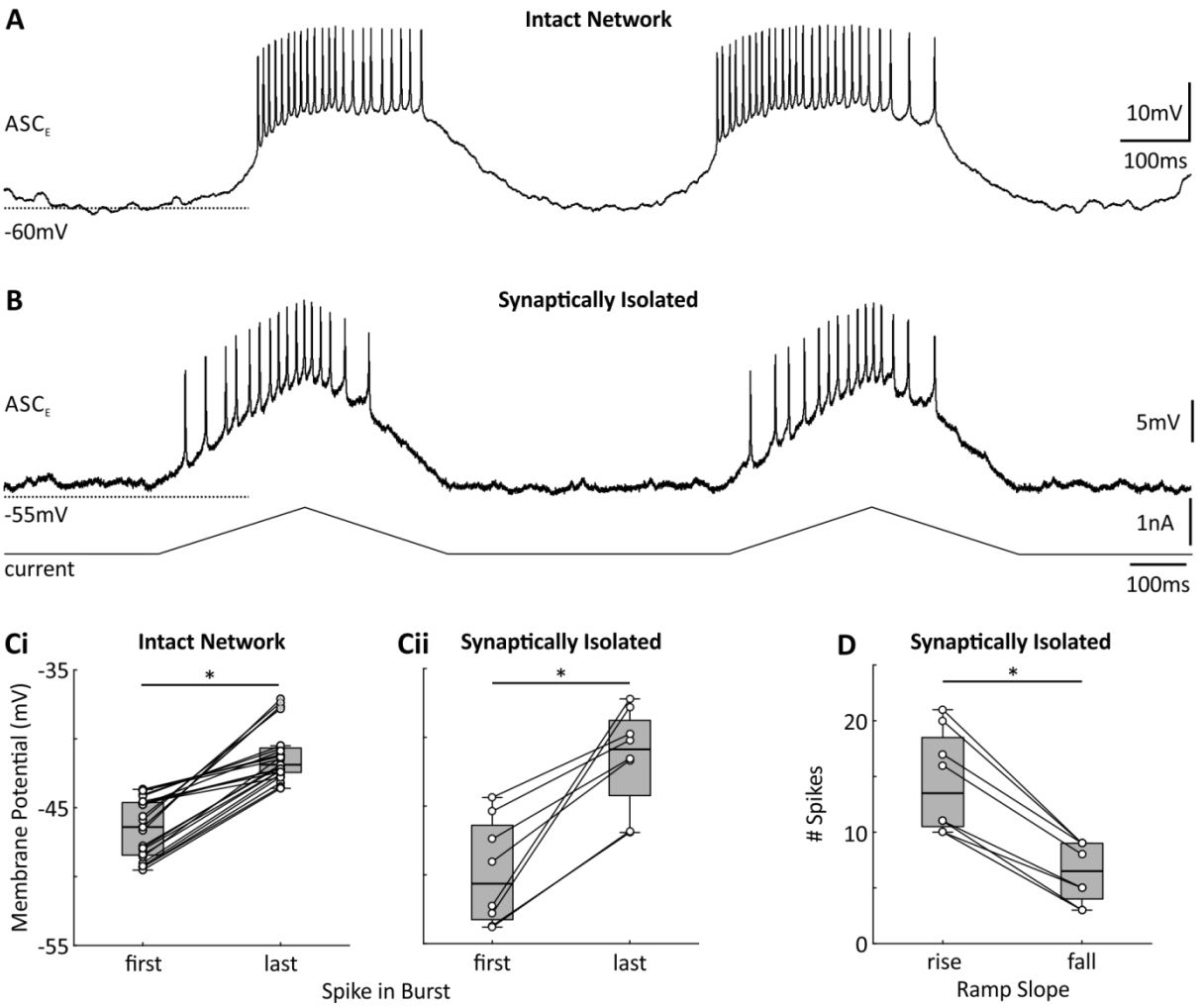

Figure 15: Intraburst hysteresis in ASC_E. A: Intracellular recording of ASC_E activity in the intact network. B: Intracellular recording and ramp stimulation of a synaptically isolated ASC_E. C: Both in the intact network (Ci; N = 5, n = 5) and in synaptic isolation (Cii; N = 4, n = 2) V_m of the first spike in response to ramp stimulation was more hyperpolarized than that of the last spike. V_m of the first spike was more hyperpolarized in the isolated ASC_E compared to ASC_E in the intact network. D: More spikes were elicited on the ramp's ascending slope compared to the descending slope (N = 4, n = 2). Data in Cii and D for 500ms 1nA ramps in 2µM carbachol. * $p < 0.05$.

Furthermore, I investigated if a preceding ramp stimulus affected the neuronal response to a second ramp stimulus. Across all ramp durations and amplitudes, the first ramp elicited 1 - 2 spikes more than the second did (median 21 vs. 19.5, Figure 16 A, B; 4 of 4

experiments). In accordance, the latency from stimulus begin to the first spike was shorter for the first ramp than for the second (median 32.7ms vs. 45.5ms, Figure 16 A, C; 4 of 4 experiments).

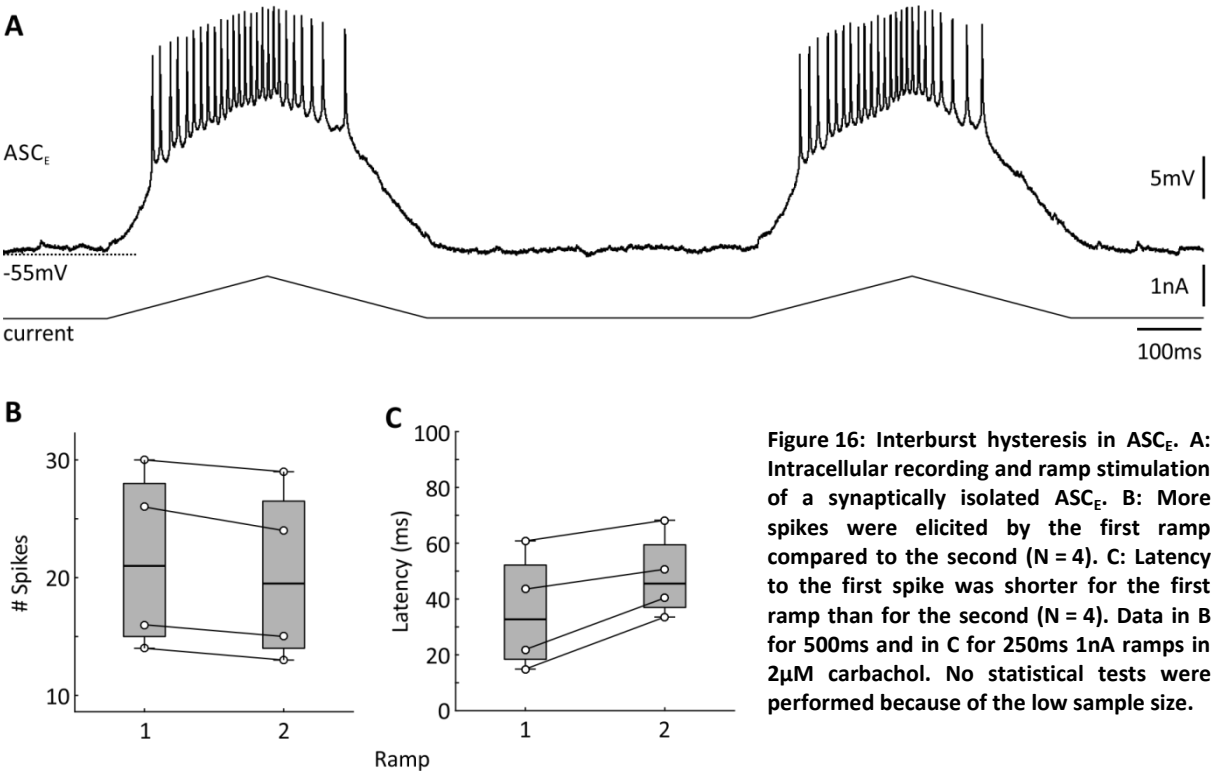

Figure 16: Interburst hysteresis in ASC$_E$. A: Intracellular recording and ramp stimulation of a synaptically isolated ASC$_E$. B: More spikes were elicited by the first ramp compared to the second (N = 4). C: Latency to the first spike was shorter for the first ramp than for the second (N = 4). Data in B for 500ms and in C for 250ms 1nA ramps in 2µM carbachol. No statistical tests were performed because of the low sample size.

This shows that history affects the neurons' activity at least on two time scales. The short-term effect within a burst caused spike threshold to increase during activity. Hence, fewer spikes were generated on the falling slope of the ramp stimulus, and the threshold of the last spike was more depolarized than that of the first spike. The long-term effect across bursts influenced spike number based on preceding activity. Hence, the second ramp elicited fewer spikes than the first ramp, and latency to the first spike was longer for the second ramp compared to the first ramp. As these results were obtained from synaptically isolated neurons, they must be caused by intrinsic properties.

Network Effect Masked Rebound Properties

Many oscillating neurons possess a hyperpolarization-activated cation current (I_h) that helps with escape from inhibition, as seen in leech heart interneurons (Angstadt and Calabrese, 1989). One indication for the presence of I_h is the development of a sag-potential when the neuron is hyperpolarized, and a post-inhibitory rebound after this hyperpolarization. As the coordinating neurons in the swimmeret system receive periodic

inhibitory input from the CPG (Smarandache-Wellmann and Grätsch, 2014) I asked if they have I_h to participate in shaping the bursts.

Even after brief current injections (≤ 100ms), coordinating neurons showed post-inhibitory rebound (5 of 8 ASC_E, 2 of 7 DSC, Figure 17 A). When I injected long (> 1s) hyperpolarizing currents in the coordinating neurons in the intact network, they continued to oscillate with a stable but hyperpolarized trough potential. Only when ASC_E and DSC were isolated, hyperpolarizing the neurons revealed a low-amplitude sag-potential (1mV-2mV, 5 of 8 ASC_E, 1 of 7 DSC). Upon release from hyperpolarization, coordinating neurons increased their spike frequency or generated rebound spikes (Figure 17 B, 6 of 6 ASC_E, 5 of 5 DSC).

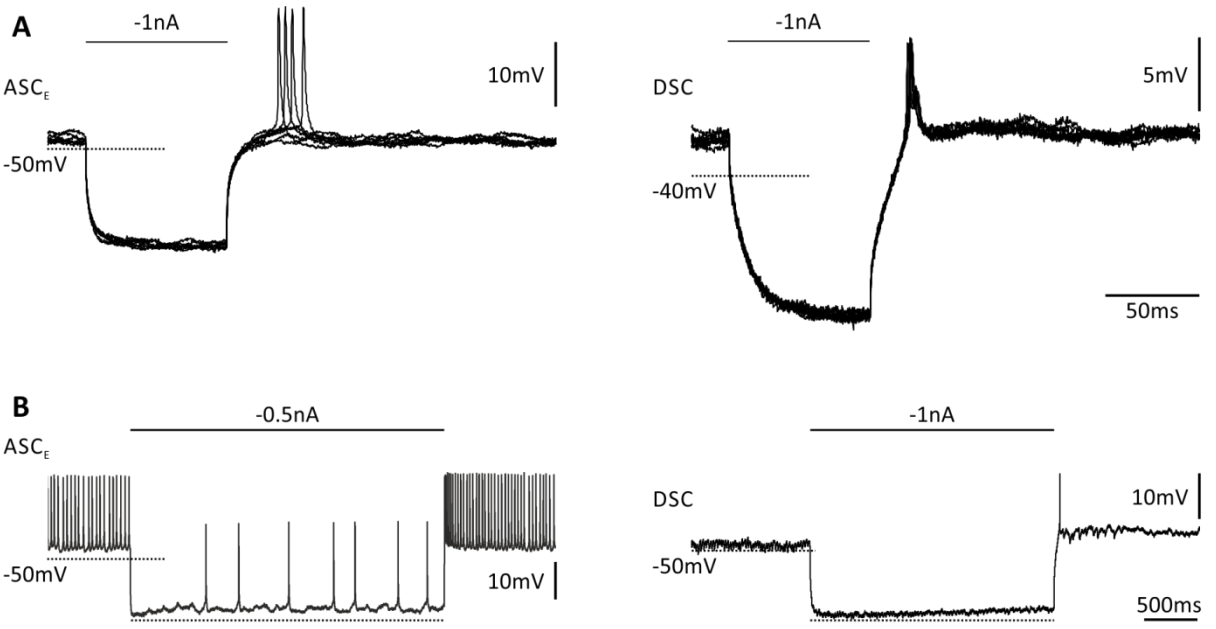

Figure 17: Application of $LowCa^{2+}$ reveals rebound properties of ASC_E and DSC. A: Post-inhibitory rebound in ASC_E and DSC (overdraw from 7 sweeps) aligned to the onset of a hyperpolarizing current injection. B: Sag potential in ASC_E and DSC. When released from hyperpolarization, ASC_E's tonic spike frequency increased and DSC fired a rebound spike.

3.3 Setting the Excitation Level with Carbachol and EdCl

To set the system's excitation level, I used different concentrations of carbachol and EdCl. In contrast to reports on experiments from extracellular recordings by Mulloney and Hall (2007b), PS burst strength did not correlate to the chemical's concentration when recording intracellularly from coordinating neurons (Figure 18). Depending on the preparation, burst strength could increase, or decrease, or first increase then decrease, or vice versa with increasing carbachol or EdCl concentrations. However, burst strength differed significantly between concentrations in 19 of 20 experiments (Supplementary Figure 3, Supplementary Figure 4). Burst strength could not be calculated in 1 of 21

experiments because of noisy PS recordings. If comparing burst strength between lowest and highest carbachol or EdCl concentrations only, burst strength was increased at the high concentration in five experiments, decreased in two and not significantly different in one carbachol experiment. In EdCl, bust strength was increased in four, decreased in three and not significantly different in one experiment. Thus, higher concentrations resulted in higher burst strength in about half of the experiments.

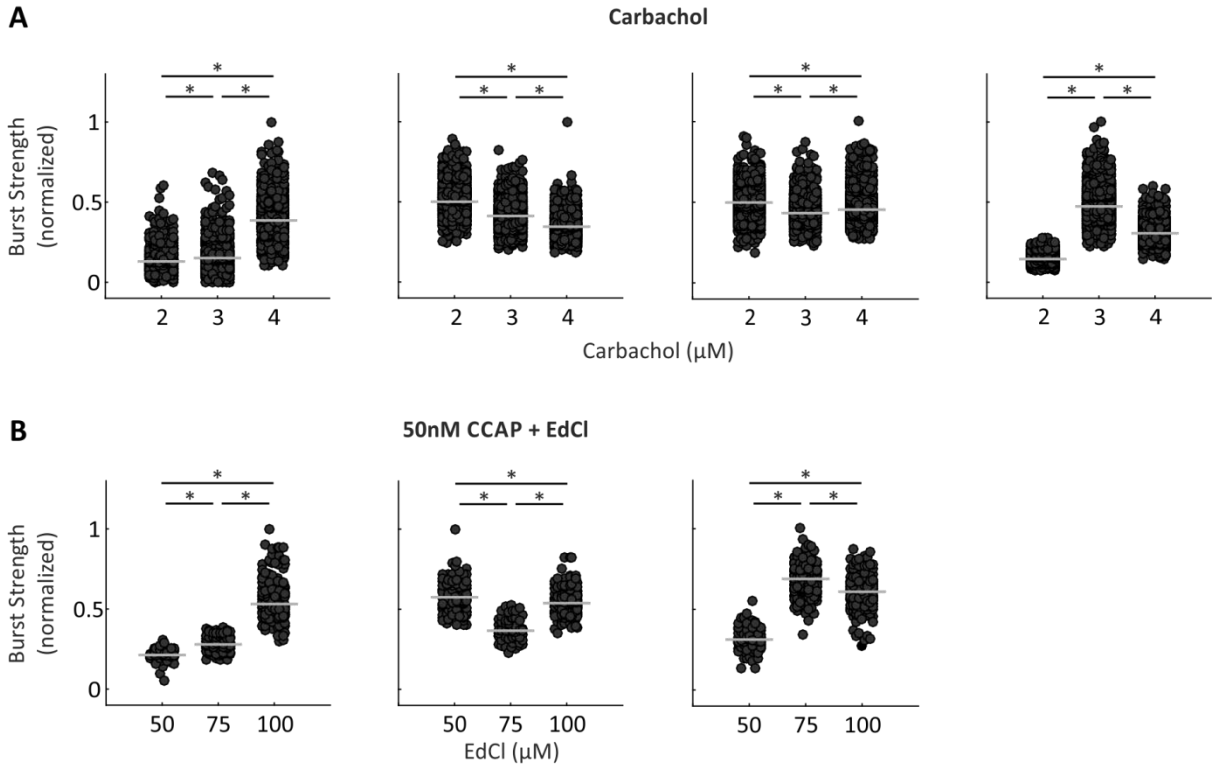

Figure 18: Exemplary changes in PS burst strengths at different carbachol (A) or EdCl (B) concentrations. Each plot illustrates a representative experiment, showing the different effects of applied substances. Each dot represents a single burst strength value. Grey bars indicate median. * p < 0.05.

When carbachol was applied, periods ranged on average from 660ms to 360ms. In 4 of 5 experiments period decreased with increasing carbachol concentration (94ms ± 41ms average difference between 2µM and 4µM; Figure 19 A). In one experiment, period did not change. As I never had rhythmic activity in normal saline without carbachol, I have no data for periods in 0µM carbachol. In 50nM CCAP with different EdCl concentrations periods ranged on average from 1.3s to 440ms. In all 6 experiments period decreased with increasing EdCl concentrations (440ms ± 140ms average difference between 0µM and 100µM EdCl in 50nM CCAP, Figure 19 B). This shows that both carbachol and EdCl influence the system's excitation level by shortening cycle period.

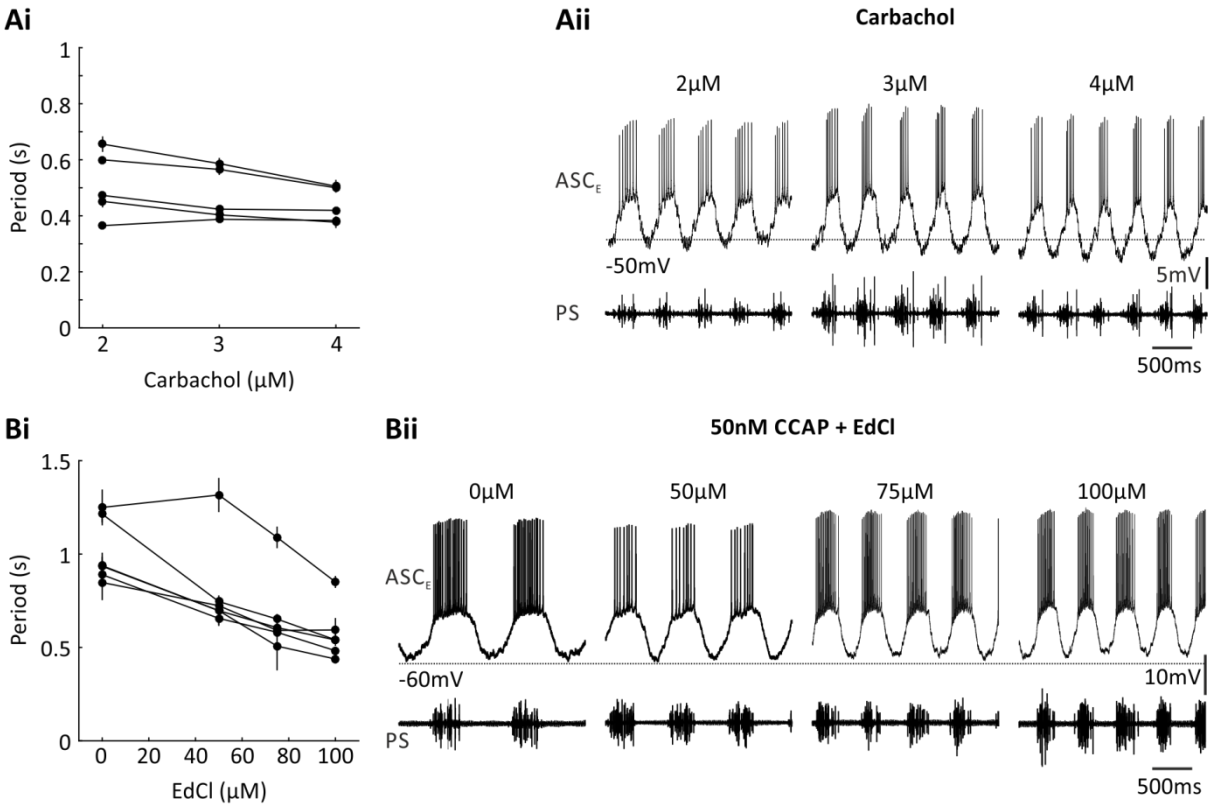

Figure 19: Effect of carbachol and EdCl concentration on period. Ai: Period decreased with increasing carbachol concentration in 4 of 5 experiments (n > 15). Aii: Exemplary intracellular ASC_E and PS recording in different carbachol concentrations. Bi: Period decreased with increasing EdCl concentration in 6 of 6 experiments (n = 19). Bii: Exemplary intracellular ASC_E and PS recording in different EdCl + 50nM CCAP concentrations. Ai, Bi: Mean with standard deviation. Lines connect individual experiments.

Both in carbachol and EdCl ASC_E fired significantly more spikes per burst than DSC (Figure 20, multiple comparison $p < 0.001$ in both cases). ASC_E spikes per burst did not differ between carbachol (N = 7) and EdCl (N = 6; $p = 0.10$), DSC fired fewer spikes in EdCl (N = 4) compared to carbachol (N = 3; $p < 0.01$). It has to be mentioned that one DSC in carbachol generated an unusually amount of spikes per burst, which could be a result of damage upon electrode penetration (see also Figure 25 Aii).

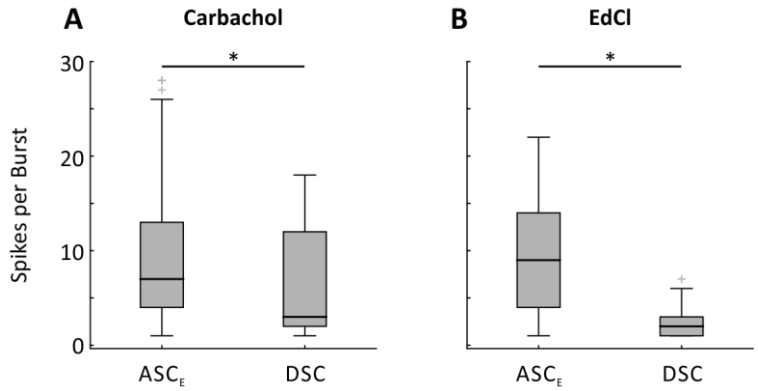

Figure 20: ASC_E and DSC spikes per burst in carbachol (A; 7 ASC_E experiments, 3 DSC experiments, all concentrations pooled) and EdCl (B; 6 ASC_E experiments, 4 DSC experiments, all concentrations pooled). n > 800; * p < 0.05.

Effect on Membrane Potential

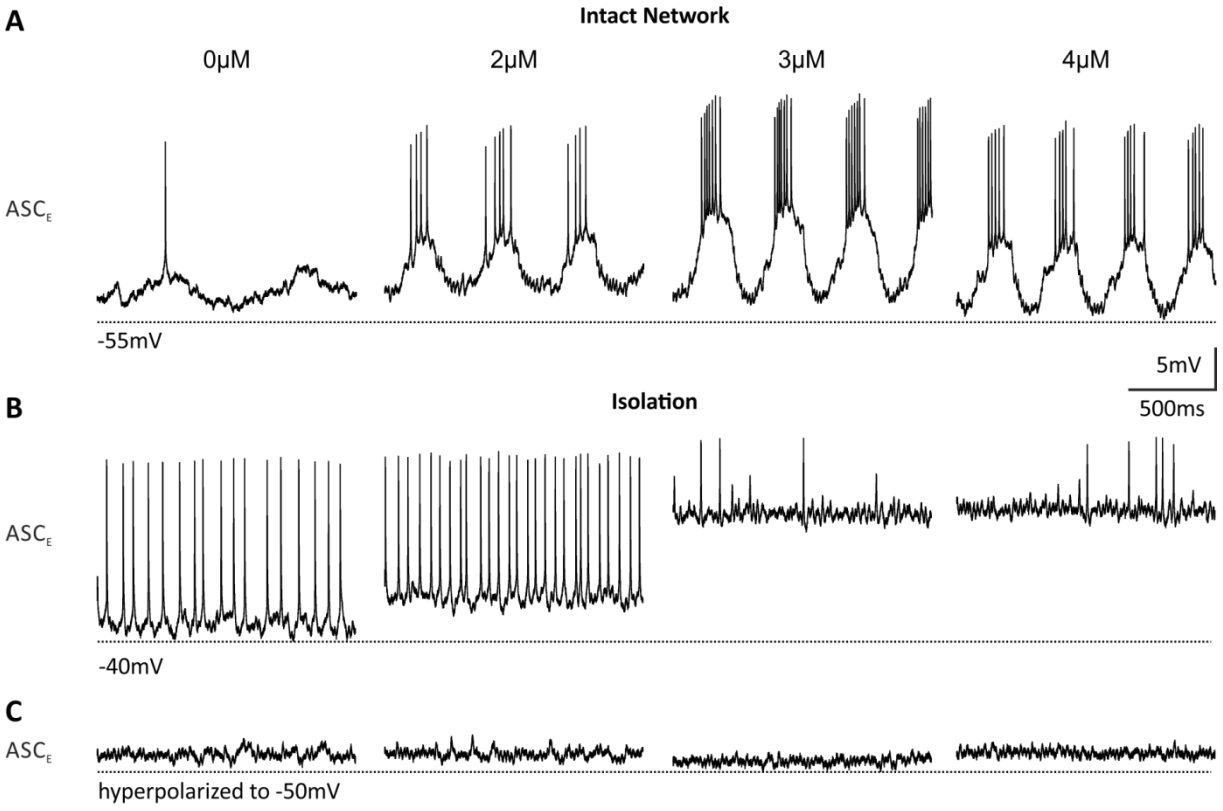

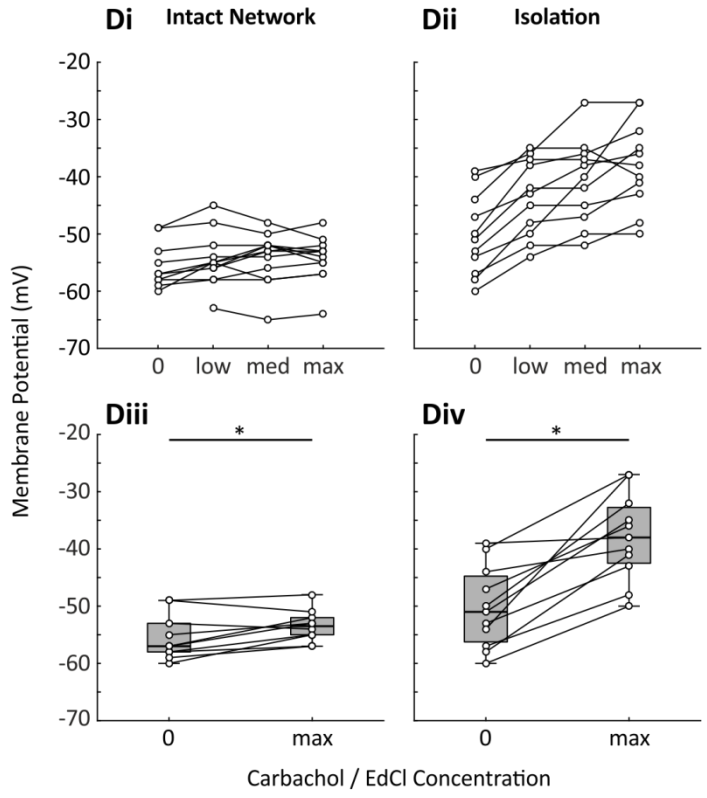

Figure 21: Carbachol effect on ASC$_E$'s membrane potential. A: Exemplary intracellular recording with different carbachol concentrations in the intact network. The trough potential was stable. B: Exemplary intracellular recording with different carbachol concentrations in the isolated neuron. V_m depolarized with increasing concentrations. In 3µM and 4µM carbachol spike amplitude became irregular. C: Hyperpolarizing the same neuron as in B subthreshold did not elicit any spikes (c.f. Figure 23 C). D: Changes in V_m with different carbachol and EdCl concentrations. Data from carbachol and EdCl experiments were pooled in the intact network condition. Accordingly, data from experiments with and without TTX were pooled in the isolated condiction. See text for justification. Lines connect individual experiments. Diii, Div: V_m from Di and Dii was compared between lowest and highest (max) concentration. * $p < 0.05$.

The trough potential of individual ASC_Es ranged from -50mV to -60mV in normal saline (Figure 21). When applying different carbachol or EdCl concentrations, V_m changed only slightly (Figure 21 A, Di). Between normal saline and maximum carbachol/EdCl concentration (intact network) it depolarized by 2mV ± 2.4mV (Wilcoxon $p = 0.041$, Figure 21 Diii). This was not correlated to changes in PS burst strength (data not shown). When isolated with $LowCa^{2+}$ saline with or without TTX, ASC_E depolarized by 12.3mV ± 7.1mV between minimum and maximum carbachol concentrations (Wilcoxon $p < 0.001$, Figure 21 B, Dii, Div). Accordingly, spike frequency of the tonically firing neuron increased, with 4 of 8 ASC_Es going into sodium block at the depolarized V_m. If the isolated ASC_E was hyperpolarized to the V_m that was subthreshold without carbachol it never spiked (eight experiments; Figure 21 C).

The depolarization of the isolated ASC_E indicated an increased excitability because V_m was closer to threshold. Therefore, I asked whether higher carbachol concentrations also resulted in more spikes in response to stimulation. Interestingly, when stimulating the isolated ASC_E with the paired current ramps at 2µM and 4µM carbachol, fewer spikes were elicited in the high carbachol concentration across ramp duration and amplitude (4 of 4 experiments; Figure 22, Supplementary Figure 5). This indicated that carbachol had a differential effect on ASC_E's excitability. On the one hand, excitability was increased by depolarizing V_m. On the other hand, excitability was decreased because sodium channel inactivation was reached earlier.

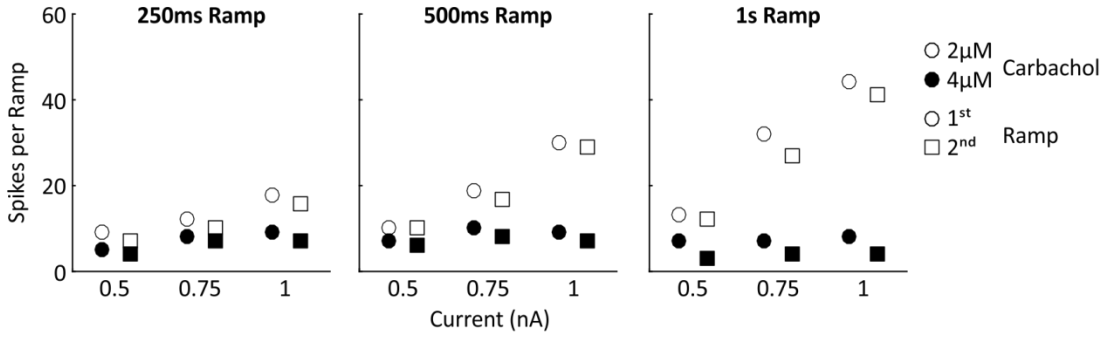

Figure 22: Number of spikes elicited by the different paired ramp stimulations. Exemplary data for 1 of 4 experiments.

Behavior of DSC was similar to ASC_E. Its trough potential was more variable than ASC_E's, ranging from -45mV to -65mV (Figure 23). When applying the different chemical concentrations with the network intact, its V_m remained stable (Figure 23 A, Di), changing by 0mV ± 4.5mV (Wilcoxon not significant, Figure 23 Diii). This was not correlated to changes in PS burst strength (data not shown). When isolated, its V_m depolarized by 12mV ± 4.8mV between minimum and maximum carbachol concentrations (Wilcoxon $p < 0.001$,

Figure 23 B, Dii, Div). Like in ASC_E, tonic firing frequency increased with the increased V_m. 2 of 5 DSCs went into sodium block at the depolarized V_m. If the isolated DSC's were hyperpolarized to the V_m that was subthreshold without carbachol, it spiked at higher carbachol concentrations, indicating a lowered threshold (2 of 5 experiments; Figure 23 C).

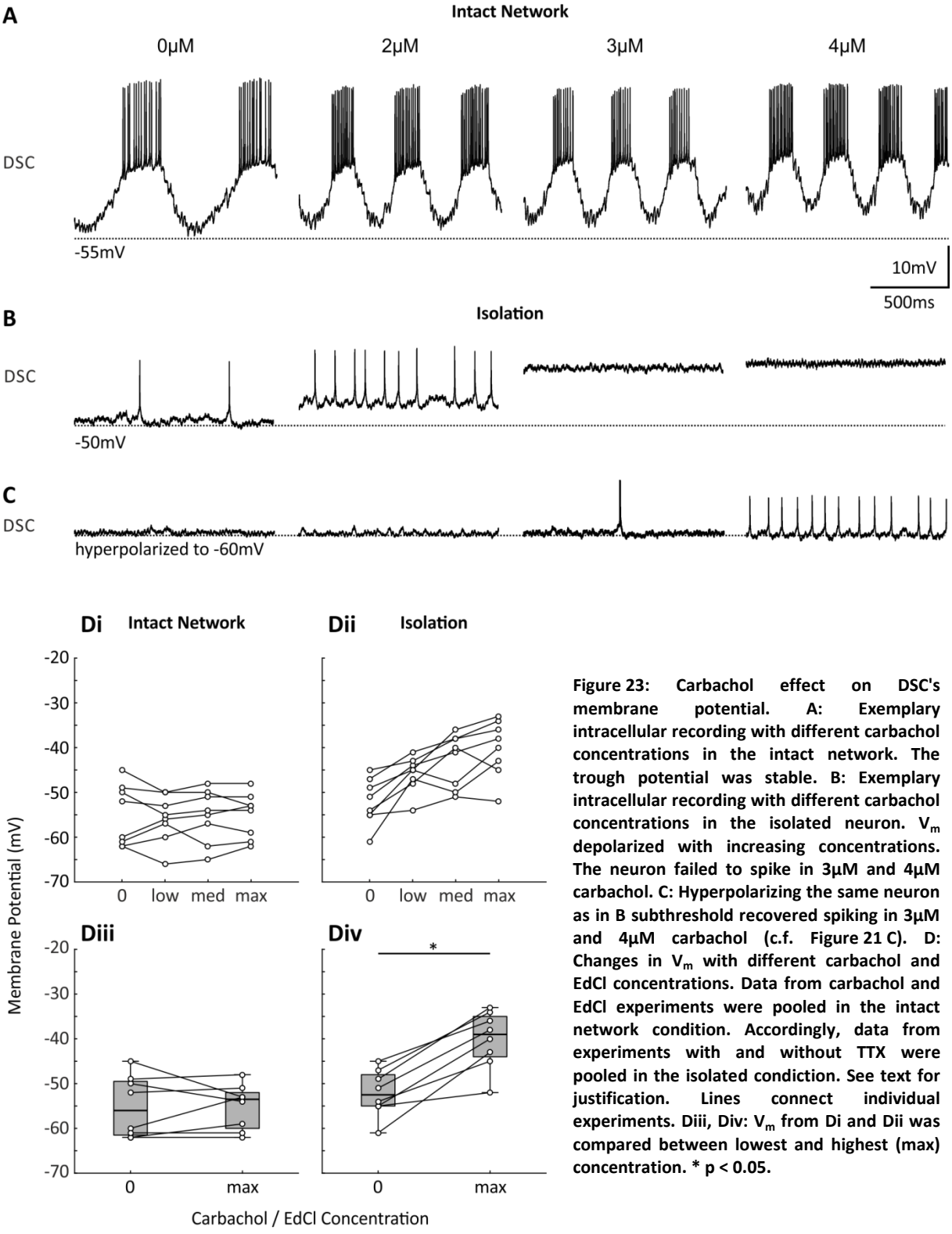

Figure 23: Carbachol effect on DSC's membrane potential. A: Exemplary intracellular recording with different carbachol concentrations in the intact network. The trough potential was stable. B: Exemplary intracellular recording with different carbachol concentrations in the isolated neuron. V_m depolarized with increasing concentrations. The neuron failed to spike in 3µM and 4µM carbachol. C: Hyperpolarizing the same neuron as in B subthreshold recovered spiking in 3µM and 4µM carbachol (c.f. Figure 21 C). D: Changes in V_m with different carbachol and EdCl concentrations. Data from carbachol and EdCl experiments were pooled in the intact network condition. Accordingly, data from experiments with and without TTX were pooled in the isolated condiction. See text for justification. Lines connect individual experiments. Diii, Div: V_m from Di and Dii was compared between lowest and highest (max) concentration. * $p < 0.05$.

Effect on Tuning Curves

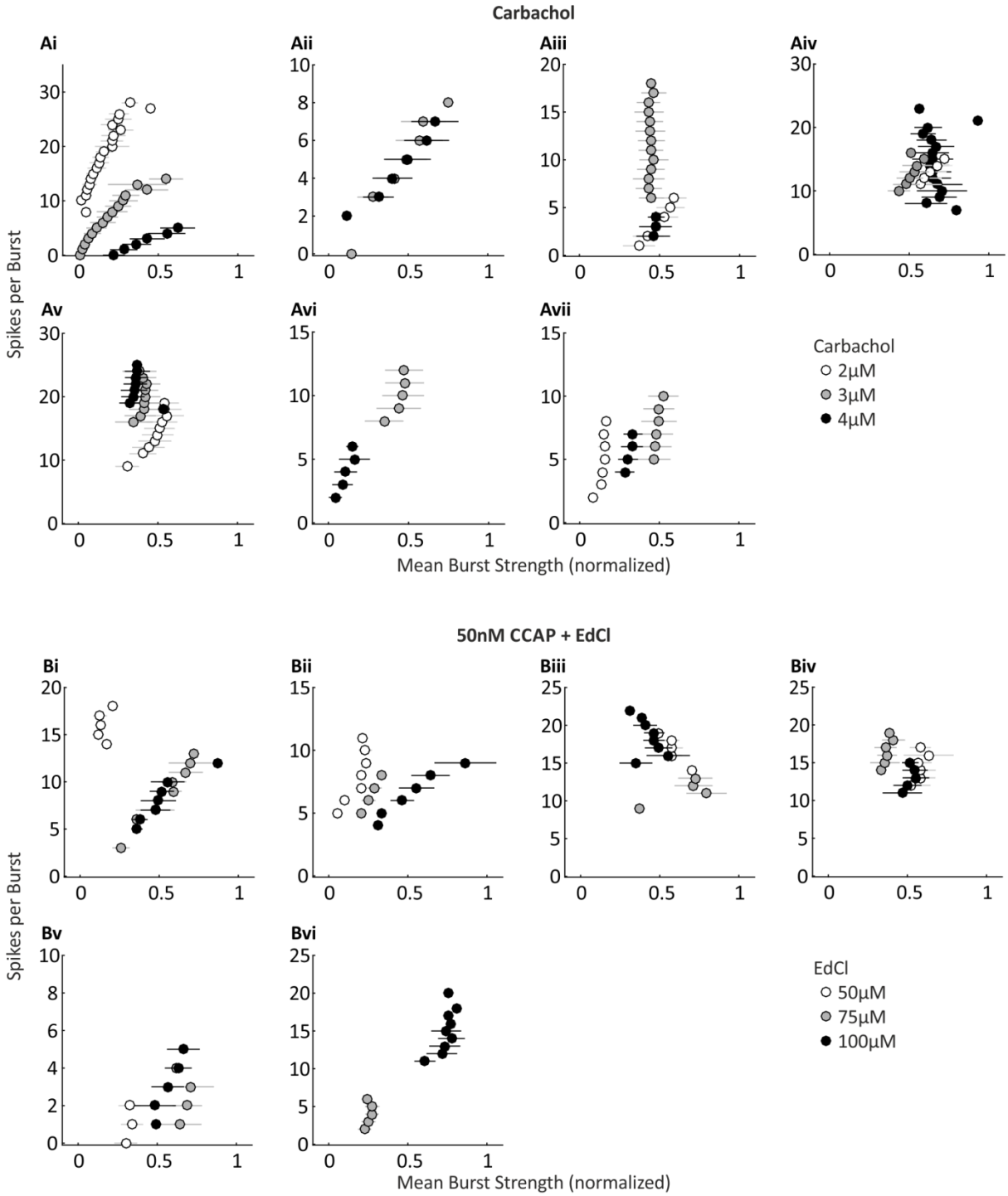

Figure 24: Number of ASC_E spikes per burst vs. mean normalized PS burst strength at different excitation levels in 13 different experiments. Excitation levels were set with different concentrations of carbachol (A; N=7) or 50nM CCAP + EdCl (B; N=6). Error bars are standard deviation.

Mulloney and Hall (2007b) used split-bath experiments to set the system's excitation to different levels across the preparation. They noticed that ASC_E spikes no longer precisely tracked PS burst strength across different concentrations. In contrast to their experiments, I did not average both burst strength and number of spikes. For each experiment, I calculated the mean PS burst strength for each occurring number of coordinating spikes per burst. With this, I was able to observe how the encoding of burst strength changed at different excitation levels.

ASC_E tracked even small changes in average PS burst strength at each carbachol concentration but not across concentrations (Figure 24 A). On average, at each concentration, stronger bursts were correlated with more ASC_E spikes. Exceptions were 3µM in Figure 24 Aiii, and 4µM in Figure 24 Aiv. In 6 of 7 experiments, the same number of spikes could code for different burst strengths at different carbachol concentrations. Hence, the tuning curve shifted with excitation level. The same pattern was present when the system's excitation was set with EdCl (Figure 24 B). In 5 of 6 experiments, the same number of ASC_E spikes encoded different bursts strengths across concentrations. In 5 of 6 experiments, stronger bursts correlated with more ASC_E spikes at each concentration.

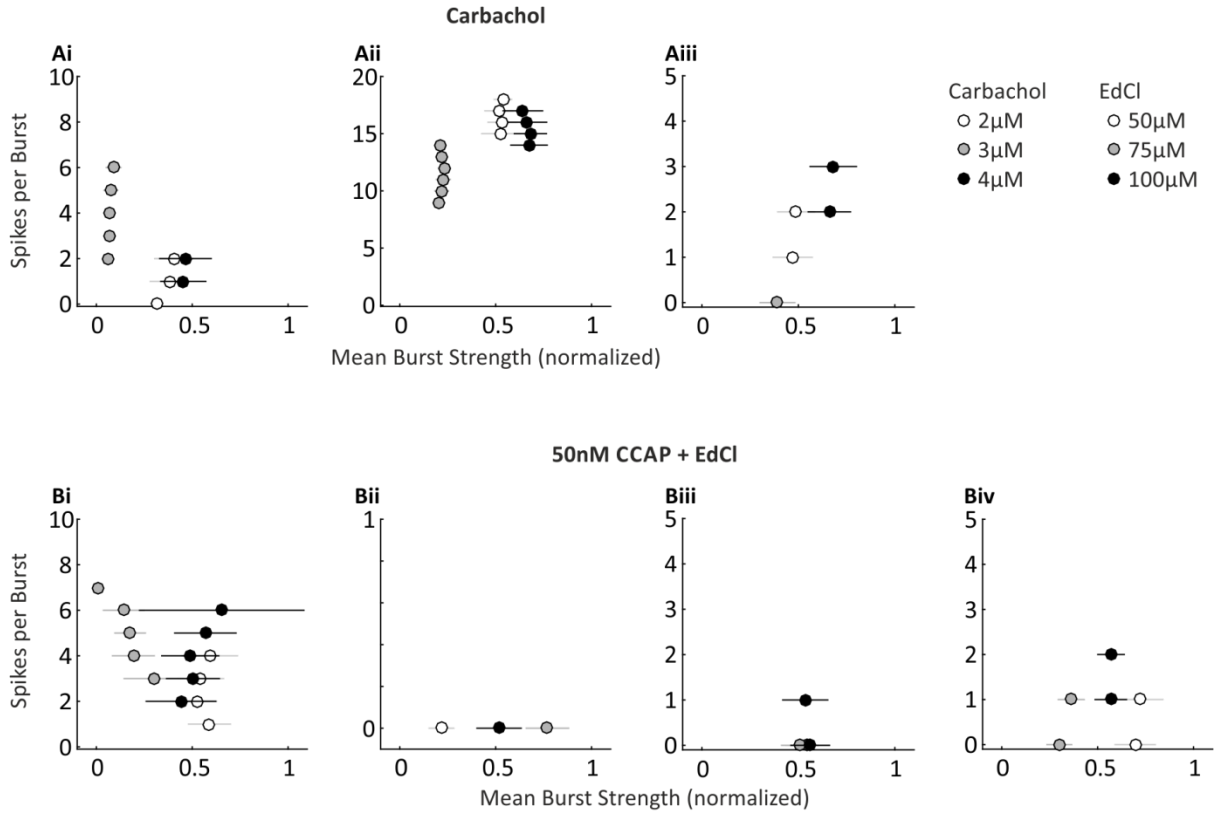

Figure 25: Number of DSC spikes per burst vs. mean normalized PS burst strength at different excitation levels in 7 different experiments. Excitation levels were set with different concentrations of carbachol (A; N=3) or 50nM CCAP + EdCl (B; N=4). Error bars are standard deviation.

On average, DSC fired fewer spikes per burst than ASC_E (median 7 vs. 3, Figure 20). Under these circumstances, interpretation of DSC spikes per burst vs. mean burst strength was nondescript. However, different PS burst strengths matched the same number of spikes across concentrations in 3 of 3 carbachol experiments (Figure 25 A) and 2 of 4 EdCl experiments (Figure 25 B). In 1 of 4 EdCl experiments, DSC was not spiking, possibly as result to damage by electrode penetration.

In contrast to the number of spikes per burst, mean spike frequency per burst did not correlate to PS burst strength in individual carbachol (7 of 7 ASC_E, 3 of 3 DSC) or EdCl concentrations (6 of 6 ASC_E, 4 of 4 DSC; Figure 26, Supplementary Figure 6, Supplementary Figure 7). Therefore, the number of spikes but not the frequency encoded information about the network's motor output.

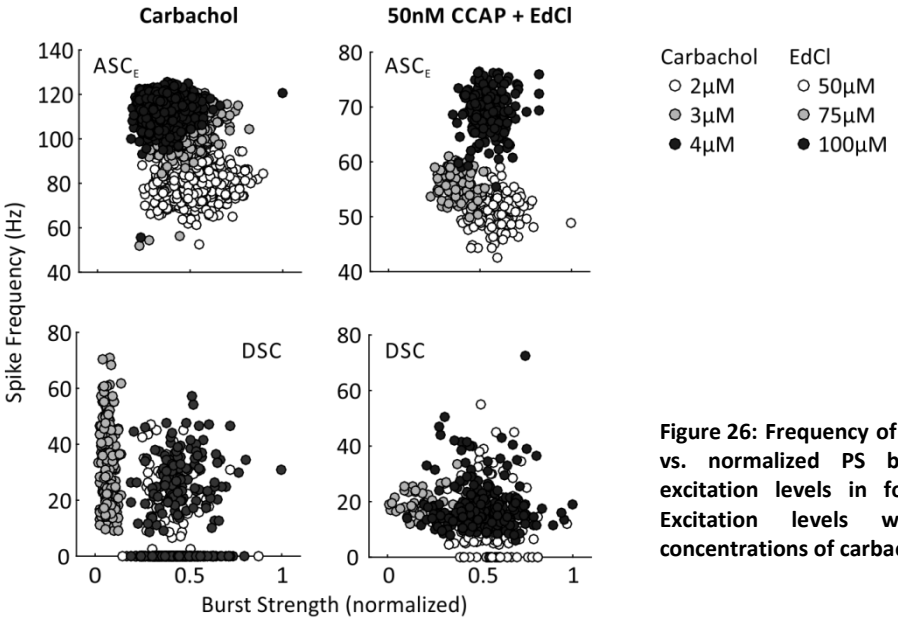

Figure 26: Frequency of ASC_E or DSC spikes per burst vs. normalized PS burst strength at different excitation levels in four exemplary experiments. Excitation levels were set with different concentrations of carbachol or 50nM CCAP + EdCl.

Effect on Input Resistance

A neuron's R_{in} depends on the number of open or closed ion channels. More channels that are open decrease R_{in}, increasing conductance for specific ions; more closed channels increase R_{in}, decreasing conductance. As the coordinating neurons' V_m behaved differently in isolation compared to the intact network, I hypothesized that the chemicals I used acted both directly and indirectly, i.e. via the network, on those neurons. This would cause excitation-dependent changes the neurons' R_{in}. As the system and coordinating neurons' properties behaved similarly in carbachol and EdCl, or LowCa^{2+} saline with and without TTX, respectively, I distinguish only between intact network and isolated neuron condition in the following.

The coordinating neurons' R_{in} ranged between 10MΩ and 30MΩ. ASC_E's and DSC's R_{in} changed with phase. Both were highest during their peak oscillation and lowest during their interburst interval (Figure 27 A for ASC_E, Supplementary Figure 8, Supplementary Figure 9). To compare R_{in} at different excitation levels I pooled the values across phase. Correlating them to carbachol or EdCl concentration did not result in clear tendencies (Figure 27 B). Therefore, I correlated them to the mean burst strength at any concentration (Figure 27 C), and statistically compared R_{in} at those concentrations yielding minimum and maximum mean burst strength (Figure 27 D). See 4.4 in the discussion for an explanation why burst strength is a better representation of excitation level than the concentration of applied chemicals. Because burst strength could not be calculated for the isolated experiments, I compared R_{in} at lowest and highest carbachol concentrations in those cases. This could be used as approximation because in half of the experiments with the network intact PS burst strength correlated with the chemicals' concentration.

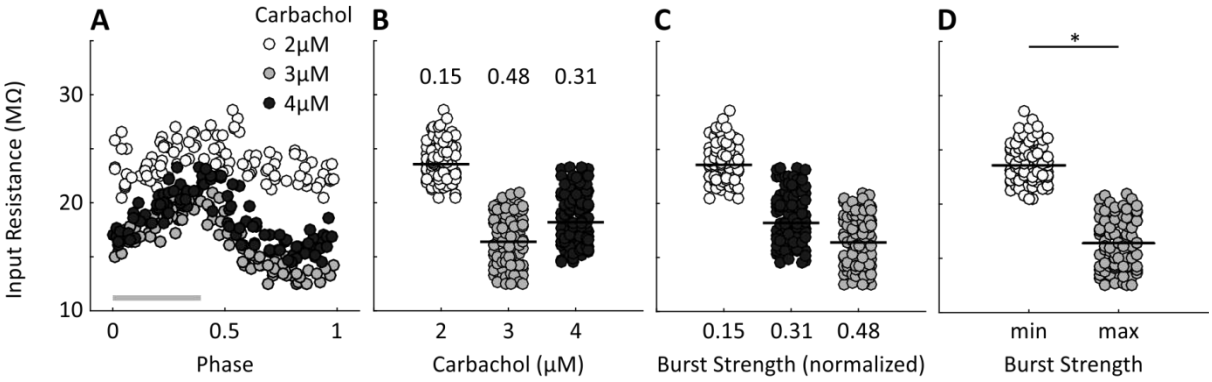

Figure 27: Workflow for analyzing R_{in} of an exemplary ASC_E. Each dot represents a single R_{in} measurement. A: R_{in} was dependent on the stimulus' phase (reference is the beginning of the home ganglion's PS). It was highest during the depolarized phase of the neuron's membrane potential oscillations. Grey bar indicates phase of PS activity. B: R_{in} from A was pooled for each concentration. Numbers above each column indicate average PS burst strength at that concentration. C: R_{in} sorted by average PS burst strength from B. D: Only R_{in} at the condition with the minimal (min) and maximal (max) PS burst strength from C were compared with a rank-sum test. * $p < 0.05$.

For better visualization, exemplary results of individual experiments are depicted in Figure 28 A, illustrating the most common changes in R_{in} for ASC_E and DSC with the network intact and in isolation. Comparison of medians for all experiments is depicted in Figure 28 B. Significant differences between medians are color-coded (rank sum, $p < 0.05$). Raw data of R_{in} vs. phase and R_{in} vs. excitation level are in Supplementary Figure 8 - Supplementary Figure 13.

In the intact network, ASC_E's R_{in} decreased in 10 of 13 experiments and increased in 3 experiments (Figure 28 B). DSC was similar with a decreased R_{in} in 4 of 7 experiments, an increase in 2 experiments, and no significant change in 1 experiment.

When the coordinating neurons were isolated from the network, carbachol had the opposite effect on ASC_E. R_{in} increased in 7 of 13 experiments, decreased in 4 experiments, and did not significantly change in 2 experiments. The effect on DSC was more variable, with an increased R_{in} in 3 of 8 experiments, decrease in 3 experiments and no change in 2 experiments (Figure 28 B).

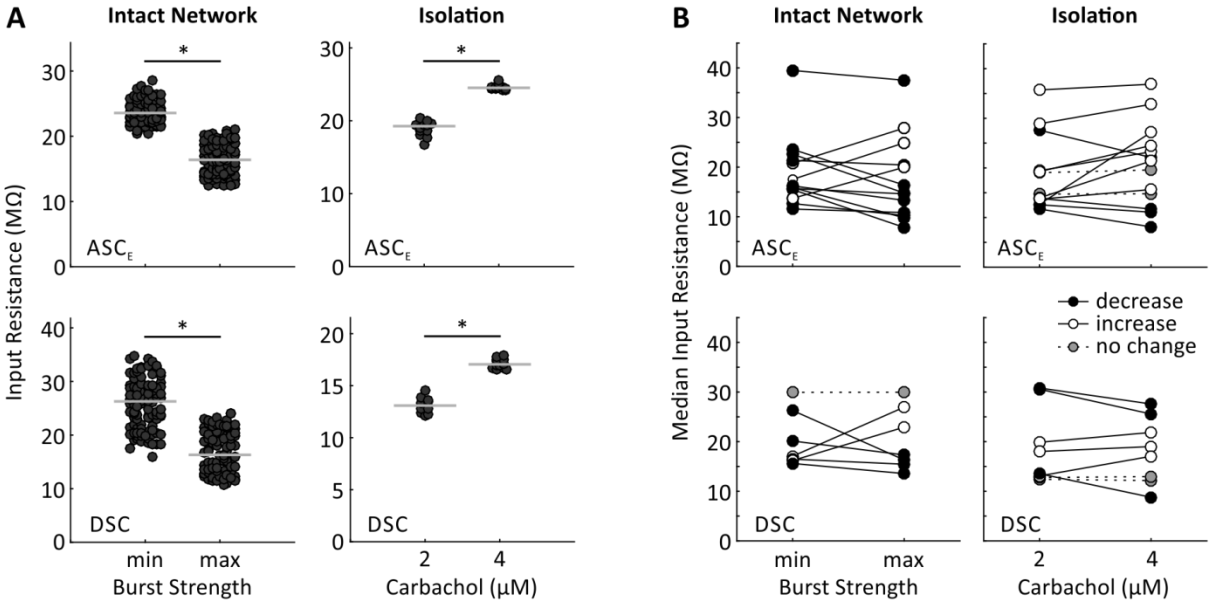

Figure 28: Differences in the coordinating neurons' input resistance at different excitation levels with the network intact and in isolation. A: Exemplary results for ASC_E and DSC in both conditions. Each dot represents a single R_{in} measurement. Medians are indicated by bars. B: Medians for all experiments in both conditions. Individual experiments are connected by lines. Colors indicate statistical differences in R_{in} between excitation levels. * $p < 0.05$.

In the ongoing rhythm, the coordinating neurons' R_{in} is higher during their depolarized phase and lower in their hyperpolarized phase (Smarandache-Wellmann and Grätsch, 2014). To investigate whether synaptic input or intrinsic features of the neurons cause this, I injected de- and hyperpolarizing current with different amplitudes. Both in isolation and the intact network injection of positive or negative current de- or hyperpolarized the coordinating neurons to a different degree (Figure 29, Supplementary Figure 14, Supplementary Figure 15). To determine the neuron's R_{in} with the de- and hyperpolarizing currents I fitted linear regression lines to describe the V-I relationship, respectively. Their slope is the input resistance. Because of the low number of data points, I omitted statistics for the linear regression models.

When depolarized in the intact network, ASC_E's R_{in} was higher in three experiments and similar (less than 1MΩ difference) in two experiments compared to hyperpolarization. DSC's R_{in} was higher in two experiments and lower in one experiment. With depolarization in the isolated neurons, ASC_E's R_{in} was higher in two experiments and lower in one

experiment. DSC's R_{in} was lower in one experiment. This matches the changes in R_{in} in the oscillating neurons, in which R_{in} is higher during the depolarization compared to the hyperpolarization.

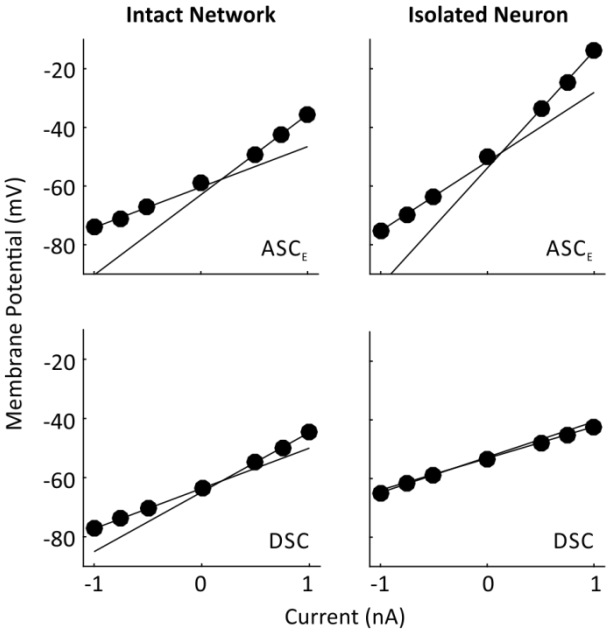

Figure 29: V-I curves for exemplary ASC_Es and DSCs in the intact network (50nM CCAP without EdCl) and isolated neuron (without carbachol). Neurons were de- and hyperpolarized with three different current amplitudes, respectively. The V-I relationships were fitted with linear regression lines. Regression lines were calculated separately for positive and negative current injections, and extrapolated across the whole range of injected currents. Coordinating neurons showed this rectification in most experiments.

In summary, across experimental conditions R_{in} mainly increased when the coordinating neurons were depolarized, and decreased when they were hyperpolarized. This suggests the involvement of voltage-gated ion channels. Likely candidate channels to explain these results would be HCN channels that underlie I_h, and voltage-dependent sodium channels. These ion channels close at depolarized V_m.

The increased R_{in} taken together with the results that the isolated coordinating neurons failed to generate more spikes in response to a stimulus at higher carbachol concentrations, although V_m was more depolarized, further supports the idea that sodium channel inactivation can help to regulate the amount of spikes per burst at different excitation levels.

PART II: Neurotransmitters

The important neurons for generating and coordinating the motor activity in the swimmeret system are identified and their connections characterized. It has been shown, for example in the STNS, that neuromodulators can alter the motor output by influencing synaptic strengths and changing ionic conductances (Flamm and Harris-Warrick, 1986a, 1986b; Johnson and Harris-Warrick, 1990). Hence, it is of equal importance to know the transmitters of a system as well as the network's connectivity. I used an immunohistochemical approach and mass spectrometry to identify the transmitters of the coordinating neurons. Previous experiments have already shown that the excitatory synapse between the coordinating neurons and ComInt 1 is mainly chemical, and that the transmitter is most likely of small molecular weight (pers. comm. Carmen Wellmann, see also 1.2).

3.4 Antibody Labeling Against Serotonin

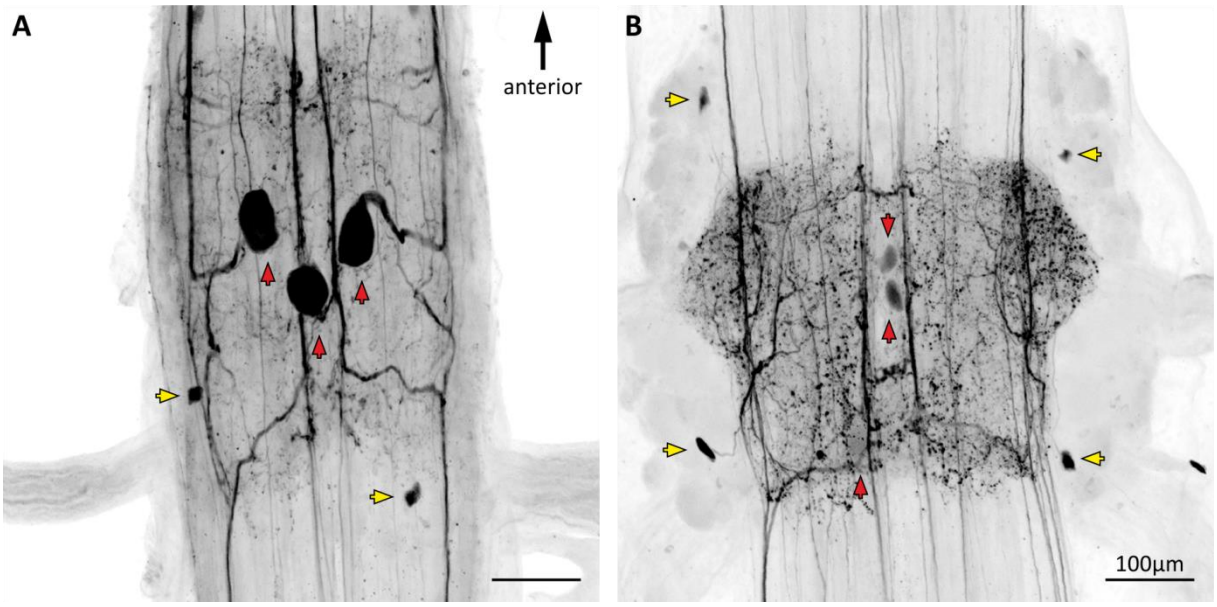

Figure 30: Anti-5-HT labelling in abdominal ganglion 1 (A) and abdominal ganglion 3 (B). A: A1 contained three large medial (red arrows) and two small (yellow arrows) lateral somata. B: Other abdominal ganglia contained four small (yellow arrows) and up to three large medial (red arrows) 5-HT-ir somata.

Beltz and Kravitz (1983) reported serotonin-like immunoreactivity (ir) in a medial (MFB) and lateral fiber bundle (LFB) in the lobster's abdominal nerve cord. The MFBs run close to the midline, in the area where ASC_E's and DSC's axons are located. To investigate whether the coordinating neurons are part of the 5-HT-ir neurons, I stained the former

intracellularly and the latter with anti-5-HT antibody labeling. Antibody labeling did not work if the fixative contained glutaraldehyde, even with sodium borohydride epitope rescue.

Abdominal ganglion 1 (A1) had a different distribution of 5-HT-ir neurons than A2 to A5. A1 contained ventrally two paired and one unpaired medial large serotonergic soma (Figure 30 A). Additionally, two smaller cell bodies were located laterally posterior to the ganglion's core region. This distribution of 5-HT-ir cell bodies was present in 4 of 4 A1s. A2 to A5 had two paired small lateral somata, anterior and posterior to the ganglion's core region (4 somata in 12 ganglia, 3 somata in 4, and 0 in 1). Ventrally, up to three large somata were located at the midline (3 somata in 4 ganglia, 2 somata in 1, 1 soma in 3, and 0 somata in 9).

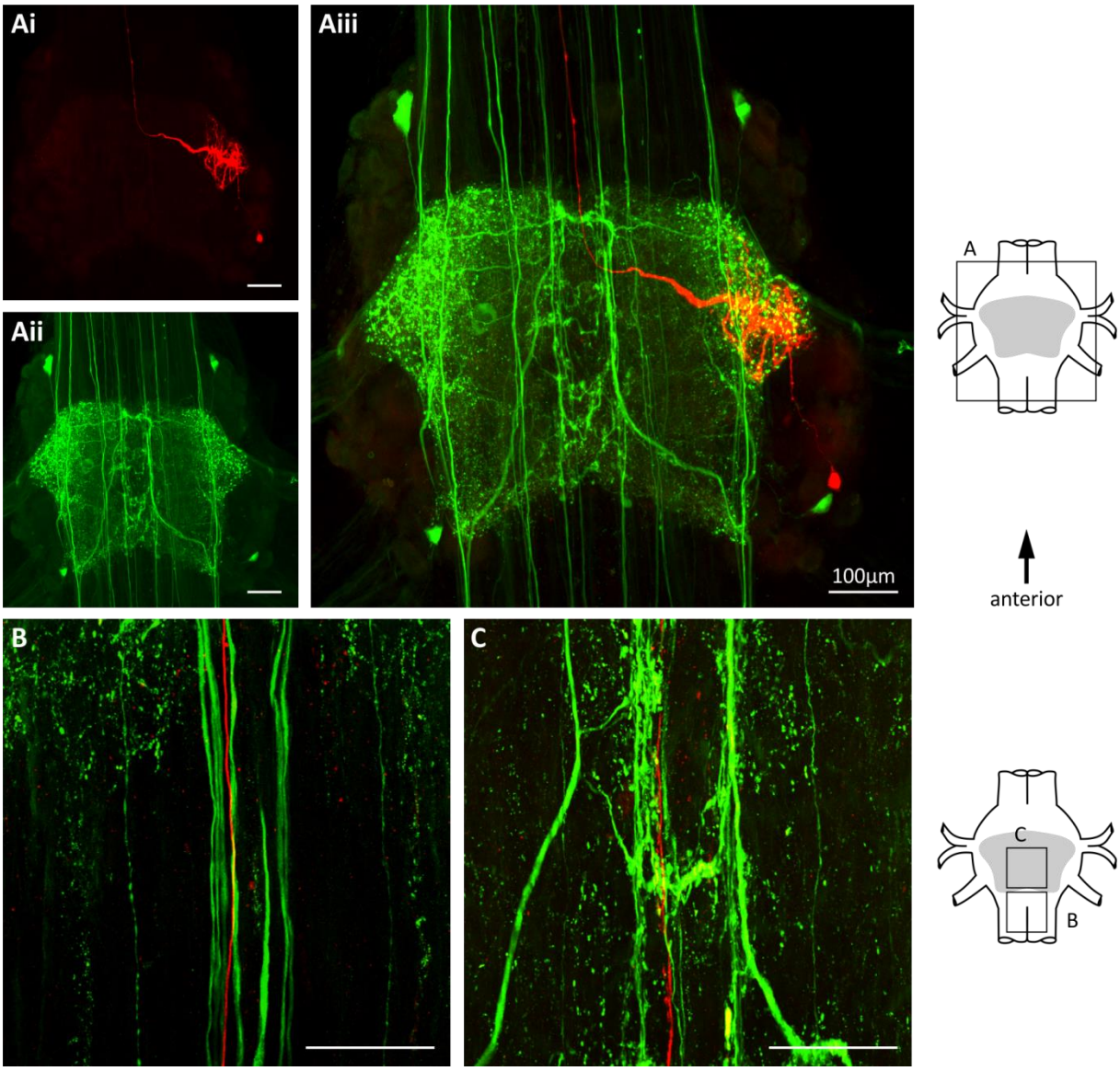

Figure 31: Intracellular staining (red) of ASC_E and 5-HT expression pattern (green). ASC_E is not co-localized with 5-HT-ir neurons in its home ganglion (A), in the posterior (B), or medial (C) part of the anterior target ganglion.

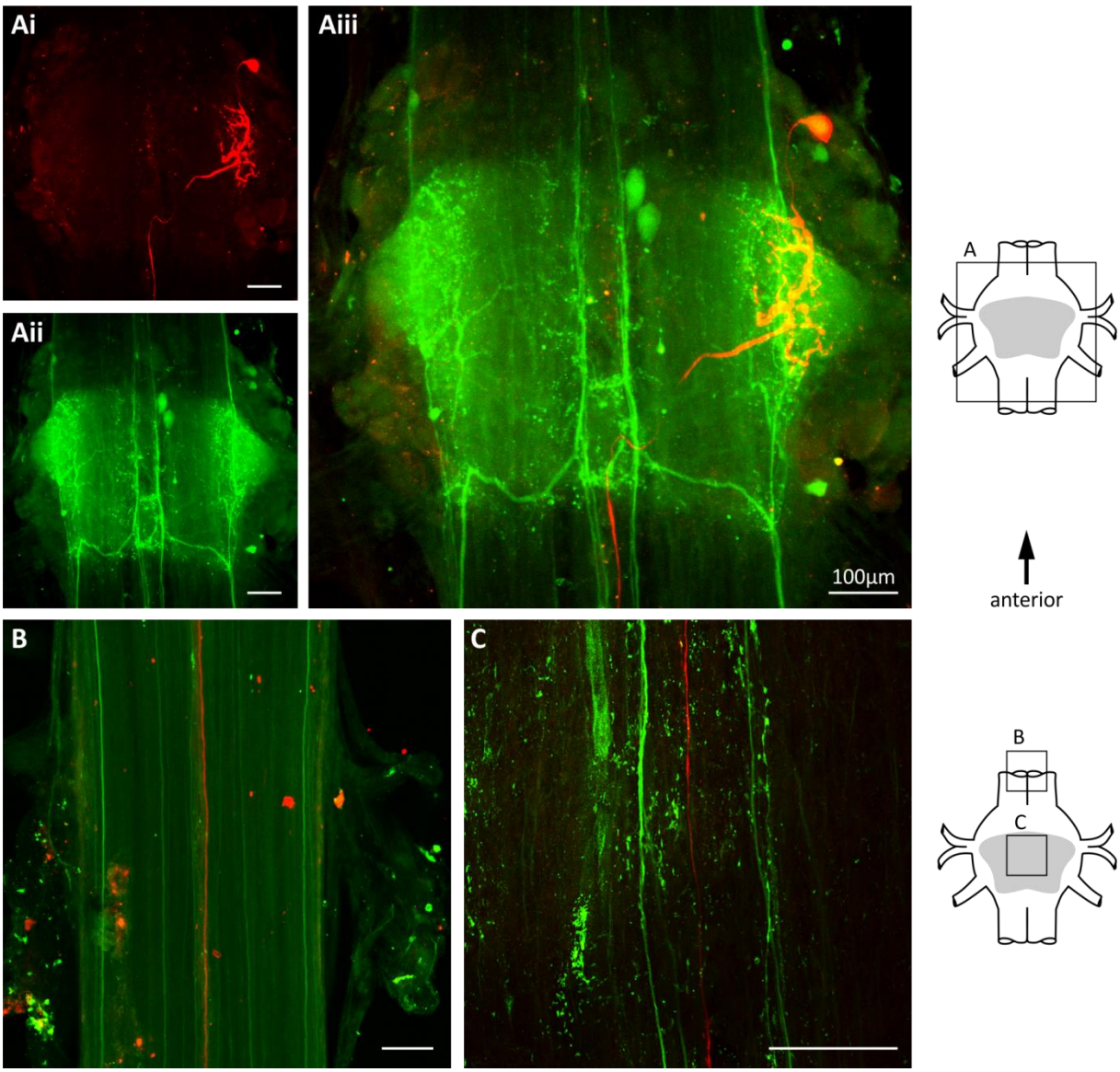

Figure 32: Intracellular staining (red) of DSC and anti-5-HT expression pattern (green). DSC is not co-localized with 5-HT-ir neurons in its home ganglion (A), in the connective (B), or medial (C) part of the posterior target ganglion.

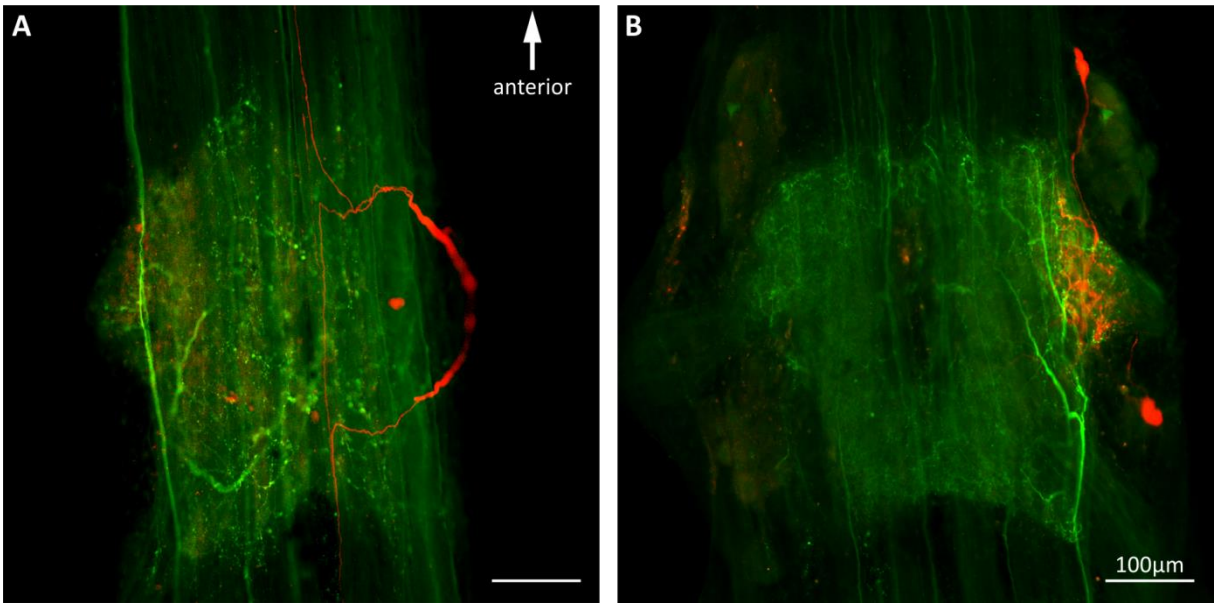

Figure 33: Intracellular staining (red) of ASC_E, DSC and an unidentified descending axon, and anti-5-HT expression pattern (green). A: Dorsal plane with coordinating axons. B: Medial plane with coordinating somata and dendrites.

In A1 to A5 two lateral and two medial fiber bundles were visible, in addition to smaller axons crossing the ganglia in rostrocaudal direction. At the posterior border of the ganglia's core region, fibers passed between the LFBs and the MFBs. In A2 to A5 one anterior and two posterior commissures connected the MFBs. The LN showed dense 5-HT-ir branches.

Double labeling of coordinating neurons and serotonin never showed co-localization of the two dyes (Figure 31, Figure 32, Figure 33; 7 of 7 ASC_E ganglia, 9 of 9 DSC ganglia). Any appearances of overlap are caused by the 2D projection of the z-stacks. ASC_E's and DSC's axons were located closer to the midline and more dorsally than the MFBs (Figure 33 A). Their somata were close to but not identical with the small lateral serotonergic cells (Figure 31 Aiii, Figure 32 Aiii, Figure 33 B). Coordinating and 5-HT-ir neurons were also separate in the connective (Figure 32 B) and the coordinating neuron's target ganglia (Figure 31 B and C, Figure 32 C). Therefore, the synapse between the coordinating neurons and ComInt 1 cannot be serotonergic.

3.5 MALDI-TOF Mass Spectrometry

To analyze neurons with MALDI-TOF mass spectrometry I stained them intracellularly with dTR so that the somata could be dissected under visual control using a stereo fluorescence microscope with an appropriate filter set (Figure 34 C). We used motor neurons as control because they are known to be GABAergic or glutamatergic (Takeuchi and Takeuchi, 1964, 1965; Mulloney and Hall, 1990). Fragmentation of all ASC_E (5 experiments) and DSC (3 experiments) samples showed a clear ion signal at mass/charge (m/z) 146.12Da (Figure 34 A) that was distinct from the matrix signal at m/z 146.05Da (Figure 34 A inset). These ions were selected for MS/MS analysis to verify the structure of the molecule. Resulting fragmentations were compared to fragmentation patterns generated from synthetic ACh (Figure 34 B). The ion signal at m/z 146.12Da was not detectable in motor neurons (9 experiments). The nearby ion signal at m/z 146.09Da in the MNs corresponded to CHCA fragmentation (Figure 35). In addition, PCA illustrated a dense cluster of motor neurons and wide spread but distinct clusters of ASC_E and DSC samples, corroborating the difference in molecular composition (Figure 36). It is therefore most likely that both ASC_E and DSC have a cholinergic synapse onto ComInt 1.

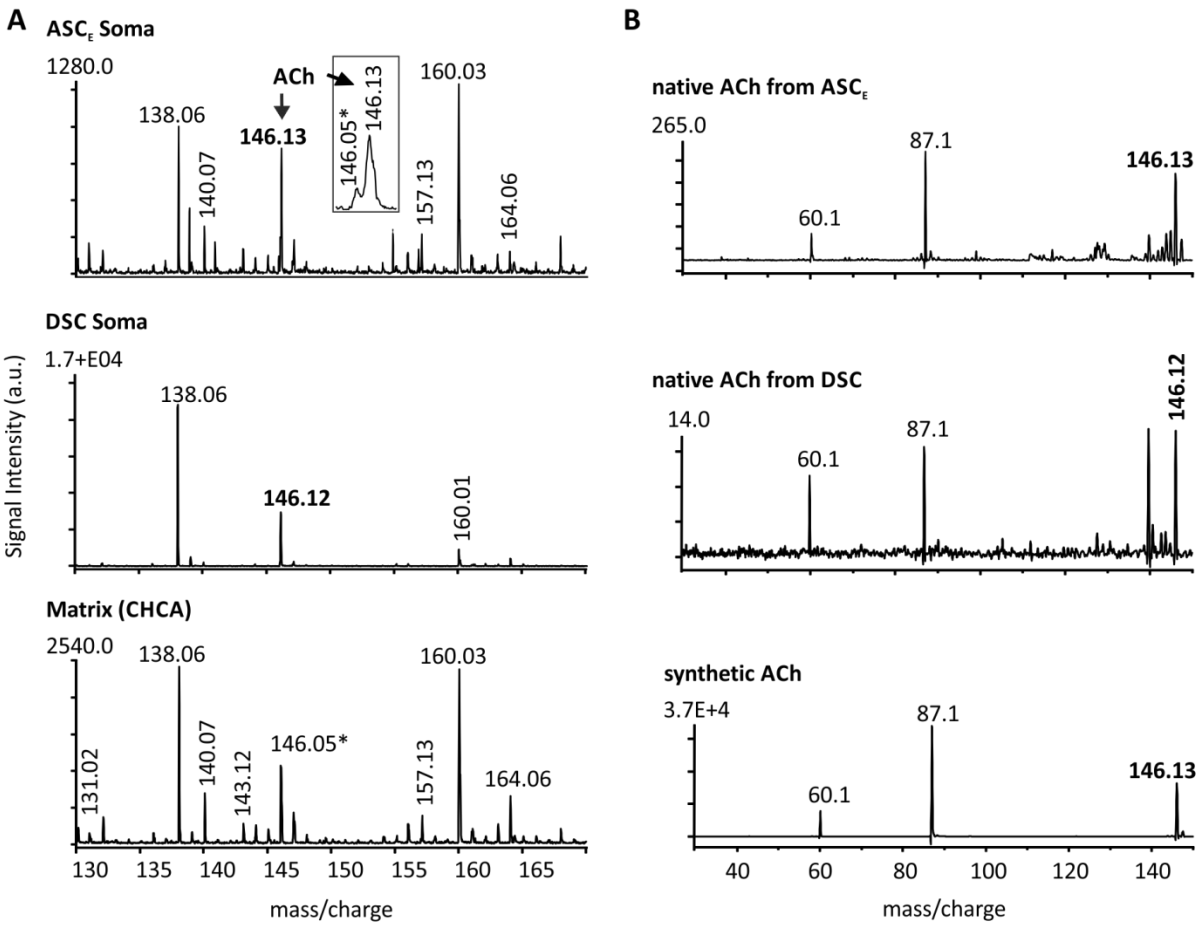

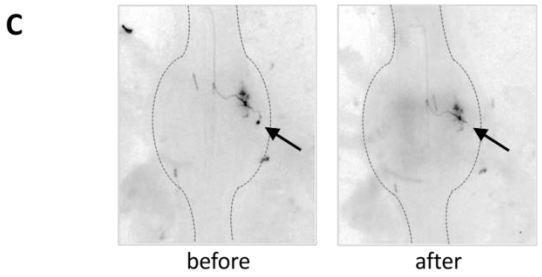

Figure 34: MALDI-TOF mass spectra of ASC$_E$ and DSC somata. A: MS spectrum of a single ASC$_E$ soma, a single DSC soma, and CHCA as matrix in a mass range of 130Da – 170Da. Asterisk indicates close but distinct matrix ion. B: To confirm mass/charge at 146.12Da analyzed in ASC$_E$ and DSC samples as ACh, resulting MS/MS fragment patterns were compared to those generated from synthetic ACh. C: Ganglion with stained ASC$_E$ before and after dissection.

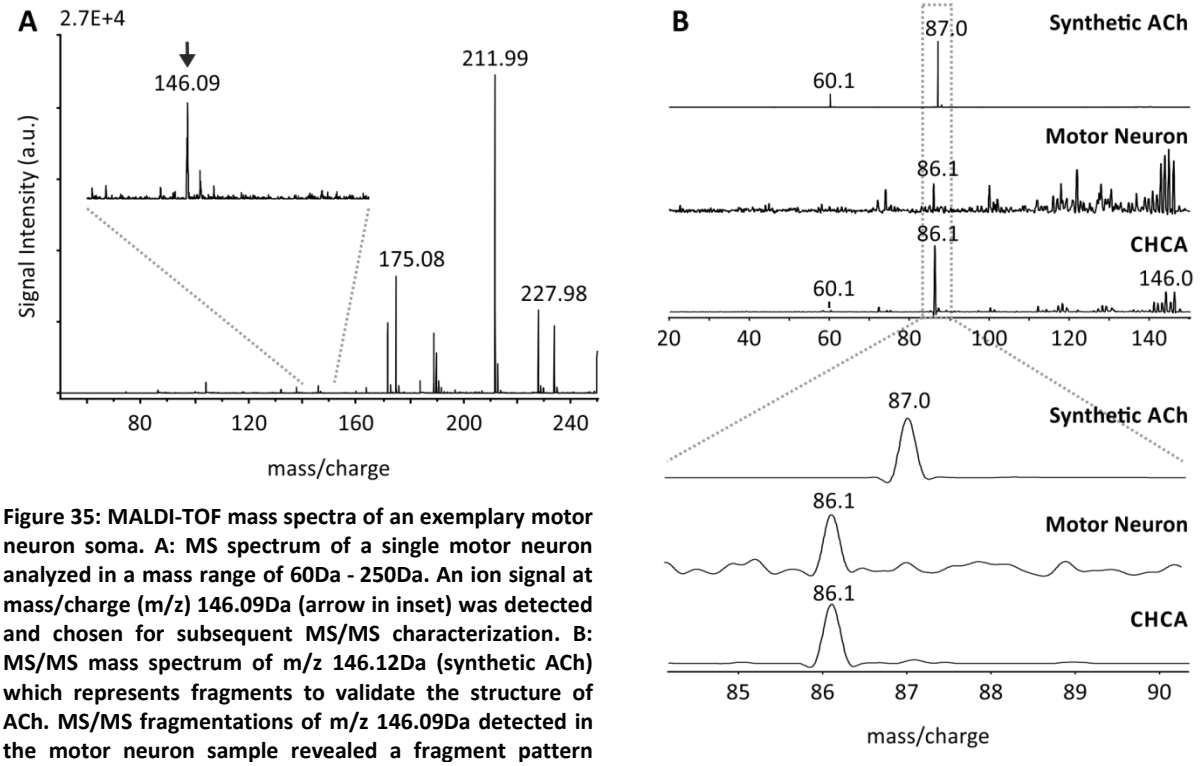

Figure 35: MALDI-TOF mass spectra of an exemplary motor neuron soma. A: MS spectrum of a single motor neuron analyzed in a mass range of 60Da - 250Da. An ion signal at mass/charge (m/z) 146.09Da (arrow in inset) was detected and chosen for subsequent MS/MS characterization. B: MS/MS mass spectrum of m/z 146.12Da (synthetic ACh) which represents fragments to validate the structure of ACh. MS/MS fragmentations of m/z 146.09Da detected in the motor neuron sample revealed a fragment pattern which do not confirm ACh. However, a comparable ion pattern was observed by fragmentations of m/z 146.09Da, an ion signal corresponding to CHCA.

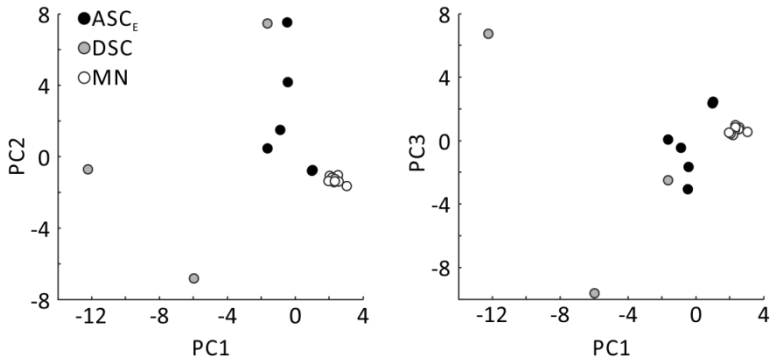

Figure 36: Principal component analysis of three different cell types based on MALDI-TOF MS analysis. Motor neurons (MN; N = 3 and n = 9) formed a distinct cluster from ASC$_E$ (N = 5) and DSC (N = 3).

4 Discussion

In this study, I tested the Adaptive Encoding Hypothesis of matched encoders and a decoder that are tuned by the system's excitation level. I used the crayfish swimmeret system as model. Each swimmeret is driven by its own neuronal oscillator, and all oscillators are coordinated in a posterior-to-anterior metachronal wave (Hughes and Wiersma, 1960; Ikeda and Wiersma, 1964). Ipsilateral oscillators are connected by coordinating neurons. They send information about their home ganglion's activity state as corollary discharge to the other oscillators. Usually, the number of spikes per burst in the coordinating neurons linearly encodes the burst strengths of the motor output. Surprisingly, if the burst strength is altered by the influence of chemicals this is no longer the case: The same number of coordinating spikes may encode for a weak burst at low excitation and a strong burst at high excitation.

4.1 Isolating Neurons

Bath application of chemicals affects all neurons in the preparation. To distinguish direct and network effects of altered excitation in the coordinating neurons, I synaptically isolated them with LowCa^{2+} saline.

When coordinating neurons were isolated in this way they still received synaptic input from an unknown source that resulted in V_m modulation. The low Ca^{2+} concentration should prevent transmitter release at chemical synapses (Sherff and Mulloney, 1996; Mulloney et al., 1997; Tschuluun et al., 2009). This indicates that Ca^{2+} concentration might still be high enough to render chemical synapses functional. Another possibility would be that chemical synapses were only functional in LowCa^{2+} saline during long depolarizations (as seen for MNs in Figure 10) of the neurons because these depolarizations kept Ca^{2+} channels longer open. The long depolarizations could arise from positive feedback through electrical synapses, which have been demonstrated for MNs (Sherff and Mulloney, 1996). Longer opening of Ca^{2+} channels would allow ionic influx for a longer time so that eventually intracellular Ca^{2+} concentration for transmitter release would be reached. That this could have happened in my experiments might be suggested by the V_m modulations that only appeared during erratically long, synchronized burst-like PS activity but not during irregular tonic PS activity (cf. Figure 9, Figure 10), and that these modulations did not occur when spikes were blocked with TTX. Further lowering the Ca^{2+} concentration could improve blocking of chemical synapses.

Because V_m was no longer regularly oscillating and the preparations were tonically active in LowCa^{2+} saline, the CPG was apparently no longer functional, i.e. either isolated or at least locked in a steady state. Paul and Mulloney could stop the swimmeret rhythm by depolarizing IPS or hyperpolarizing IRS (1985a, 1985b). The authors stated that IPS (formerly known as Interneuron 1A) was depolarized during quiescent states that interrupted long periods of swimmeret rhythm expression (Paul and Mulloney, 1985a). Hence, it might seem obvious to assume that IPS is depolarized and IRS hyperpolarized in quiescent preparations. Because of their graded transmitter release (Mulloney, 2003) ASC_E would then be inhibited and DSC is disinhibited. This is supported by findings from Namba and Mulloney (1999), who illustrated that ASC_E is only sporadically firing and DSC tonically active in quiescent preparations. The experiments in which ASC_E and PSEs were tonically active indicated that the CPG was not only locked but neurons were completely isolated because ASC_E and MNs were no longer subject to IPS inhibition. This extends the argument mentioned above that the Ca^{2+} concentration in the LowCa^{2+} saline was low enough to prevent chemical synaptic transmission under normal circumstances.

Coordinating neurons were still able to spike in LowCa^{2+} saline, meaning that the spikes were mainly generated by Na^+ influx and not by Ca^{2+}. In isolation, the coordinating neurons were more depolarized and spike amplitudes were smaller. At depolarized V_m positive to -35mV, the neurons did not spike anymore. A possible explanation could be the inactivation of sodium channels at these depolarized values. This sodium block was not obvious when depolarizing the neurons with the network intact. Therefore, calcium-activated outward currents could play a role in regenerative processes like sodium channel deinactivation by sufficiently hyperpolarizing the neurons during the oscillations. This could be tested by substituting Ca^{2+} with Ba^{2+} in normal saline, which carry the same charge but greatly reduce calcium-dependent potassium conductances.

4.2 Burst Shaping Mechanisms

Burst Shaping in ASC_E

When the swimmeret system switched from a quiescent to an active state, ASC_E's V_m tonically depolarized and then began to oscillate with spikes during peak oscillation. The same is seen in PSE when the system is activated (Mulloney et al., 1997). Like in PSE the oscillations in ASC_E are due to synaptic drive from the CPG's IPS neurons (Smarandache-Wellmann and Grätsch, 2014). The source for the underlying depolarization has not yet been identified. It could be a release from IPS' strong tonic inhibition that is imposed on

ASC_E when the system is at rest. In this state the CPG is locked with IRS hyperpolarized and IPS depolarized. As these are non-spiking neurons their transmitter release is graded, and the amount of release depends on V_m (Burrows and Siegler, 1978; Ivanov and Calabrese, 2000; Simmons and van Steveninck, 2005).

An alternative, but not mutually exclusive, explanation to the release from inhibition is the depolarization via neuromodulator action. CCAP depolarizes the membrane of chemically isolated PSEs. In the intact network, this is followed by an successive activation of the CPG (Mulloney et al., 1997). The similarities between the effects of Mulloney's experiments and the here described depolarization upon switching into the active state are remarkable and suggest similar causes for both observations. Also the wide distribution of CCAP-immunoreactive (ir) positive neurites in the Lateral Neuropil (LN) (Trube et al., 1994; Mulloney et al., 1997) and similarities in morphology of PSE and ASC_E support the assumption that, next to a possible lack of inhibition from IPS, also the action of CCAP could have had the depolarizing effect on ASC_E. This could be clarified by CCAP application to isolated ASC_Es, or simultaneous recordings of ASC_E and CCAP-ir positive neurons. If stimulation of the CCAP-ir neurons results in depolarization of ASC_E, one additional source of input to those neurons would be identified. Latency between stimulation and response could give indications for a mono- or polysynaptic pathway (Sherff and Mulloney, 1996; Smarandache-Wellmann and Grätsch, 2014).

Another possible mechanism for the sustained depolarization could be the activation of persistent inward currents that underlie plateau potentials. Expression of plateau potentials do not apply to ASC_E as discussed below in 4.3 for intraburst and interburst hysteresis.

In addition to chemical activation, the swimmeret system can also be activated by stimulation of 'command neurons' (Wiersma and Ikeda, 1964). Three of the five excitatory command neurons release proctolin, and proctolin-ir positive axons branch in the LN. Furthermore, bath application of proctolin activates the swimmeret rhythm in the isolated preparation (Acevedo et al., 1994; Mulloney and Smarandache-Wellmann, 2012). Therefore, proctolin is another candidate for causing the tonic depolarization of ASC_E.

I observed this tonic depolarization in about two thirds of the experiments. In the other third ASC_E's V_m oscillated on top of the resting potential. In these cases it could be possible that the system was already in a primed state that caused a depolarization without activating the CPG. Such primed states are common in many CNSs. For example, leeches possess a preparatory network that responds with rapid depolarization to sensory stimuli. This network readies the system for complex behavior by bringing motor- and interneurons closer to threshold before a decision about which motor program to execute has been made

(Frady et al., 2016). The authors compare this to the interaction of postural and limb control systems, which allows animals to keep their balance by postural changes even before limb movement starts. A similar enhancement in MN responsiveness has been reported in *Manduca* larvae by tactile stimulation and activation of a cholinergic pathway (Trimmer and Weeks, 1993; Trimmer, 1994).

An alternative explanation to ASC_E's oscillations without any observed preceding depolarization would be that the recording electrode was far away from the site of synaptic input that underlies the preceding tonic depolarization. ASC_E branches extensively in the LN and changes in V_m spread passively in its dendrites. Therefore, if the electrode has been too far away from the source of tonic depolarization it would not have been detectable. If the main reason for the depolarization is to bring the neuron closer to spike threshold it would be most effective if the activated ion channels would be close to the spike-initiating zone and not far away in the area of dendritic arborization.

When ASC_E was hyperpolarized, its oscillation amplitude decreased, although it never reached reversal potential. The decrease in oscillation amplitude demonstrates that the oscillations are caused by phasic inhibition. So far, the only known source for inhibition of ASC_E are the non-spiking IPS (Smarandache-Wellmann and Grätsch, 2014). The conclusion drawn from this for burst shaping in ASC_E is that the neuron receives tonic depolarization as soon as the system is activated. Subsequently, bursts are shaped by phasic inhibition on top of this depolarization. Never reaching reversal potential was most likely a result of insufficient space clamping and not applying enough hyperpolarizing current. When I hyperpolarized coordinating neurons with more than -2nA, the neurons did not recover afterwards. Their V_m remained more hyperpolarized than before and they did not spike anymore, which is why I refrained from current injections larger than ± 1.5nA. The injected current might have dissipated in the neuron's many branches in the LN, therefore never sufficiently affecting the site of synaptic input responsible for the oscillations to reverse the oscillations.

The rather smooth appearance of ASC_E's oscillations pointed to a main drive by graded transmitter release of the non-spiking CPG. The additional small IPSPs indicated input from inhibitory spiking neurons that was either weak or the recording site was distant from those synapses. Recording from different areas along ASC_E's neurite could clarify this matter. If IPSPs do not change drastically in size at different recording sites it is likely that they are caused by weak synaptic input.

The appearance of PSPs together with the tonic depolarization indicated that ASC_E received input from other neurons than the CPG, which are not identified yet. One way to

find presynaptic neurons would be simultaneous recordings. Depending on the latency between presynaptic simulation and ASC_E's response estimations of a mono- or polysynaptic connection would be possible. Latencies between 2ms and 3.5ms would indicate a monosynaptic connection (Sherff and Mulloney, 1996; Smarandache-Wellmann and Grätsch, 2014; Smarandache-Wellmann et al., 2014). Additionally, application of high divalent ion saline increases spike threshold so that only monosynaptic connections evoke PSPs in the postsynaptic neuron upon stimulation of the presynaptic neuron.

Burst Shaping in DSC

Burst shaping in DSC was quite different to ASC_E. During each PS burst, DSC was inhibited, showing large, distinct IPSPs. The source of these IPSPs is not yet known. The CPG can be discarded as direct source for the IPSPs because CPG neurons are non-spiking and gradually release transmitter (Heitler and Pearson, 1980; Mulloney, 2003). This might account for the graded inhibition during PS but cannot explain the distinct IPSPs. They occurred as soon as PS was active, suggesting similar drive as for the MNs. This could be mediated by interneurons that also receive input from the CPG or from PS MNs. Because of the regular interval between the IPSPs, it is most likely that they come from one individual spiking neuron. If multiple neurons were involved, IPSP intervals would be spaced less regularly. To find the source of the additional inhibitory synaptic input simultaneous intracellular recordings of DSC and putative presynaptic neurons are needed. Double staining of the two neurons could then further clarify where the synapse for this distinct inhibitory input is located.

The strength of DSC's inhibition correlated with PS strength, a further indication that the putative inhibitory interneuron might receive the same input as the PSEs. This correlation only became evident when burst strength was widely varying over time, and not in the regular carbachol- or CCAP-induced rhythms. Because in regular chemical-induced rhythms burst strength varied only slightly, so that the correlation was not apparent in the system's noise.

When hyperpolarized, DSC's V_m oscillations decreased. In one experiment, oscillations were flat at approximately -90mV, and then reversed with further hyperpolarization. Therefore, inhibition seemed to be carried by K^+ ions, which have their equilibrium potential at approximately -90mV, whereas Cl^- equilibrium potential is at approximately -60mV. The recording in which I was able to hyperpolarize DSC below reversal potential indicated that the recording site might influence this outcome. In the respective DSC recording, spikes were smaller than in average DSC recordings and the large IPSPs during the interburst were not clearly visible. This suggests that the recording electrode was

further away from the spike-generating zone and the input site for inhibition by spiking neurons. Presumably, inhibition from the CPG and spiking neurons occurred at different compartments along the neurites, which may influence the neuron's computational properties.

Post-inhibitory Rebound in ASC_E and DSC

Both ASC_E and DSC were able to generate rebound spikes even after brief hyperpolarizations, and showed slight sag potentials during longer hyperpolarizations. This was most obvious in the chemically isolated neurons. When the network was intact, the coordinating neurons continued to oscillate when hyperpolarized so that the 1mV - 2mV sag could easily be lost in the noise of the ongoing oscillations. The presence of a sag potential indicated the presence of I_h in the coordinating neurons. Generally, this current is rather small, compared to other ionic currents in a neuron, activates at V_m more hyperpolarized than approximately -50mV to -60mV, and can contribute to rhythmogenesis (reviewed in Pape, 1996; Robinson and Siegelbaum, 2003). The small amplitude of the sag in my experiments could be explained with insufficient hyperpolarization, I_h being not that pronounced in those neurons, or the respective channels being distant to the recording electrode. This can only be answered by a thorough investigation of ionic currents in the coordinating neurons, e.g. holding the neuron at a specific potential and hyperpolarize with incrementing current amplitude and duration, or blocking I_h with chemicals like extracellular Cs^+ or more specific blockers like ZD-7288. Recently, such systematic experiments increased evidence for the presence of I_h in ASC_E (pers. comm. Laura Schläger).

Rebound spikes or an increase in firing frequency was common in both ASC_E and DSC after long hyperpolarizations. This could be mediated by I_h, which was not immediately deactivated after stopping the hyperpolarization, or de-inactivation of voltage-gated sodium channels during the hyperpolarization. Again, this could be clarified by using channel blockers and standardized stimulation protocols. If rebound responses were absent when using h-current blockers, it would be a strong indication that I_h underlies the otherwise observed rebound.

Rebound spikes after brief hyperpolarization were less often observed in DSC compared to ASC_E. This could be because of different channel densities at the recording sites in ASC_E and DSC, or because of general differences in rebound properties between the coordinating neurons. The ability to generate rebound spikes might help with burst shaping when the inhibition by the CPG decreased during each cycle. More spikes could be generated at a higher frequency as soon as the neurons are released from inhibition. The resulting

increased spike count in ASC_E at the beginning of its burst might depolarize ComInt 1 and its connected IRS more, facilitating the beginning of PS in an anterior ganglion.

Burst Shaping in Other Neurons and Systems

The swimmeret MNs seem to share similar mechanisms for burst shaping with the coordinating neurons. MNs receive periodic inhibition from the CPG, and no evidence for periodic excitation has been found (Mulloney, 2003). Similar to ASC_E, Mulloney et al. (1997) revealed that PSE and RSI first depolarize and then begin to oscillate if the abdominal ganglia chain is perfused with CCAP to activate the rhythm. Similar to DSC, RSE and PSI hyperpolarize and begin to oscillate. ASC_E's soma is located in the pool of PSE and RSI, DSC is located with RSE and PSI. Both coordinating neurons are active in the same phase as their respective MN pool. Based on these similarities in location, morphology, innervation, and response to system activation, it could be possible that the coordinating neurons evolutionary developed from MNs, only sending their axon to other ganglia instead of muscles.

Stick insect leg MNs show a similar activation pattern as ASC_E and swimmeret MNs. They are tonically depolarized during movement. In contrast to ASC_E, these bursts are then shaped by both periodic inhibition and excitation. Unlike inhibitory swimmeret MNs, which apparently receive only inhibitory input, bursts in stick insect inhibitors are also generated by tonic depolarization with overlaying phasic excitation and inhibition (Büschges et al., 2004; Ludwar et al., 2005b; Rosenbaum et al., 2015). This mechanism of tonic depolarization and additional alternating phasic excitation and/or inhibition is quite common for MNs and interneurons in invertebrates and vertebrates. For example, locust flight elevator MNs depolarize by wind stimulation of the head (Hedwig and Pearson, 1984), neonatal rat MNs depolarize before oscillations occur when the CPG is chemically activated in the isolated spinal cord (Cazalets et al., 1996), and oscillations in lamprey MNs and interneurons are driven by alternating excitation and inhibition (Kahn, 1982; Russell and Wallén, 1983). In the *Tritonia* swim network, interneurons and MNs express a ramp depolarization on which additional bursts occur during fictive swimming. With each cycle, this depolarization decreases until swimming stops (Lennard et al., 1980; Getting and Dekin, 1985). The tonic depolarization is sustained by feedforward mechanisms (Frost and Katz, 1996), and bursts are shaped by interaction of CPG neurons (Getting et al., 1980).

Compared to ASC_E, the burst shaping mechanism of DSC is less common. Similar to DSC, heart interneurons (HN) 3 and 4 in leech are tonically active if synaptic transmission is blocked. In the intact network, bursts are terminated by inhibition from the contralateral HN (Angstadt and Calabrese, 1989). Their intrinsic I_h allows them to escape from inhibition

so that a new burst can start. In the STNS, pyloric neurons are conditional bursters. They are tonically active or silent if modulatory input is missing. Isolated from each other but with modulatory influence present they burst irregularly. Only when they are coupled by inhibitory synapses is the coordinated pyloric rhythm generated (Bal et al., 1988; Elson et al., 1999). Thalamic neurons can produce both tonic and bursting activity. However, these neurons are intrinsically capable of rhythm generation. V_m, T-type Ca^{2+} channels and I_h, and modulatory input determine the switch between tonic spiking and bursting (Jahnsen and Llinás, 1984; McCormick and Huguenard, 1992; Sherman, 2001).

The expression of a sag-potential upon hyperpolarization in both ASC_E and DSC indicated that the neurons might have I_h. This current plays an important role in many bursting neurons. In STNS neurons, the phase at which rebound spikes are generated is strongly influenced by interplay of I_h and the transient outward K^+ current (I_A) (Harris-Warrick et al., 1995). Hyperpolarization deinactivates I_A, which delays spiking when it is activated during subsequent depolarization. Because during faster rhythms neurons are inhibited for a shorter duration than during slow rhythms, I_A is less deinactivated, therefore delay to rebound spikes is shorter (Bose et al., 2004). In the swimmeret system such a mechanism could ensure that ASC_E's and DSC's activity is phase-locked to PS and RS (Namba and Mulloney, 1999) over the wide range of frequencies the system can express. Furthermore, Edman et al. (1992) have shown that in the lobster stretch receptor I_h contributes to V_m and stabilizes it under different external influences like varying temperatures, pH, or potassium concentration, which might further ensure phase-locking of coordinating neurons to the motor output.

Burst Shaping: Conclusions

Although ASC_E's and DSC's activity appeared quite similar during the ongoing rhythm (but with a 50% phase lag in the same home ganglion) the mechanisms that underlie their bursts of spikes are different. My experiments indicated that ASC_E received tonic excitation on top of which V_m oscillations are driven by the CPG and by presumably weak input from unknown spiking inhibitory neurons. DSC bursts were shaped only by two inhibitory mechanisms: Graded inhibition from the CPG and spiking inhibition from an unknown neuron. This is interesting because until now the only identified afferents to the coordinating neurons are inhibitory from the CPG (Smarandache-Wellmann and Grätsch, 2014).

Mathematical modeling studies suggest that input solely from the CPG to the coordinating neurons is sufficient to achieve the proper coordination of oscillators (Skinner and Mulloney, 1998). This raises the question why additional inhibition is present in those

neurons. One possibility could be a feed-forward mechanism in which the CPG also drives the inhibitory presynaptic neurons to enhance the inhibitory input to the coordinating neurons. This would ensure a precise burst termination in ASC_E and DSC.

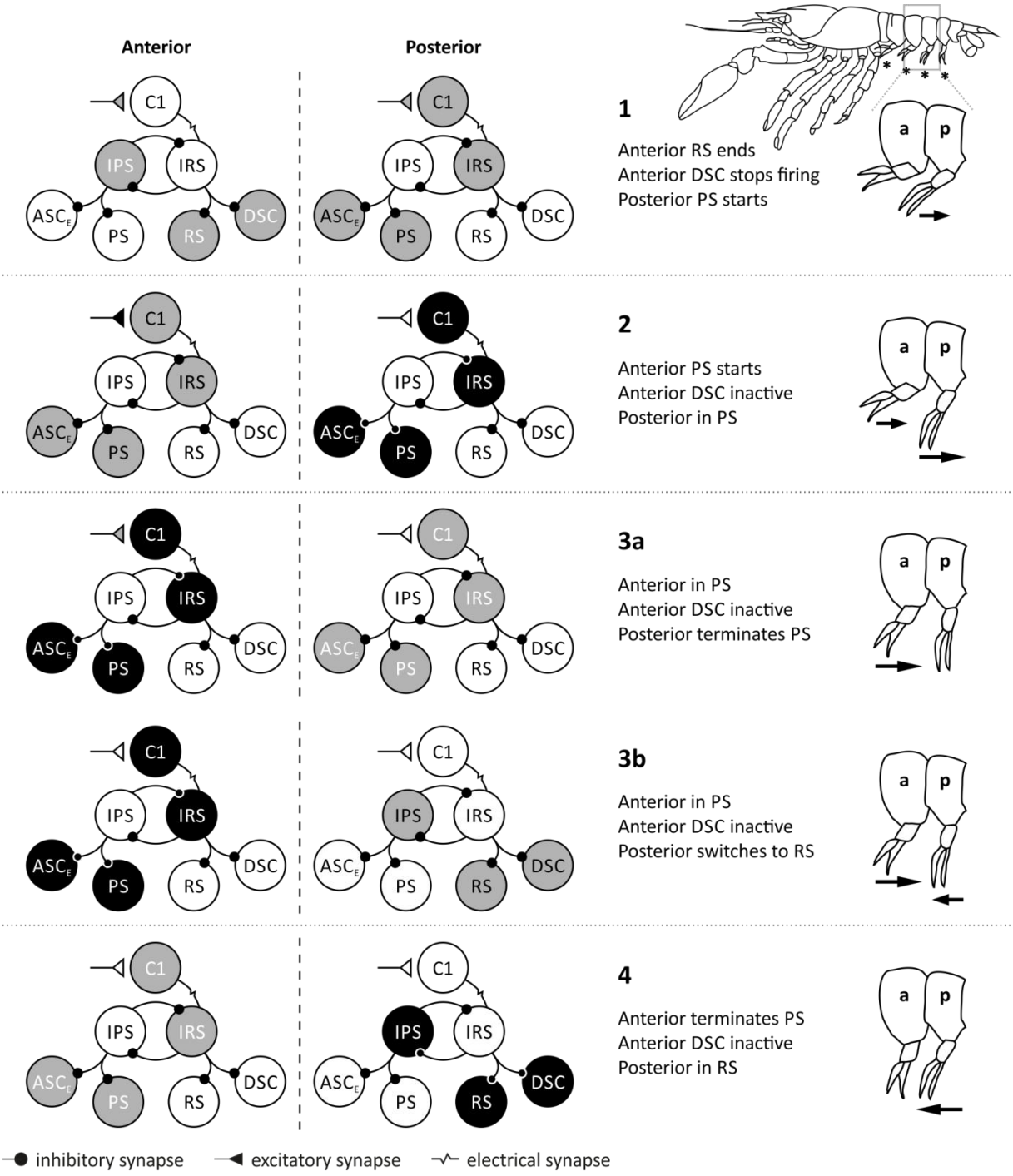

Figure 37: Putative switching mechanism from PS to RS, depending on descending coordinating information. Left panel depicts schematics of descending interactions between an anterior and a posterior microcircuit, which control their respective swimmerets. Black neurons are active, white neurons are inactive. Grey neurons switch from active to inactive (white letters), or from inactive to active (black letters). For simplification, coordinating input to ComInt 1 is illustrated by only one synapse because spikes from neighboring ASC_E and DSC arrive simultaneously. Right panel depicts schematics of an anterior (a) and posterior (p) abdominal segment with the according swimmeret movements. Arrows indicate the direction of swimmeret movement. Short arrows indicate beginning of movement. Long arrows indicate ongoing movement. Asterisks mark swimmerets. See text for additional details.

Previous studies have shown that DSC activity is loosely correlated to RS and PS (Paul and Mulloney, 1986; Mulloney et al., 2006). Additionally, I demonstrated that DSC inhibition is correlated with PS burst strength. As DSC is characterized by tonic activity in the quiescent state of the system, and the number of spikes do not have such a strong effect on the target ganglion compared to ASC_E (Namba and Mulloney, 1999), the important information about its home ganglion's activity state that reaches its target may be the interburst interval.

Consider the following: PSE have approximately 40% duty cycle (Mulloney et al., 2006), which means because of the 25% phase lag that an anterior PS starts before the posterior PS has ended. As soon as the anterior PS starts, DSC spiking is terminated (Figure 37, 1 and 2). If DSC is not spiking, it is not depolarizing the target ComInt 1. Because of the electrical synapse from ComInt 1 to IRS (Smarandache-Wellmann et al., 2014), IRS is also not depolarized. This disinhibits IPS, terminating PS in the posterior ganglion (Figure 37, 3a). The lacking input to the posterior ComInt 1 could thus facilitate the termination of the posterior PS and the switch to RS in order to maintain the approximately 25% phase lag between segments (Figure 37, 3b and 4). In turn, ASC_E's rebound properties could facilitate execution of an anterior PS if a posterior PS is active (see above).

4.3 Hysteresis of Coordinating Neurons

Spike-Frequency Adaptation

Both coordinating neurons were influenced by their history. When depolarized for several cycles, the spike count per burst decreased from one burst to the next. In their investigation of the coordinating neurons' firing pattern, Namba and Mulloney (1999) reported a decrease in instantaneous firing frequency within each burst. Such spike-frequency adaptation can be caused by several different mechanisms. Input adaptation at the postsynaptic receptors can be excluded for my experiments as the neurons were stimulated by intracellular current injection (Figure 14). More likely is the activation of adaptive currents. These can be voltage-gated potassium currents that activate at high voltages, like the M-current (Brown and Adams, 1980). At high spike frequencies, the time between spikes is not long enough for this current to deactivate completely. As the current builds up between spikes, it counteracts the Na^+ influx, decelerating spiking. Calcium-activated potassium currents are activated if the intracellular calcium concentration is increased, typically by calcium influx through voltage-gated Ca^{2+} channels that are activated during spiking. This has been shown for example in *Aplysia* (Gorman and

Thomas, 1978; Lewis and Wilson, 1982). In addition, inactivation of Na^+ channels can decrease spike frequency (see discussion on intraburst hysteresis below).

Which ionic currents cause the spike-frequency adaptation in the coordinating neurons is unknown. Adaptation was still present in $LowCa^{2+}$ saline (Figure 15 B, Cii, D). This might indicate that calcium-activated currents played only a minor role, or that Ca^{2+} concentration in the bath was still high enough to activate calcium-dependent currents. In $LowCa^{2+}$ saline, transient Na^+ channels were completely inactivated around -35mV in most experiments. As peak oscillation amplitude is close to this potential, a large fraction of Na^+ channels could already be inactivated and could therefore contribute to spike-frequency adaptation. Experiments in which specific channels are blocked could help to identify contributing currents.

Chrachri (1995) conducted a detailed investigation on ionic currents in swimmeret system MNs. He identified I_A and the delayed K^+ rectifier current by blocking them with 4-aminopyridine (4-AP) or TEA, respectively. Furthermore, he identified a fast transient inward Na^+ current that could be blocked by TTX, and an L-type Ca^{2+} current that could be suppressed by nifedipine. He concluded that the Na^+ current is active during spike depolarization, that the K^+ currents are active during spike repolarization and that the Ca^{2+} current is generating the MN's oscillations. Under the assumption that coordinating neurons share physiological similarities with MNs, their K^+ and Ca^{2+} currents can be blocked with the mentioned substances. The role of the remaining Na^+ currents in spike-frequency adaptation could then be examined in detail by injecting constant current or ramp currents. If inactivation of Na^+ channels is the reason for spike-frequency adaptation, it should still be present when K^+ currents and Ca^{2+} currents are blocked. Subsequently, blocking only Ca^{2+} channels could reveal if K^+ currents contribute to the adaptation. If Ca^{2+} dependent K^+ currents were necessary for adaptation, it would not be present in $LowCa^{2+}$ saline.

Intraburst Hysteresis

In the isolated ASC_E, hysteresis appeared to have an intraburst and an interburst component. Due to the intraburst component, the last spike of a burst was elicited at a more depolarized V_m than the first spike. In addition, fewer spikes were generated on the descending slope of the ramp stimulus than the ascending. The notion that spike threshold increased in ASC_E during the burst has been corroborated by modeling the neuron's response to ramp stimulations. Only if a variable for an adaptive threshold was introduced in the model, which increased over time during the stimulation, it was able to capture ASC_E's response to ramp stimulation appropriately (pers. comm. T. Michael Wright).

Ramp stimuli have been used to characterize plateau properties in vertebrate motor neurons (e.g. Hounsgaard et al., 1988; Bennett et al., 2001). Such plateau potentials could also explain ASC_E's tonic depolarization during active swimmeret rhythms. Due to the self-sustained firing in neurons with plateau characteristics, more spikes are generated on the descending slope of a triangular ramp stimulus, and the last spike occurs at lower injected current than the first. As this was not observed in ASC_E, it probably does not have the prerequisites in which persistent inward currents could cause plateau potentials that might aid burst shaping.

Spike threshold adaptation has been described as early as 1936 (Hill, 1936). It can be a result of fast Na^+ channel inactivation or increased K^+ outward currents (Hodgkin and Huxley, 1952). Henze and Buzsáki (2001) reported for pyramidal neurons in rat hippocampus that slower rates of membrane depolarization correlate with a higher spike threshold, and that both single and multiple spikes preceding up to 1s increase threshold. In one experiment, the authors briefly hyperpolarized the membrane after each spontaneous spike, which reversed the negative correlation between spike threshold and inter-spike interval. They concluded that spike-dependent modulation of voltage-activated conductances is the underlying mechanism. According to their argumentation, slow recovery from inactivation of Na^+ channels is more likely than activation of K^+ conductances, partly because maximum spike rising slope becomes shallower with decreasing inter-spike intervals.

ASC_E features both of the mentioned correlations. During the sinusoidal oscillations depolarization rate decelerated and the slow changes in V_m close to peak depolarization shifted sodium currents along their activation and inactivation curves. Additionally, inter-spike intervals are short within a burst and could be shorter than the sodium channels' inactivation time constant. To test the hypothesis of sodium channel inactivation I could do a similar analysis of changes in spike shape within an ASC_E burst. I would expect spikes to have lower maximum rising slopes and therefore a longer half-width, and reduced amplitude, as fewer activated Na^+ channels are available for the spike. Another argument supporting the assumption that a lack of Na^+ channel inactivation is responsible for the changes in spike threshold is the observed increase in R_{in} during the bursts.

Platkiewicz and Brette (2010) demonstrated in a modeling study the interplay of voltage-gated fast Na^+ channel inactivation and delayed rectifier K^+ channel activation for dynamic thresholds. However, the authors also conclude that spike threshold is mainly determined by sodium channel inactivation (Platkiewicz and Brette, 2010, 2011). In contrast to this,

Higgs and Spain (2011) demonstrated pharmacologically in rat pyramidal motor cortex neurons a major role of potassium conductances for fast threshold accommodation.

Because different neuron types have different molecular mechanisms to mediate hysteresis means that a detailed analysis of channel kinetics in the neurons of the swimmeret system is necessary to unravel the underlying mechanism. Threshold adaptation might contribute to the encoding of duration and burst strength information in the coordinating neurons because it can influence spike frequency and spike count within a burst.

Interburst Hysteresis

The interburst component of ASC_E's hysteresis caused the neuron to fire fewer spikes on the second ramp than the first, and increased the delay of the first spike. This demonstrates that the prior activity of ASC_E influenced the response to the second ramp.

In contrast to intraburst hysteresis, it is less likely that Na^+ channel inactivation mediates interburst hysteresis. The interval between ramps lasted several seconds which should be enough time to remove inactivation from sodium channels (Henze and Buzsáki, 2001). In this case, the activation of outward K^+ currents could be the dominant mechanism. These outward currents could counter the depolarization and hence increase the time until a spike is generated. To test this hypothesis, isolated ASC_Es could be stimulated with paired ramps without and with blocking of K^+ currents, for example with TEA. Blocking should then abolish the interburst hysteresis. Another possible experiment would be to use calcium-free saline to investigate if calcium-activated potassium channels are involved. This is hard to conclude when using LowCa^{2+} saline because the Ca^{2+} concentration might still be high enough to activate the calcium-activated potassium channels.

Another explanation for the interburst hysteresis that comes to mind is an underlying plateau potential that is modulated over time. This plateau potential might be activated during ASC_E's tonic depolarization when the system switches to the active state. In vertebrate neurons with plateau characteristics, e.g. cat motor neurons or turtle sensory neurons, the response to subsequent stimuli is stronger compared to the preceding (Russo and Hounsgaard, 1994; Bennett et al., 1998). This 'warm-up' occurred even with 3s - 6s interstimulus intervals. The plateau potentials in those neurons are mediated largely by L-type Ca^{2+} currents with slow kinetics. The opposite effect of repetitive stimulation in my experiments indicated that plateau potentials are not involved in ASC_E burst shaping.

Hysteresis: Conclusions

Intra- and interburst hysteresis were most likely caused by different mechanisms because they differed in their time scales. The mechanisms that cause the interburst hysteresis might also be responsible for the more depolarized spike threshold when the network is intact, compared to that of the isolated neurons: The interburst effects caused a delay and increased threshold for the first spike on the second ramp. In the ongoing steady state rhythm, interburst hysteresis probably reaches a steady state that keeps spike threshold elevated. As hysteresis lasts longer than a single period, it could help to stabilize the encoding of coordinating information against small fluctuations in synaptic input. In this context it would be interesting to do multiple subsequent ramp stimulations or vary interstimulus intervals to determine how long the interburst hysteresis lasts and how many subsequent bursts are affected. Furthermore, the rise-time of the ramp could be adjusted to better mimic the depolarization in the intact network.

Smarandache-Wellmann and Grätsch (2014) demonstrated hysteresis in the effectiveness of ASC_E inhibition by IPS. If inhibition increases to some value ASC_E generates more spikes per burst than if inhibition decreases to that same value, i.e. the previous inhibition affects the spike count per burst. This does not match my results when investigating synaptically isolated ASC_Es. Based on my experiments, I would expect that if ASC_E is initially weakly inhibited by IPS, and therefore quite depolarized, interburst hysteresis would cause a relatively high spike threshold. If inhibition then strengthens, therefore hyperpolarizing ASC_E, hysteresis would gradually lower spike threshold. Vice versa, if ASC_E is initially strongly inhibited, and therefore quite hyperpolarized, interburst effects would cause a relatively low spike threshold. If inhibition then weakens, therefore depolarizing ASC_E, hysteresis would increase spike threshold. My experiments in which spike threshold differed between ramps have shown that the threshold increase happens faster, on a cycle-to-cycle basis, than threshold decrease. Under these circumstances, I would expect ASC_E to spike more in the case in which inhibition decreases to some value, compared to an increase in inhibition to that same value. This would be opposite to the results from Smarandache-Wellmann and Grätsch. The discrepancy might be due to the different experimental conditions. Those by Smarandache-Wellman and Grätsch rather resemble the transition between the active and quiescent system in which ASC_E inhibition ranges from weak to complete, while mine resembled ongoing activity during which inhibition by IPS is not that variable. This indicates that the neuron's computational properties are different during the transition from active to quiescent compared to ongoing activity.

DSC bursts were shaped differently than ASC_E bursts. Repeating the ramp stimulations in the isolated DSC could give more information about how information about the activity state of DSC's home ganglion is encoded. To mimic DSC's input, ramps should be hyperpolarizing. If hysteresis affects it in the same way as seen for ASC_E, its own activity would likewise suppress spike generation, extending the interburst. As discussed above (see 4.2 and Figure 37), this might facilitate PS termination and switch to RS in the posterior ganglion.

Hysteresis is also commonly found in sensory neurons or other neurons in sensory pathways, for example in chordotonal organs (Zill, 1985; Zill and Jepson-Innes, 1988), sensorimotor integration (Siegler, 1981a, 1981b), or decoding of social communication (Carlson, 2009). My experiments were carried out in the isolated nervous system; therefore, it is unknown which role sensory input would have had in the activity of the swimmeret system. The hysteresis of coordinating neurons might reflect hysteresis in sensory pathways that could influence the motor output. By tuning the coordinating neurons via history mechanisms, their activity may match those of sensory neurons.

4.4 Effect of Carbachol and EdCl on the Swimmeret System's Excitation Level

No Dose-Dependent Effect on Burst Strength

Bath application of different carbachol and EdCl concentrations significantly changed PS burst strength. In contrast to the literature, this change was not dose-dependent but varied among different preparations (Braun and Mulloney, 1993; Mulloney, 1997; Mulloney and Hall, 2007b). Only in about half of the experiments, burst strength was increased at the highest concentration compared to the lowest concentration. Several below discussed explanations are possible, as the effect of concentrations on burst strength has never been thoroughly investigated.

A method to reliably calculate burst strengths from recordings with overlapping spikes was first established in 2005 (Mulloney, 2005). Before that time, changes in burst strength were estimated by visual inspection of the recorded traces, or calculations did not factor in burst duration (as in Mulloney et al., 1997). Therefore, only prominent changes in burst strength between extreme concentration differences might have been noticed.

The authors of the above mentioned publications used other carbachol concentrations than in my experiments, ranging from less than 1.5µM to more than 10µM. In preliminary experiments, I was never able to obtain a steady physiological motor output with carbachol

concentrations lower than 2µM or higher than 6µM. With low concentrations, the rhythm was prone to collapse, if activated at all, when searching with a sharp electrode for coordinating neurons in the LN. With high concentrations, PS bursts were no longer clearly delineated, and some MNs were often tonically active. This can be explained by differences in the preparations. The authors only used the abdominal ganglia chain from A1 to A6 and desheathed only those ganglia innervating the swimmerets. My preparations also contained the last two thoracic ganglia as their presence stabilizes the swimmeret motor output (pers. comm. Carmen Wellmann), presumably by interactions between the walking system and the swimmeret system (Chrachri and Neil, 1993). In addition, I desheathed all ganglia of my preparations. This may have made the system more susceptible to carbachol, leading to rhythm deterioration at higher carbachol concentrations.

Mulloney an Hall compared burst strengths from quite extreme carbachol concentrations ≤ 1.5µM and ≥ 3µM (2007b). These large concentration differences can account for the detected dose-dependent effect in burst strength. I too observed an increase in burst strength in half of my experiments when comparing burst strengths at the lowest concentrations with burst strengths at the highest concentration. As burst strength was nonetheless statistically different between all concentrations, bath application may cause differential and state-dependent activation at certain synapses so that a dose-dependent effect of carbachol concentration on burst strength is lost in stochastic jitter for small dosage increments. This argument is supported by results from Bacqué-Cazenave et al. (2013), who found out that 5-HT de- or hyperpolarizes crayfish walking depressor MNs, depending on the site of focal application along the neurite.

ASC_E and DSC activity have both been shown to influence strength and timing of their target ganglion's output (Namba and Mulloney, 1999). Furthermore, ASC_E activity also affects its home ganglion, especially when descending information from anterior ganglia is blocked (Mulloney and Hall, 2007a). Impaling an electrode into the coordinating neurons may cause different amounts of damage to those neurons. That damage might result in an increased or decreased activity of the coordinating neurons, which can influence their target ganglia and home ganglion. As the change in motor output of the target ganglia is then fed back into the home ganglion, and from there fed back to the target ganglia, the motor output of the whole system could be changed by damaging one coordinating neuron. ComInt 1 receives information from three coordinating neurons, therefore some of that arriving information might be redundant and a failsafe mechanism if one ganglion is damaged (Tschuluun et al., 2001). Because successful recordings were often a result of searching the LN for a long time in different ganglia, it is possible that coordinating neurons

or CPGs from certain ganglia were also damaged or destroyed. This might lead to incorrect information arriving at ComInt 1 so that the apparently not-dose-dependent changes in burst strength reflect some of that damage. This might also explain why EdCl as well had no dose-dependent effect on burst strength.

Dose-Dependent Effect on Period

Both carbachol and EdCl shortened the system's period in a dose-dependent manner, although EdCl had a stronger influence. This could be caused by two reasons. It is likely that the carbachol and EdCl concentrations used did not match in their ability to excite the system. Higher EdCl concentrations and smaller increments might have resulted in similar frequency changes as carbachol. To determine which changes in concentrations change period in the same way, dose-response curves are needed for both chemicals.

Another reason could be the fundamental difference in how these chemicals act on the swimmeret system. Carbachol as a cholinergic agonist is able to activate all muscarinic and nicotinic ACh receptors in the system (Braun and Mulloney, 1993). EdCl inhibits the ACh esterase, delaying enzymatic ACh breakdown. This means that activity at already active synapses is prolonged, but not that inactive synapses are activated, possibly causing a more physiological modulation of the system's activity than with carbachol. This argument is weakened to some extend by taking into account that EdCl's action requires an already active system, which I obtained by bath application of CCAP. This might also have activated synapses that would otherwise be inactive in the intact animal.

No CCAP receptors have been identified yet in the swimmeret system. In the STNS a transcript is identified that is similar to insect CCAP receptors (Garcia et al., 2015), which are G-protein coupled and different from muscarinic ACh receptors (Park et al., 2002). Additionally, in other arthropod preparations, motor activity is induced and modulated by CCAP application, indicating an similar underlying mechanism for CCAP-induced activation of systems (Gammie and Truman, 1997; Weimann et al., 1997). Trube et al. (1994) and Mulloney et al. (1997) investigated CCAP-immunoreactivity (ir) in different crayfish species and found a similar distribution of CCAP-ir positive neurons. Each abdominal ganglion has three paired neurons. Their somata are located anterior and ventral in the ganglia. Neurites are present in the connective, run in the ganglia's outer Ventral Lateral Tract, and branch in the LN of their home ganglion, admitting the possibility of connections to the CPG neurons. Mulloney et al. (1997) also reported that CCAP modulates burst intensity (burst duration was not factored in the calculation, so this intensity represents the burst area) and duration in a dose-dependent manner but had no significant effect on

period. In their experiments, some preparations were locked in PS phase with CCAP concentrations >25nM, which I did not observe in my experiments.

Taken together, these results demonstrate that CCAP activates and modulates the swimmeret system in a different way than carbachol because carbachol does not lock the system in any phase or change duty cycles of motor activity. The system's activation by CCAP in my experiments could in turn have led to activation of cholinergic synapses. Because of the EdCl-induced prolonged activity at those cholinergic synapses, activity could then have been modulated via the nicotinic pathway. The possibly unphysiological activation of all cholinergic synapses by carbachol application might have had opposing effects in the system. This could be a reason why the changes in period were greater in EdCl experiments than in carbachol experiments.

Excitation Level: Conclusions

Using both period and PS burst strengths as criteria to deduce the system's excitation level was difficult because both could change independent of each other. Period shortened dose-dependently but burst strength changed not always in the same way, which is contradictory to results from literature (Mulloney, 1997; Mulloney and Hall, 2007b).

In the living animal, excitation level could indeed mean independent changes in burst strength and frequency. If the animal moves through the water, its swimmerets are subjected to drag, depending on velocity and water current. If the animal is moving fast or river current is strong, the swimmerets have to move more forcefully to overcome the drag. This does not necessarily require an increase in swimmeret beating frequency. Force-velocity relationships for shortening muscle in several crustacean fiber types show that less force can be generated at faster contractions (Galler and Rathmayer, 1992). Thus, at short cycle periods the fast-beating swimmerets cannot exert that much force.

Force generation might also depend on the behavior in which swimmeret movement is involved. For example, in supporting walking less force would be required than during swimming because the walking legs generate the main forward thrust. If females have eggs attached to their swimmerets, their weight is increased, which would require larger movement force. While the CNS could control the gross forces necessary for a certain behavior, the fine-tuning might require sensory input, which is missing in the isolated abdominal ganglia chain. In this context, Davis and Kennedy (1972a, 1972b) could show that spike frequency of single motor neurons increases and more motor neurons are recruited (i.e. burst strength increases) with increased stimulus frequency or number of stimulated excitatory command neurons in lobster. Because the coordinating neurons' spike number

depended on burst strength but not period, 'excitation level' refers to changes in burst strength in this thesis.

Differences in the Number of ASC_E and DSC Spikes

On average, ASC_E fires more spikes per burst than DSC. The number of ASC_E spikes ranges on average from 10 to 20, of DSC spikes from 3 to 10 (Namba and Mulloney, 1999; Mulloney et al., 2006; Mulloney and Hall, 2007b). This relation was not changed by application of carbachol or EdCl.

DSC fired fewer spikes per burst in EdCl than carbachol, whereas ASC_E's spike number did not change. Mulloney et al. (1997) stated that CCAP biases the swimmeret system towards PS. DSC is inhibited during PS, so if PS duration is increased DSC inhibition is also increased. This reduces the duty cycle so that fewer spikes can be generated. As results investigating hysteresis suggests (see 4.3), ASC_E might possess internal mechanisms to limit the maximum number of spikes, which could explain why there was no difference in spikes per burst between carbachol and EdCl (see also 3.2 and 4.2 about mechanisms of burst generation).

Another possibility for the significant decrease in DSC's spike number in EdCl could be the low number of experiments (3 in carbachol, 4 in EdCl) for this analysis. In one carbachol experiment, DSC spike number was exceptionally high (cf. Figure 25 Aii). This could have been caused by damaging the neuron's membrane when impaling it with the electrode. The seal around the electrode could have been incomplete, leading to additional leak conductances for all ions and bringing V_m closer to threshold near the spike-initiating zone. Similar damage in two EdCl experiments (cf. Figure 25 Bii, Biii) could have caused a hyperpolarization to subthreshold V_m.

In my experience, DSC seemed more vulnerable than ASC_E to electrode penetration. This might be caused by the angle at which the electrode was oriented to the preparation. The best way to find and record from coordinating neurons is to orient the electrode perpendicular to the primary neurite. In some preparations, I found DSC while searching for ASC_E, so the electrode was oriented parallel to DSC's primary neurite. This configuration could have resulted in additional pressure on the neurite, inferring with membrane sealing around the electrode. To test this possibility, it would be necessary to record from ASC_E with a perpendicular oriented electrode. This could prove difficult, as I was never able to record from ASC_E when the electrode was oriented for recording DSC.

In summary, the differences in the number of spikes between ASC_E and DSC is based on their intrinsic properties. The differences in spike number between chemicals could arise from effects mediated by those chemicals or from experimental conditions.

4.5 Encoding Coordinating Information at Different Excitation Levels

Changes in Membrane Potential

When the network was intact, changing the excitation level had only a minor effect on ASC_E's and no effect on DSC's trough potential across all experiments. Although V_m change in ASC_E is statistically significant across all experiments, V_m depolarized only in some preparations. In others, it did not change or hyperpolarized. It is questionable if the average 2mV depolarization is also of biological significance in an oscillating neuron, especially if compared to the six-fold depolarization in isolation. On the other hand, several examples exist in which small changes in V_m are the result of an obvious change in a system's state. For example, the lateral gastric neuron in the STNS hyperpolarizes by 2mV to 3mV at elevated temperatures due to an increased leak conductance that prevented rhythmic bursting (Städele et al., 2015). In the leech, HN(5)'s trough potential is depolarized by about 2mV in the active state compared to the inactive (Gramoll et al., 1994). In stick insect, mesothoracic MNs tonically depolarize no more than 5mV in response to front leg stepping (Ludwar et al., 2005b). However, in all these examples the relatively small changes in V_m might have been larger at the spike-initiating zone because of the distance to the recording electrode. Hence, the effect of that synaptic input on the neuron's activity might have been greater than expected from the observed recording. In contrast to those reports from the literature, the changes in trough potential in my experiments were not correlated with any differences in motor output and therefore might be negligible.

When synaptically isolated, both ASC_E and DSC depolarized by about 12mV at maximum carbachol concentrations. This depolarization could not arise from synaptic input, which demonstrates that the coordinating neurons must have cholinergic receptors. This is interesting because so far no excitatory or cholinergic afferents to the coordinating neurons have been identified. In ASC_E, the preeminent tonic depolarization when the system switches to activity could be mediated by these cholinergic receptors. Which role they play in DSC is enigmatic because I never observed depolarization in DSC with the network intact. Generally, ACh is present in many crustacean sensory neurons (Barker et al., 1972; Florey, 1973; Hildebrand et al., 1974). The influence of sensory feedback on the swimmeret system has not been studied in detail because of the system's ability to produce a well-coordinated motor pattern in isolation. Thus, the coordinating neurons might be a site for integration of sensory input to influence the swimming pattern. This is discussed in detail in 4.7.

Two mechanisms can cause depolarization of V_m: activation of inward currents, like Na^+ or Ca^{2+}, or deactivation of K^+ outward currents. For swimmeret MNs a carbachol-activated depolarizing inward current has been confirmed, although it is still unclear by which ions it is carried (Tschuluun et al., 2009). Because of the many similarities between coordinating neurons and MNs, it is possible that carbachol activates the same current in both. To test this hypothesis, carbachol-activated currents in coordinating neurons could be measured by single-electrode voltage clamp. Another possibility would be to systematically omit different ions from the saline or block ion channels and test if the neurons still depolarize. In rat, synaptically isolated entorhinal pyramidal projection neurons depolarize upon carbachol application (Gloveli et al., 1999). The depolarization is caused by activation of Ca^{2+} currents. In my experiments, the depolarization only became obvious in LowCa^{2+} saline but not normal saline. Hence, a depolarization due to Ca^{2+} influx seems to be unlikely.

That the dose-dependent depolarization of ASC_E and DSC is not present when the network is intact means that carbachol might additionally enhance their inhibition by the CPG. This reveals a balancing mechanism in the swimmeret system: Intrinsic depolarization of ASC_E and DSC and external inhibition by the CPG neurons are co-regulated in a manner that keeps V_m stable if the system's excitation changes. To allow a better understanding of this relationship, the effect of cholinergic agonists and antagonists on the CPG neurons needs to be investigated. If the assumption is correct that enhanced inhibition counteracts the carbachol-induced depolarization of ASC_E and DSC, the CPG neurons should be more depolarized at higher excitation levels for an overall increase of their graded transmitter release. Liu et al. (2007) state that carbachol has a biphasic effect via nicotinic ACh receptors on neuronal excitability in chick basal ganglia. After an initial short-term increase in spike rate, firing frequency dropped below control value after three minutes. The short-term effect is due to activation of postsynaptic ACh receptors, whereas the delayed effect is due to activation of presynaptic ACh receptors that enhance the presynaptic release of GABA. Long-term effects by activation of presynaptic neurons can be excluded for my experiments in which synaptic transmission was blocked. However, presynaptic activation (e.g. transmitter release from the CPG) seemed to be important to stabilize V_m of coordinating neurons when the network was intact.

Ramp stimulations at different carbachol concentrations showed that although the system's excitation increased ASC_E's excitability decreased. Ramps elicited fewer spikes at high carbachol concentrations than at low concentrations although neurons were held at -55mV. Usually, carbachol is known to depolarize neurons and increase their excitability, i.e. neurons generate more spikes in response to stimulation (e.g. Szczupak et al., 1998; Gloveli

et al., 1999; Tschuluun et al., 2009; Ohkuma et al., 2013). Studies reporting a decrease in excitability found this only together with a hyperpolarization of the membrane after carbachol or ACh application, such as in songbird premotor neurons (Meng et al., 2016), or cat and guinea pig geniculate nucleus neurons (McCormick and Prince, 1987). The following might give an explanation why higher carbachol concentrations depolarized ASC_E but reduced the number of spikes at ramp stimulations. R_{in} increased with carbachol concentration in isolated neurons and threshold decreased. Thus, positive current injection might cause a greater depolarization so that spike number is reduced because of inactivation of fast Na^+ channels. Reduction of spike current threshold by carbachol has been studied by Ohkuma et al. (2013) in newt olfactory receptor cells. In this case, carbachol increases voltage-gated Na^+ and Ca^{2+} currents. However, the pathway in the swimmeret system is still unknown.

Shift of Tuning Curves

As described by Mulloney et al. (2006), Smarandache-Wellman and Grätsch (2014), and in my study, PS burst strength is encoded by the number of coordinating spikes per burst. I did not find a relationship between burst strength and spike frequency. The relationship between PS burst strength and DSC spike count was difficult to interpret because of the low number of spikes per burst.

Burst strength was not as variable if the swimmeret rhythm was induced by application of carbachol compared to spontaneously occurring rhythms. This could distort the relation between PS burst strength and DSC spike count similar as seen for PS burst strength and inhibition strength in DSC (Figure 13 C): Correlations were lost in the system's noise because the low number of spikes in DSC are not able to track small changes in burst strength. This distortion could explain why the correlation between burst strength and coordinating spikes per burst did not appear as accurate as described in the literature. Furthermore, burst strength calculations of noisy recordings are difficult. On the one hand, small units are lost in noise, and on the other hand, the calculated integral of the smoothed and rectified trace is small after subtraction of noise. Therefore, small changes in burst strength could be easily missed in noisy recordings. This might explain why in some experiments the number of spikes per burst changed over a wide range while burst strength did not seem to change at all. In two experiments, burst strength negatively correlated with the number of coordinating spikes per burst at least at one excitation level. Possible reasons could be damage of the preparation or impure impalement of the neuron so that spikes from another neuron were additionally recorded.

The shift in the tuning curves as response to changed excitation means that the coordinating neurons adapted to the changed condition. 'Efficient coding' (Barlow, 1961) matches the stimulus distribution's probability density to the cumulative distribution of a neuron's response so that the neuron responds to all probable stimuli with equal likeliness. This was first experimentally demonstrated in blowfly visual system by Laughlin (1981). If a stimulus' statistical distribution changes, the neuron needs to adapt to maximally utilize its response range (reviewed for sensory systems in Wark et al., 2007). The results of my study suggest that this might have happened in the swimmeret system. Different carbachol and EdCl concentrations changed the distribution of PS burst strength and the coordinating neurons adapted accordingly so that the same number of spikes per burst encoded different absolute burst strengths under different excitatory conditions. An analysis of the temporal change of PS burst strength and coordinating neurons' spikes per burst during the changing of excitation levels (i.e. wash-in or -out of carbachol or EdCl) could reveal on which time-scale the adaptation occurs. An additional detailed investigation of coordinating neurons' responses to ramp stimulation at different excitation levels could further elucidate excitation-induced changes in their input/output functions.

The shift in tuning curves means that the coordinating neurons only encoded relative burst strength. This gain rescaling suggests that the underlying excitation level determined the range of burst strengths in the whole swimmeret system and rescaled the encoding properties of the coordinating neurons accordingly. These results are in accordance with the Adaptive Encoding Hypothesis. Similar results from rat barrel cortex show that adaptive neurons conserve the amount of information transmitted per spike (Maravall et al., 2007). That study investigated how stimulus features were encoded during high and low background excitation, i.e. changes in stimulus statistics. Non-adapting neurons conveyed less information about a stimulus if background excitation was high. Another example is the coding of sound level in the guinea pig inferior colliculus (Dean et al., 2005). The auditory pathway was stimulated with white noise at different sound pressure levels (SPL) so that some SPL ranges occurred with a higher probability than others did. The coding accuracy in inferior colliculus neurons shifted so that it was highest in the range of high stimulus probability. In order to adapt to stimulus statistics a neuron needs to 'be aware' of such changes which can be mediated by hysteresis. Therefore, the hysteresis effects that contributed to ASC_E's burst shaping might very well be involved in the neuron's adaptation to excitation level.

DSC activity is weakly correlated with both PS and RS (Mulloney et al., 2006). Because DSC is spiking during RS it would be interesting to match spikes per burst and RS burst

strength at different excitation levels. Possibly a stronger relationship would emerge to RS than to PS burst strength. In this context, the correlation between ASC_E and RS should also be investigated. This could give information about redundancy in distribution of coordinating information by both ASC_E and DSC, and the relationship between PS and RS parameters, which have not yet been investigated.

Differential Effect on Input Resistance

During ongoing swimmeret activity the coordinating neurons' R_{in} was highest when they were spiking and lowest in the interburst. This is in accordance with results from Smarandache-Wellman and Grätsch (2014), who demonstrated this for ASC_E the first time. In this regard, coordinating neurons were similar to PSE and RSE whose R_{in} is also highest during their active phase (Tschuluun et al., 2009). Several extra- and intracellular processes could have contributed to the distinct changes in R_{in} of ASC_E and DSC. The decrease in R_{in} might result from the increased inhibition by the CPG that hyperpolarized the neurons. The increase in R_{in} during the neurons' active phase could then be a combined effect of the diminished input from the CPG and from additional inactivation of voltage-gated Na^+ channels. As there were indications for I_h in ASC_E and DSC, the deactivation of these channels may also contribute to the increased R_{in} during spiking, and the decreased R_{in} in the hyperpolarized interburst. The contribution of intracellular mechanisms to R_{in} was also obvious when R_{in} was calculated at de- and hyperpolarization of the coordinating neurons. R_{in} was higher when the neuron was depolarized and lower when it was hyperpolarized, even when chemically isolated, demonstrating inward rectification.

Such rectification is present in cat neocortical neurons (Stafstrom et al., 1982). Depolarization towards spike threshold activates a persistent inward current, which paradoxically increases R_{in}. Such a 'negative slope conductance' non-linearly influences the integrative properties for synaptic input in oscillating rat hippocampal neurons (Economo et al., 2014). The authors demonstrate that this leads to selective amplification of both excitatory and inhibitory synaptic input during peak oscillation compared to trough oscillation, which could help in phase-locking the neurons to theta rhythm. Changes in R_{in} depending on membrane potential were also found in locust non-spiking interneurons (Laurent, 1990). There, the decreased R_{in} upon depolarization led to shunting of synaptic input. Conductance increases if resistance decreases, which lowers efficacy of electrotonic propagation. In the case of ASC_E and DSC, the gain of synaptic input would have been decreased in the interburst when R_{in} was low. Hence, the electrotonic propagation of PSPs would be lower in the interburst. This would mean for ASC_E, which appeared to receive mixed IPSPs and EPSPs, that EPSPs in the interburst are less likely to elicit a spike than

during the depolarized phase. This might be a further contribution to determine the spiking phase of the coordinating neurons.

R_{in} also changed when the system's excitation level changed. If the network was intact, R_{in} decreased in both ASC_E and DSC with increased excitation. This is in accordance with the finding that V_m was stable with the network intact although it depolarized with increased excitation if the neurons were isolated. If V_m was stable because of increased inhibition from the CPG R_{in} would decrease accordingly. In contrast, R_{in} increased in the isolated ASC_E with higher carbachol concentration. One current that both depolarizes a neuron and increases its R_{in} is the M-current (I_M, reviewed in Brown, 1988). This is a non-inactivating voltage-gated low threshold K^+ current that can be inhibited by stimulation of muscarinic ACh receptors, first identified in frogs (Brown and Adams, 1980). I_M is present in many vertebrate neurons, e.g. bullfrog sympathetic neurons (Adams et al., 1982), guinea pig hippocampus (Halliwell and Adams, 1982), or turtle motor neurons (Alaburda et al., 2002). It is associated with neuronal excitability because of V_m hyperpolarization in response to depolarization, or V_m depolarization upon muscarinic inhibition. Channels consist of KCNQ3 subunits that form heteromultimers with either KCNQ2 (Wang et al., 1998) or KCNQ5 (Yus-nájera et al., 2003) subunits. Evolutionary, KCNQ2/3 arose during the divergence of extant jawless and jawed vertebrates (Hill et al., 2008). Consequently, I_M has never been described in invertebrates.

However, KCNQ-like K^+ channels have been detected in *C. elegans* (Wei et al., 2005). Those KQT-1 and KQT-2 channels share kinetic similarities with vertebrate KCNQ channels when expressed in *Xenopus* oocytes, including the inhibition by muscarinic agonists. In the cockroach giant interneuron, application of muscarinic agonists depolarizes V_m, which the authors interpret as result of a decreased K^+ conductance (Corronc and Hue, 1993). In crayfish walking leg MNs, the inactivation of a voltage-gated outward K^+ current, which underlies a long-lasting, exclusively muscarine-induced depolarization, has been revealed by Cattaert et al. (1994). This shows that M-like currents can indeed be present in invertebrates. As cholinergic agonists are both able to activate and modulate the swimmeret motor output (Braun and Mulloney, 1993; Mulloney, 1997) it would also be plausible that they help balancing ASC_E's excitability. To reveal I_M-like mechanisms in the swimmeret system, muscarinic and nicotinic agonists could be applied separately to the isolated neurons as first step. One or both pathways could be involved in inhibiting K^+ conductances, which would be represented by depolarization and increase in R_{in}.

Results for changes in DSC's R_{in} in isolation are inconclusive. Further experiments could help to clarify this matter. The discrepancies in R_{in} might arise because of the unknown

channel density for any kind of current at the recording site. Because recordings were made in the dendritic region it is unsure if the recording site was similar across experiments or distributed along the dendritic branches. Like the several different responses of crayfish walking leg MNs to ACh excitation, which all have different underlying mechanisms (Cattaert et al., 1994), different pathways could be activated by cholinergic agonists in the swimmeret system. The observed result would then depend on their relative magnitude near the recording electrode.

The differential effect of system excitation on the isolated and synaptically connected coordinating neurons demonstrates a balancing mechanism by which changes in neural excitability might be counteracted so that a limited number of spikes can encode burst strength distributions.

Encoding Coordinating Information: Conclusions

As discussed above, excitation level could both directly and indirectly influence the activity of the coordinating neurons. Network and intrinsic effects balanced each other. As excitation level increased, PS burst strength also increased but these chemically induced differences in burst strength were not encoded by the coordinating neurons. Rather, these neurons seemed to adapt to the range of expressed burst strengths, therefore encoding relative burst strength. Increasing carbachol concentrations also increased the neurons' excitability by depolarizing V_m. This was opposed by increased inhibition, presumably from the CPG, and intrinsic mechanisms, such as inactivation of Na^+ channels at more depolarized V_m. The possibility to shunt synaptic input during the inhibitory phase might help to determine the spiking phase because this enhances the coordinating neuron's response to driving input during the depolarized phase.

What has not been thoroughly investigated in this study, but was indicated, is that spike threshold could decrease with increased excitation level (Figure 23 C). This would suggest that more Na^+ channels are inactivated in the voltage range covered by V_m oscillations at higher excitation, which in turn supports burst termination as discussed above.

It is still unknown how the system is excited exactly. It can be activated via a proctolinergic and muscarinic pathway, and modulated via a nicotinic pathway (Braun and Mulloney, 1993). Excitatory command neurons release proctolin and unknown transmitters (Acevedo et al., 1994). CCAP-ir positive neurons run through the whole CNS (Trube et al., 1994; Mulloney et al., 1997), and both CCAP and cholinergic agonists directly depolarize isolated MNs (Mulloney et al., 1997; Tschuluun et al., 2009). Morphologically it might be possible that the unknown transmitter of the command neurons is CCAP because CCAP-ir fibers are located in areas that contain their axons (Mulloney et al., 1997). Thus, stimulation

of command neurons would directly release CCAP. On the other hand, command neuron activity could induce CCAP or ACh release from interneurons that would in turn influence the swimmeret system. A third option would be transmitter release from sensory afferents caused by sensory stimulation. Without additional knowledge about transmitter release in the swimmeret system or about command neuron targets this matter remains unresolved.

4.6 Transmitters of Coordinating Neurons

Intracellular Staining and Immunohistochemistry

Intracellular dye injection reliably stained ASC_E and DSC in their home ganglion, the morphology as described by Namba and Mulloney (1999). Details were best preserved if the fixative contained glutaraldehyde. Fixation in paraformaldehyde often let the dye appear clustered because of neurite rupture and leakage during fixation. This is in agreement with Eldred et al. (1983), who investigated the influence of different fixatives for electron microscopic immunohistochemistry. It was not possible to obtain antibody labeling in glutaraldehyde-fixed samples, despite epitope rescue.

5-HT is known to be involved in social status and aggressive motivation (Huber et al., 1997), as well as expression of anxiety-like behavior (Fossat et al., 2014). Furthermore, it can modulate the excitability of the LG (Teshiba et al., 2001) that is involved in the escape tail-flip. A direct effect on the swimmeret system has not been observed (Mulloney et al., 1987), although serotonergic fibers are present in all abdominal ganglia of lobster, especially branching in the LN (Beltz and Kravitz, 1983).

Distribution of serotonergic somata and fibers was similar in all investigated abdominal ganglia. The three ventromedial somata were not as brightly stained in A2 - A5 compared to A1, and not always all three were visible. This could be because the ganglia were larger and antibodies needed longer to penetrate the tissue. Extending the incubation time or removing the ventral ganglion sheath could enhance the antibody staining. Not all of the four lateral small somata were present in all samples. Because of their lateral location, they could have been damaged or destroyed during desheathing. Differences in the number and size of serotonergic somata in A1 compared to A2 - A5 might be a result of the ganglia's different function. In *P. leniusculus*, only A2 - A5 carry functional swimmerets. The limbs of A1 are either missing in females or transformed to gonopods in males.

As neither coordinating neurons' soma nor dendrites nor axon in the home or target ganglion were 5-HT positive it is safe to assume that coordinating neurons are not

serotonergic. Any apparent co-localizations in the images depicted above (see 3.4) are artifacts from projecting the z-stacks in one plane.

Serotonergic fibers branched extensively in the LN so that connections to swimmeret system neurons are possible. However, no effects of 5-HT on active and quiet preparations has been observed (Mulloney et al., 1987). However, the ganglionic sheath was not removed in that study, which might have prevented that an effective amount of 5-HT reached the neurons. In contrast, 5-HT has been shown to have differential effects on walking leg MNs, depending on the presynaptic release location (Bacqué-Cazenave et al., 2013). Together with the differential effect on LG it emphasizes the role of 5-HT as modulator in the crayfish CNS. Assuming that the overall neural organization for limb control is similar in all crayfish ganglia, 5-HT could possibly also modulate the swimmeret system.

MALDI-TOF Mass Spectrometry

With MALDI-TOF MS, we could screen the coordinating neurons for molecules with a certain mass to narrow down the list of putative transmitters. ACh is mainly associated with sensory neurons in the crustacean CNS (Barker et al., 1972; Florey, 1973; Hildebrand et al., 1974). Both ASC_E and DSC but not control MN samples were positive for ACh. Although ACh is released in the axon terminals, it can be detected throughout the cell (pers. comm. Susanne Neupert). The characteristic ions obtained by MS/MS emerge from the loss of trimethylamine from the residual $C_4H_7O_2^+$ (peak at m/z 87.1Da) by a neighboring group attack and formation of protonated trimethylammonium (peak at m/z 60.1Da) (Lioe et al., 2009).

In single-cell mass spectrometry, samples could always be contaminated by surrounding tissue so that false-positive results might be obtained. However, as the somata of coordinating neurons and MNs are located in the same area, and ACh could not be detected in MNs, it is unlikely that the ACh in the samples from coordinating neurons is due to contamination. With PCA analysis, MNs clustered distinctly from the coordinating neurons, further corroborating that ACh is present in coordinating neurons but not MNs. This extenuates the hypothesis that coordinating neurons and MNs originated from the same precursor. Furthermore, the wide spread of data points from coordinating neurons indicates differences in their molecular composition.

Although sample contamination is unlikely in my experiments it cannot be excluded based on the MALDI-TOF MS results. Complementary histochemical and/or electrophysiological experiments should be conducted to confirm ACh as transmitter. Until now, cholinergic neurons have not been identified in the swimmeret system. Braun and Mulloney (1994) investigated ACh esterase activity in the swimmeret system. They found

activity in some somata located in the MN pools, neurites in the LN and MnT, and axons in the connectives. ASC_E is present in all the mentioned locations, so that it could have been among the labeled neurons. ACh esterase is no reliable marker for cholinergic neurons but antibody labeling of ACh transferase has failed so far (Mulloney and Smarandache-Wellmann, 2012). To bypass this problem, antibodies against ACh receptors could be used. If the coordinating neurons use ACh, the postsynaptic neurons, including ComInt 1, should possess cholinergic receptors. Positive labeling of ACh receptors in ComInt 1 would be further evidence that coordinating neurons indeed use ACh at the synapse to the target ComInt 1.

Additionally, electrophysiological experiments with bath application and focal application of ACh agonists and antagonists on ComInt 1 should be conducted. Braun and Mulloney (1993) reported that the antagonists atropine and scopolamine stop the carbachol-induced swimmeret rhythm but do not influence proctolin-induced rhythms. Also, the nicotinic antagonist mecamylamine does not interrupt the proctolin rhythm. As the putative cholinergic synapses in the swimmeret system are between the coordinating neurons and ComInt 1, it is more likely that ACh antagonists would affect the coordination between segments but not the rhythm itself. Whether there were differences in the coordination pattern or not was not investigated in the study by Braun and Mulloney. Recent experiments have shown that bath application of EdCl induced summation of EPSPs in ComInt 1 and therefore an increase in oscillation amplitude (pers. comm. Felix Blumenthal). This supports the hypothesis of a cholinergic synapse in the coordinating circuit. If ASC_E and DSC release ACh onto ComInt 1 and EdCl inhibits the ACh esterase, EPSPs in ComInt 1 would be prolonged and increased in amplitude. The prolongation would also support EPSP summation which is usually not seen in ComInt 1 (Mulloney and Hall, 2003; Smarandache et al., 2009).

4.7 Comparison to Coordination in Other Systems

Coordination of neural networks is studied in many other systems. Until now, the crayfish swimmeret system is the only one investigated that generates the exact same coordinated motor pattern in isolation as the intact animal and in which the necessary and sufficient coordinating interneurons are identified (Mulloney et al., 1987, 2006; Braun and Mulloney, 1993; Namba and Mulloney, 1999). Modeling studies in the swimmeret system revealed that one prerequisite for the specific coordination is the asymmetric coupling by one ascending and one descending coordinating neuron per hemiganglion (Jones et al., 2003;

Zhang et al., 2014). Results from models that are symmetrically coupled by either ascending or descending connections did not match experimental results in phase lag.

In contrast to that, other systems depend to varying extend on sensory feedback for well-organized coordination of distinct CPGs. Leech locomote mainly by either swimming or crawling. Locomotor CPGs are present in each ganglion. The animals swim by sinusoidal anterior to posterior undulations with approximately 20° phase lag between segments (Kristan et al., 1974). In the isolated nervous system, at least six ganglia have to be connected to express robust fictive swimming (Kristan and Calabrese, 1976; Pearce and Friesen, 1985). In contrast to the intact animal, phase lag between segments in the isolated preparation is only 10° (Kristan and Calabrese, 1976; Pearce and Friesen, 1984). In this system, central coordination is achieved by a subset of CPG neurons. Like in crayfish, the intersegmental coordinating connections are asymmetric in that some neurons project in anterior and others in posterior direction. Inhibitory interneurons project in both anterior and posterior direction. Excitatory interneurons project solely posteriorly (Brodfuehrer et al., 1995). As in crayfish, coordinating axons project across multiple segments (Poon et al., 1978; Weeks, 1982; Friesen and Hocker, 2001), and this coupling is sufficient for the anterior to posterior progression of movement (Cang and Friesen, 2002). Despite the presence of central coordinating projections, leeches are also able to coordinate the swimming pattern with sensory feedback only. In this case the intersegmental phase lag is longer than in the intact animal (Yu et al., 1999).

A vertebrate model for swimming is the lamprey. The intact lamprey and its isolated spinal cord generate (fictive) swimming with a phase lag about 1% (McClellan, 1990; Miller and Sigvardt, 2000). Specific coordinating neurons have not been identified in lamprey but neural classes that span the experimentally determined coupling range from 5 to 40 segments are likely candidates (Dale, 1986; Mullins et al., 2011). These candidate neurons also display an asymmetrical organization as in leech and crayfish with ascending and descending projections. Unlike in leech, the phase lag can be maintained in the transected nerve cord by mechanosensory coupling only (McClellan, 1990). Modeling experiments by Ekeberg and Grillner (1999) showed that lampreys need to incorporate mechanosensory input in order to counteract water current and hold their course in running water. Similarly, modelling studies in leech swimming revealed that sensory input is sufficient to directly adapt CPGs to environmental changes (Iwasaki et al., 2014). Those experiments in invertebrates and vertebrates demonstrate that a central mechanism for coordination exists, which is refined by sensory input to exert the proper motor output.

An example for coordinated locomotion that depends - in different species to variable extends - on sensory feedback is insect walking. Terrestrial insects navigate a more heterogeneous environment than swimming animals so that movement patterns need to be more flexible. Central mechanisms in *Manduca* help to generate coordinated motor patterns that are different for larval and adult isolated CNS (Johnston and Levine, 2002). This shows that central coordination can adapt to produce different motor patterns during an animal's life. However, the authors reported that the fictive motor output from the isolated adult CNS differs in details from the activity pattern of intact walking animals. This indicates that sensory input can refine the motor pattern. Another example is deafferented cockroach nervous systems that can generate a coordinated but highly variable motor output without sensory feedback. Movement of single legs is able to entrain all leg CPGs to physiological phases by reducing variability between phases, thus reinforcing the centrally generated patterns (Fuchs et al., 2011, 2012).

In contrast to this example of well-demonstrated central coordinating mechanisms in a fast walking insect is the rather slow walking stick insect. In stick insects, it has been shown that each joint of the three walking legs is driven by its own CPG, respectively. In the deafferented nervous system the phase relationships of these CPGs are largely uncoupled (Büschges et al., 1995). Several experiments have demonstrated that sensory feedback of cuticular strain (i.e. load) and leg joint position signals is of paramount importance for interjoint coordination (Akay et al., 2001, 2004; Bucher et al., 2003). In addition, interleg coordination seems to be mediated predominantly by sensory input and not by central mechanisms. In isolated preparations, one active thoracic segment is not able to elicit rhythmic output from the other segments (Ludwar et al., 2005a). In contrast, sensory input from one segment in semi-intact preparations can modulate the motor activity of other segments, either by inducing rhythmic activity or generally modulate MN activity (Ludwar et al., 2005a; Stein et al., 2006; Borgmann et al., 2007, 2009).

In the insect studies mentioned above, neither the central nor the sensory pathways for coordination of the motor pattern have been identified on the cellular level. Therefore, it is also unknown how the coordinating mechanisms might response to changes in excitation level. However, recent behavioral experiments in *Drosophila* suggest that interleg coordination strength is speed-dependent (Berendes et al., 2016).

Although the swimmeret system is able to generate by central mechanisms a coordinated motor output in isolation that is indistinguishable from that in the intact animal, sensory input can alter the motor activity. Rotational movement and acceleration of the body is sensed via the statocysts located at the antennule bases (Cohen, 1955). This input induces

countersteering movements of the swimmerets to bring the body back to its primary orientation (Hughes and Wiersma, 1960; Neil and Miyan, 1986; Knox and Neil, 1991). In case of rolling in lobster, the swimmerets on the upper body side beat more forcefully than on the lower body side (Davis, 1968). Swimmeret movement on the lower body side can be uncoupled from the contralateral side or even be completely inhibited, although the metachronal wave persists (Neil and Miyan, 1986). This indicates that the circuits encoding burst strength on the two body sides can function independent of each other.

The swimmerets itself send many sensory afferents to the CNS that can modulate the motor output similar as seen in insects. Spiking sensory afferents from the rami report on cuticular deformation during movement, and deflection of the feathered hairs by water flow (Killian and Page, 1992a, 1992b). Joint angles of the swimmerets are encoded by spiking and non-spiking stretch receptors (NSSR) (Heitler, 1982; Neil and Miyan, 1986). NSSRs respond to stimulation of the basi-coxal joint with depolarization during PS and hyperpolarization during RS. Injection of de- and hyperpolarizing current decreases or increases PS activity, respectively (Heitler, 1982, 1986; MacMillan and Deller, 1989). Isolated preparations revealed that NSSRs oscillate in phase with the motor rhythm, probably driven by the CPG (Paul, 1989). Similar to single-leg stepping preparations in insects, movement of one single swimmeret can entrain the rhythm of an otherwise deafferented swimmeret system (MacMillan and Deller, 1989). If all swimmerets are attached, entrainment becomes more rigorous if three swimmerets are moved with an imposed frequency, compared to one or two swimmerets (Deller and MacMillan, 1989). Although the site of synaptic integration from sensory systems is not yet identified, recent experiments have shown that the state of the NSSRs directly influence the efference copies of ASC_E and DSC and therefore the motor output of their target ganglia (Mulloney et al., 2014). All this demonstrates that although the swimmeret system can produce the properly coordinated motor output based on its hardwiring it is flexible enough to incorporate sensory stimuli, hence adapting to the environment.

5 Conclusions and Outlook

The present study illustrates how coordinating neurons in the crayfish swimmeret system encode information about their home ganglion's activity state. The interplay of several mechanisms allows the encoding of coordinated motor output at different excitation levels. The results support the Adaptive Encoding Hypothesis in that the encoding properties were tuned by the system's excitation level.

Bursts of ASC_E and DSC were shaped in different ways. ASC_E was oscillating and spiking on top of a tonic depolarization. DSC activity occurred in bursts because the tonically active neuron was inhibited phasically during PS. At least in ASC_E, interburst history influences the amount of spikes generated in each burst. Intraburst hysteresis together with the ability to spike on rebound might help to control the correct phase of activity.

My experiments suggest that the coordinating neurons receive input from additional afferent neurons besides the CPG. Simultaneous intracellular recordings can help to identify other presynaptic neurons. Identifying these neurons further enhances our understanding in how the swimmeret system works in detail. ASC_E's depolarization could be the action of a preparatory network. Such an additional network could bring ASC_E and MNs closer to threshold so that coordinated movement can be performed accurately if needed. In other systems, voltage-sensitive dyes (VSD) (Miller et al., 2012), which have a higher fidelity to voltage changes than calcium imaging, were used to identify unknown components and connections of networks, such as in leech (Frady et al., 2016), *Tritonia* (Hill et al., 2015), or mouse (Willadt et al., 2014). Using VSD could prove difficult in the swimmeret system because all neurons that are known to participate in the execution and coordination of the swimmeret rhythm are densely packed in and around the LN in each ganglion. Electrical activity in their somata is very weak and all the neurites are intermingled in the LN. Hence, it might be hard to distinguish individual neurons. On the other hand, VSDs could help to identify ascending and descending neurons in the connectives. The parallel organization of axons in the connective could make identification of specific axons easier than in the intermingled crossing neurites in the neuropils. For example, command neurons and coordinating neurons run in different areas of the connectives and could thus be easier to delineate than the overlapping neurites in the LN.

The coordinating neurons adapted to changes in the excitation level so that they encoded relative burst strengths. Several processes appeared to be co-regulated so that the number of coordinating spikes per burst encoded the relative PS burst strength. As excitation increased, the neurons' depolarization and lowered threshold indicated that their own

excitability also increased. In the intact network, this excitability was counteracted by what seemed to be stronger synaptic inhibition as indicated by decreases in R_{in}. Additionally, the mechanisms underlying hysteresis may contribute to an intrinsic reduction in excitability: Spike-frequency adaptation can limit the amount of spikes generated during each burst. Besides the inactivation of Na^+ channels and activation of K^+ outward currents, I_M and I_h have also been shown to be involved in spike-frequency adaptation. In rat hippocampal neurons, opening of M-channels or h-channels (depending on voltage) is involved in afterhyperpolarizations; thus I_M and I_h are key currents in regulating the neuron's excitability (Gu et al., 2005). How afterhyperpolarizations regulate excitability was not investigated in this study because they were not clearly detectable at the recording site.

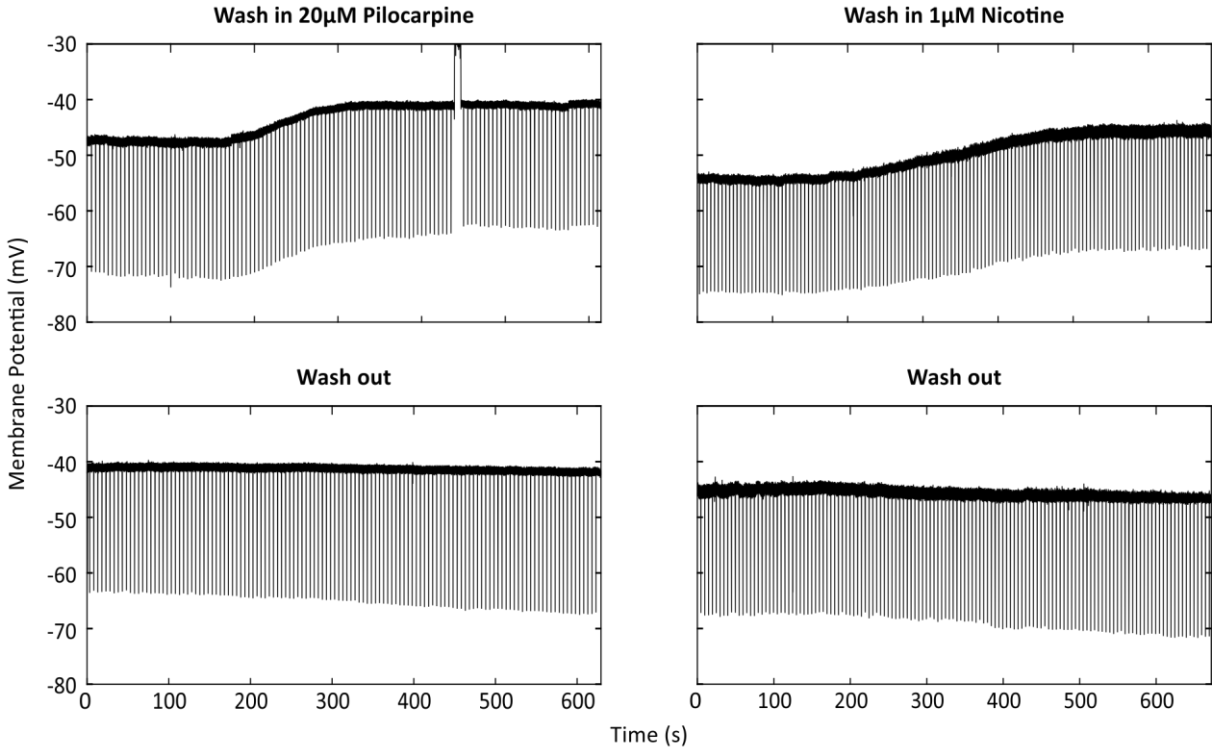

Figure 38: Effect of pilocarpine and nicotine on the membrane potential of a chemically isolated ASC_E. Both substances depolarized the neuron but wash out with $LowCa^{2+}$ saline + TTX did not hyperpolarize the neuron to its previous membrane potential. Sharp deflections in membrane potential are from current injections to measure R_{in} or compensate electrode capacity.

Besides I_h, indications for the presence of an M-like current were demonstrated in this study. This needs to be investigated further because so far only indications exist for an M-like current in invertebrates and no detailed description. Blocking of I_M by muscarinic agonists is especially interesting in the swimmeret system. The system can be activated via a muscarinic pathway, whereas modulation of the motor activity is mainly controlled by an nicotinic pathway (Braun and Mulloney, 1993). Preliminary experiments have shown that

both the muscarinic agonist pilocarpine and nicotine depolarized V_m of isolated coordinating neurons (Figure 38). Results from measuring R_{in} were so far inconclusive because the substances apparently did not wash out after 30min perfusion, in contrast to carbachol. Mulloney et al. (1987) stated that wash out of pilocarpine did not reset the system to its initial activity even after 2h washing. An alternative approach to identify a possible M-like current would be to perform single-electrode voltage clamp. With this, additional currents contributing to the coordinating neurons' adaptation could be identified. To further investigate ASC_E's and DSC's input/output functions at different excitation levels, the ramp stimulation protocol could be extended as proposed in 4.3. As the swimmeret system consists of oscillators, investigating resonance frequencies of coordinating neurons could bring additional insights of their adaptation properties. Resonance might be influenced by excitation level and period, controlling the voltage difference to threshold by oscillation amplitude.

ACh was identified by mass spectrometry as putative transmitter of ASC_E and DSC. This finding needs to be corroborated by immunohistochemical or electrophysiological experiments. So far, antibody labeling of ACh transferase has failed in crayfish (Mulloney and Smarandache-Wellmann, 2012). Recordings from ComInt 1 revealed that the EPSPs elicited by coordinating neurons summate, hence increasing and smoothing oscillation amplitude, if the preparation is perfused with CCAP + EdCl (pers. comm. Felix Blumenthal). This would be expected if coordinating neurons release ACh at the synapse to ComInt 1, when EdCl inhibits the ACh esterase. ACh would bind longer to the receptors, increasing EPSP amplitude and duration, which would result in summation. A detailed examination of this effect is necessary. Focal application of ACh agonists and antagonists at the midline could reveal any effects on synaptic transmission from the coordinating neurons.

As complementary experiments, the effect of excitation on ComInt 1's decoding properties should be investigated. The decoding properties could also be tuned as the Adaptive Encoding Hypothesis predicts. On the other hand, ComInt 1 could be a hub neuron that only integrates coordinating input and relays it to the CPG. In this case, the CPG neurons must be tuned by excitation level to interpret the coordinating information correctly.

Mathematical modeling is a valuable tool in neuroscience because it complements and predicts outcomes from real experiments. Early simplified models of the swimmeret system, before the coordinating neuron's mode of operation and connectivity was identified, made the following predictions. The coordinating neurons are driven by the CPG, the excitation level influences the oscillator's intrinsic period but not exclusively coupling strength, and

the coupling must be asymmetrical to maintain a period-independent phase lag (Skinner et al., 1997; Skinner and Mulloney, 1998; Jones et al., 2003; Zhang et al., 2014). With respect to coordination, the influence and importance of sensory feedback and central interactions have been studied in a variety of vertebrate and invertebrate models (e.g. Ekeberg and Grillner, 1999; Daun–Gruhn and Tóth, 2011; Iwasaki et al., 2014). For multi-legged walking, these models give possible solutions for transitions between coordination patterns (Daun–Gruhn and Tóth, 2011; Grabowska et al., 2015; Tóth and Daun-Gruhn, 2016). In the existing models of the swimmeret system some neuronal connections were modeled on assumptions that later turned out to be not true, e.g. excitatory synapses from the CPG to the coordinating neurons or multiple targets for coordinating information (Skinner and Mulloney, 1998; Jones et al., 2003). With an updated model, the questions could be answered if different burst shaping mechanisms in the coordinating neurons are necessary for a stable phase lag, and to which extend system excitation level needs to influence CPG and coordinating neurons to produce a stable output. Furthermore, models of single neurons could help to predict how ionic currents interact that underlie the here observed hysteresis and adaptive mechanisms. In addition, the putative influence of proprioceptive and other sensory input might be anticipated.

The small number of neurons and their identified connections to produce the well-coordinated motor output of the swimmeret system makes the system amenable to modeling studies, and to infer a canonical mechanism for coordination of distributed oscillators at diverse system states.

Bibliography

Acevedo LD, **Hall WM**, **Mulloney B**. Proctolin and excitation of the crayfish swimmeret system. *J Comp Neurol* 345: 612–627, 1994.

Adams PR, **Brown DA**, **Constanti A**. M-currents and other potassium currents in bullfrog sympathetic neurones. *J Physiol* 330: 537–572, 1982.

Akay T, **Bässler U**, **Gerharz P**, **Büschges A**. The Role of Sensory Signals From the Insect Coxa-Trochanteral Joint in Controlling Motor Activity of the Femur-Tibia Joint. *J Neurophysiol* 85: 594–604, 2001.

Akay T, **Haehn S**, **Schmitz J**, **Büschges A**. Signals From Load Sensors Underlie Interjoint Coordination During Stepping Movements of the Stick Insect Leg. *J Neurophysiol* 92: 42–51, 2004.

Alaburda A, **Perrier J-F**, **Hounsgaard J**. An M-like outward current regulates the excitability of spinal motoneurones in the adult turtle. *J Physiol* 540: 875–881, 2002.

Alving BO. Spontaneous Activity in Isolated Somata of Aplysia Pacemaker Neurons. *J Gen Physiol* 51: 29–45, 1968.

Amantonico A, **Urban PL**, **Fagerer SR**, **Balabin RM**, **Zenobi R**. Single-Cell MALDI-MS as an Analytical Tool for Studying Intrapopulation Metabolic Heterogeneity of Unicellular Organisms. *Anal Chem* 82: 7394–7400, 2010.

Angstadt JD, **Calabrese RL**. A hyperpolarization-activated inward current in heart interneurons of the medicinal leech. *J Neurosci* 9: 2846–2857, 1989.

Atwood HL, **Wiersma CAG**. Command Interneurons in the Crayfish Central Nervous System. *J Exp Biol* 46: 249–261, 1967.

Backus AR, **Schoffelen J-M**, **Szebényi S**, **Hanslmayr S**, **Doeller CF**. Hippocampal-Prefrontal Theta Oscillations Support Memory Integration. *Curr Biol* 26: 450–457, 2016.

Bacqué-Cazenave J, **Issa FA**, **Edwards DH**, **Cattaert D**. Spatial segregation of excitatory and inhibitory effects of 5-HT on crayfish motoneurons. *J Neurophysiol* 109: 2793–2802, 2013.

Bal T, **Nagy F**, **Moulins M**. The pyloric central pattern generator in Crustacea: a set of conditional neuronal oscillators. *J Comp Physiol A* 163: 715–727, 1988.

Barker DL, **Herbert E**, **Hildebrand JG**, **Kravitz EA**. Acetylcholine and lobster sensory neurones. *J Physiol* 226: 205–229, 1972.

Barlow HB. Possible Principles Underlying the Transformations of Sensory Messages. In: *Sensory Communication*, edited by Rosenblith WA. Cambridge: MIT Press, 1961, p. 217–234.

Bartos M, **Manor Y**, **Nadim F**, **Marder E**, **Nusbaum MP**. Coordination of Fast and Slow Rhythmic Neuronal Circuits. *J Neurosci* 19: 6650–6660, 1999.

Beltz BS, **Kravitz EA**. Mapping of serotonin-like immunoreactivity in the lobster nervous system. *J Neurosci* 3: 585–602, 1983.

Bennett DJ, **Hultborn H**, **Fedirchuk B**, **Gorassini M**. Short-Term Plasticity in Hindlimb Motoneurons of Decerebrate Cats. *J Neurophysiol* 80: 2038–2045, 1998.

Bennett DJ, **Li Y**, **Siu M**. Plateau Potentials in Sacrocaudal Motoneurons of Chronic Spinal Rats, Recorded In Vitro. *J Neurophysiol* 86: 1955–1971, 2001.

Berendes V, **Zill SN**, **Büschges A**, **Bockemühl T**. Speed-dependent interplay between local pattern-generating activity and sensory signals during walking in *Drosophila*. *J Exp Biol* 219: 3781–3793, 2016.

Borgmann A, **Hooper SL**, **Büschges A**. Sensory Feedback Induced by Front-Leg Stepping Entrains the Activity of Central Pattern Generators in Caudal Segments of the Stick Insect Walking System. *J Neurosci* 29: 2972–2983, 2009.

Borgmann A, **Scharstein H**, **Büschges A**. Intersegmental Coordination: Influence of a Single Walking Leg on the Neighboring Segments in the Stick Insect Walking System. *J Neurophysiol* 98: 1685–1696, 2007.

Bose A, **Manor Y**, **Nadim F**. The Activity Phase of Postsynaptic Neurons in a Simplified Rhythmic Network. *J Comput Neurosci* 17: 245–261, 2004.

Braun G, **Mulloney B**. Cholinergic modulation of the swimmeret motor system in crayfish. *J Neurophysiol* 70: 2391–2398, 1993.

Braun G, **Mulloney B**. Acetylcholinesterase activity in neurons of crayfish abdominal ganglia. *J Comp Neurol* 350: 272–280, 1994.

Braun G, **Mulloney B**. Coordination in the crayfish swimmeret system: differential excitation causes changes in intersegmental phase. *J Neurophysiol* 73: 880–885, 1995.

Brodfuehrer PD, **Debski EA**, **O'Gara BA**, **Friesen WO**. Neuronal control of leech swimming. *J Neurobiol* 27: 403–418, 1995.

Brown DA. M-currents: an update. *Trends Neurosci* 11: 294–299, 1988.

Brown DA, **Adams PR**. Muscarinic suppression of a novel voltage-sensitive K^+ current in a vertebrate neurone. *Nature* 283: 673–676, 1980.

Brown TG. The Intrinsic Factors in the Act of Progression in the Mammal. *Proc R Soc Lond B Biol Sci* 84: 308–319, 1911.

Bucher D, **Akay T**, **DiCaprio RA**, **Büschges A**. Interjoint Coordination in the Stick Insect Leg-Control System: The Role of Positional Signaling. *J Neurophysiol* 89: 1245–1255, 2003.

Burrows M, **Siegler MV**. Graded synaptic transmission between local interneurones and motor neurones in the metathoracic ganglion of the locust. *J Physiol* 285: 231–255, 1978.

Büschges A, **Ludwar BC**, **Bucher D**, **Schmidt J**, **DiCaprio RA**. Synaptic drive contributing to rhythmic activation of motoneurons in the deafferented stick insect walking system. *Eur J Neurosci* 19: 1856–1862, 2004.

Büschges A, **Schmitz J**, **Bässler U**. Rhythmic patterns in the thoracic nerve cord of the stick insect induced by pilocarpine. *J Exp Biol* 198: 435–456, 1995.

Cang J, **Friesen WO**. Model for Intersegmental Coordination of Leech Swimming: Central and Sensory Mechanisms. *J Neurophysiol* 87: 2760–2769, 2002.

Carlson BA. Temporal-Pattern Recognition by Single Neurons in a Sensory Pathway Devoted to Social Communication Behavior. *J Neurosci* 29: 9417–9428, 2009.

Cattaert D, **Araque A**, **Buno W**, **Clarac F**. Nicotinic and muscarinic activation of motoneurons in the crayfish locomotor network. *J Neurophysiol* 72: 1622–1633, 1994.

Cattaert D, **Clarac F**. Influence of walking on swimmeret beating in the lobster *Homarus gammarus*. *J Neurobiol* 14: 421–439, 1983.

Cazalets JR, **Borde M**, **Clarac F**. The synaptic drive from the spinal locomotor network to motoneurons in the newborn rat. *J Neurosci* 16: 298–306, 1996.

Chrachri A. Ionic currents in identified swimmeret motor neurones of the crayfish *Pacifastacus leniusculus*. *J Exp Biol* 198: 1483–1492, 1995.

Chrachri A, **Neil DM**. Interaction and synchronization between two abdominal motor systems in crayfish. *J Neurophysiol* 69: 1373–1383, 1993.

Cohen AH, **Wallén P**. The neuronal correlate of locomotion in fish. "Fictive swimming" induced in an in vitro preparation of the lamprey spinal cord. *Exp Brain Res* 41: 11–18, 1980.

Cohen MJ. The function of receptors in the statocyst of the lobster *Homarus americanus*. *J Physiol* 130: 9–34, 1955.

Corronc HL, **Hue B**. Pharmacological and Electrophysiological Characterization of a Postsynaptic Muscarinic Receptor in the Central Nervous System of the Cockroach. *J Exp Biol* 181: 257–278, 1993.

Dale N. Excitatory synaptic drive for swimming mediated by amino acid receptors in the lamprey. *J Neurosci* 6: 2662–2675, 1986.

Daun–Gruhn S, **Tóth TI**. An inter-segmental network model and its use in elucidating gait-switches in the stick insect. *J Comput Neurosci* 31: 43–60, 2011.

Davis WJ. Lobster Righting Responses and their Neural Control. *Proc R Soc Lond B Biol Sci* 170: 435–456, 1968.

Davis WJ. The Neural Control of Swimmeret Beating in the Lobster. *J Exp Biol* 50: 99–117, 1969.

Davis WJ, **Kennedy D**. Command interneurons controlling swimmeret movements in the lobster. I. Types of effects on motoneurons. *J Neurophysiol* 35: 1–12, 1972a.

Davis WJ, **Kennedy D**. Command interneurons controlling swimmeret movements in the lobster. II. Interaction of effects on motoneurons. *J Neurophysiol* 35: 13–19, 1972b.

Dean I, **Harper NS**, **McAlpine D**. Neural population coding of sound level adapts to stimulus statistics. *Nat Neurosci* 8: 1684–1689, 2005.

Deller SRT, **MacMillan DL**. Entrainment of the Swimmeret Rhythm of the Crayfish to Controlled Movements of Some of the Appendages. *J Exp Biol* 144: 257–278, 1989.

Economo MN, **Martínez JJ**, **White JA**. Membrane potential-dependent integration of synaptic inputs in entorhinal stellate neurons. *Hippocampus* 24: 1493–1505, 2014.

Edman Å, **Theander S**, **Grampp W**. Functional effects of a hyperpolarization-activated membrane current in the lobster stretch receptor neurone. *Acta Physiol Scand* 146: 221–232, 1992.

Ekeberg O, **Grillner S**. Simulations of Neuromuscular Control in Lamprey Swimming. *Philos Trans Biol Sci* 354: 895–902, 1999.

Eldred WD, **Zucker C**, **Karten HJ**, **Yazulla S**. Comparison of fixation and penetration enhancement techniques for use in ultrastructural immunocytochemistry. *J Histochem Cytochem* 31: 285–292, 1983.

Elson RC, **Huerta R**, **Abarbanel HDI**, **Rabinovich MI**, **Selverston AI**. Dynamic Control of Irregular Bursting in an Identified Neuron of an Oscillatory Circuit. *J Neurophysiol* 82: 115–122, 1999.

Flamm RE, **Harris-Warrick RM**. Aminergic modulation in lobster stomatogastric ganglion. I. Effects on motor pattern and activity of neurons within the pyloric circuit. *J Neurophysiol* 55: 847–865, 1986a.

Flamm RE, **Harris-Warrick RM**. Aminergic modulation in lobster stomatogastric ganglion. II. Target neurons of dopamine, octopamine, and serotonin within the pyloric circuit. *J Neurophysiol* 55: 866–881, 1986b.

Florey E. Acetylcholine as sensory transmitter in crustacea. *J Comp Physiol* 83: 1–16, 1973.

Fossat P, **Bacqué-Cazenave J**, **Deurwaerdère PD**, **Delbecque J-P**, **Cattaert D**. Anxiety-like behavior in crayfish is controlled by serotonin. *Science* 344: 1293–1297, 2014.

Frady EP, **Kapoor A**, **Horvitz E**, **Kristan Jr. WB**. Scalable Semisupervised Functional Neurocartography Reveals Canonical Neurons in Behavioral Networks. *Neural Comput* 28: 1453–1497, 2016.

Friesen WO, **Hocker CG**. Functional Analyses of the Leech Swim Oscillator. *J Neurophysiol* 86: 824–835, 2001.

Frost WN, **Katz PS**. Single neuron control over a complex motor program. *Proc Natl Acad Sci* 93: 422–426, 1996.

Fuchs E, **Holmes P**, **David I**, **Ayali A**. Proprioceptive feedback reinforces centrally generated stepping patterns in the cockroach. *J Exp Biol* 215: 1884–1891, 2012.

Fuchs E, **Holmes P**, **Kiemel T**, **Ayali A**. Intersegmental coordination of cockroach locomotion: adaptive control of centrally coupled pattern generator circuits. *Front Neural Circuits* 4: 125, 2011.

Galler S, **Rathmayer W**. Shortening velocity and force/pCa relationship in skinned crab muscle fibres of different types. *Pflüg Arch* 420: 187–193, 1992.

Gammie SC, **Truman JW**. Neuropeptide Hierarchies and the Activation of Sequential Motor Behaviors in the Hawkmoth, Manduca sexta. *J Neurosci* 17: 4389–4397, 1997.

Garcia VJ, **Daur N**, **Temporal S**, **Schulz DJ**, **Bucher D**. Neuropeptide Receptor Transcript Expression Levels and Magnitude of Ionic Current Responses Show Cell Type-Specific Differences in a Small Motor Circuit. *J Neurosci* 35: 6786–6800, 2015.

Gariépy J-F, **Missaghi K**, **Chevallier S**, **Chartré S**, **Robert M**, **Auclair F**, **Lund JP**, **Dubuc R**. Specific neural substrate linking respiration to locomotion. *Proc Natl Acad Sci U S A* 109: E84–E92, 2012.

Getting PA, **Dekin MS**. Mechanisms of pattern generation underlying swimming in *Tritonia*. IV. Gating of central pattern generator. *J Neurophysiol* 53: 466–480, 1985.

Getting PA, **Lennard PR**, **Hume RI**. Central pattern generator mediating swimming in *Tritonia*. I. Identification and synaptic interactions. *J Neurophysiol* 44: 151–164, 1980.

Gloveli T, **Egorov AV**, **Schmitz D**, **Heinemann U**, **Müller W**. Carbachol-induced changes in excitability and $[Ca^{2+}]_i$ signalling in projection cells of medial entorhinal cortex layers II and III. *Eur J Neurosci* 11: 3626–3636, 1999.

Gorman AL, **Thomas MV**. Changes in the intracellular concentration of free calcium ions in a pace-maker neurone, measured with the metallochromic indicator dye arsenazo III. *J Physiol* 275: 357–376, 1978.

Grabowska M, **Toth TI**, **Smarandache-Wellmann C**, **Daun-Gruhn S**. A network model comprising 4 segmental, interconnected ganglia, and its application to simulate multi-legged locomotion in crustaceans. *J Comput Neurosci* 38: 601–616, 2015.

Gramoll S, **Schmidt J**, **Calabrese RL**. Switching in the activity state of an interneuron that controls coordination of the hearts in the medicinal leech (*Hirudo medicinalis*). *J Exp Biol* 186: 157–171, 1994.

Gu N, **Vervaeke K**, **Hu H**, **Storm JF**. Kv7/KCNQ/M and HCN/h, but not $K_{Ca}2$/SK channels, contribute to the somatic medium after-hyperpolarization and excitability control in CA1 hippocampal pyramidal cells. *J Physiol* 566: 689–715, 2005.

Halliwell JV, **Adams PR**. Voltage-clamp analysis of muscarinic excitation in hippocampal neurons. *Brain Res* 250: 71–92, 1982.

Harris-Warrick RM. Neuromodulation and flexibility in Central Pattern Generator networks. *Curr Opin Neurobiol* 21: 685–692, 2011.

Harris-Warrick RM, **Coniglio LM**, **Levini RM**, **Gueron S**, **Guckenheimer J**. Dopamine modulation of two subthreshold currents produces phase shifts in activity of an identified motoneuron. *J Neurophysiol* 74: 1404–1420, 1995.

Hedwig B, **Pearson KG**. Patterns of synaptic input to identified flight motoneurons in the locust. *J Comp Physiol A* 154: 745–760, 1984.

Heitler WJ. Non-Spiking Stretch-Receptors in the Crayfish Swimmeret System. *J Exp Biol* 96: 355–366, 1982.

Heitler WJ. Aspects of Sensory Integration in the Crayfish Swimmeret System. *J Exp Biol* 120: 387–402, 1986.

Heitler WJ, **Pearson KG**. Non-spiking interactions and local interneurones in the central pattern generator of the crayfish swimmeret system. *Brain Res* 187: 206–211, 1980.

Henze DA, **Buzsáki G**. Action potential threshold of hippocampal pyramidal cells in vivo is increased by recent spiking activity. *Neuroscience* 105: 121–130, 2001.

Higgs MH, **Spain WJ**. Kv1 channels control spike threshold dynamics and spike timing in cortical pyramidal neurones. *J Physiol* 589: 5125–5142, 2011.

Hildebrand JG, **Townsel JG**, **Kravitz EA**. Distribution of Acetylcholine, Choline, Choline Acetyltransferase and Acetylcholinesterase in Regions and Single Identified Axons of the Lobster Nervous System. *J Neurochem* 23: 951–963, 1974.

Hill AS, **Nishino A**, **Nakajo K**, **Zhang G**, **Fineman JR**, **Selzer ME**, **Okamura Y**, **Cooper EC**. Ion Channel Clustering at the Axon Initial Segment and Node of Ranvier Evolved Sequentially in Early Chordates. *PLOS Genet* 4: e1000317, 2008.

Hill AV. Excitation and Accommodation in Nerve. *Proc R Soc Lond B Biol Sci* 119: 305–355, 1936.

Hill ES, **Vasireddi SK**, **Wang J**, **Bruno AM**, **Frost WN**. Memory Formation in *Tritonia* via Recruitment of Variably Committed Neurons. *Curr Biol* 25: 2879–2888, 2015.

Hodgkin AL, **Huxley AF**. A quantitative description of membrane current and its application to conduction and excitation in nerve. *J Physiol* 117: 500–544, 1952.

Hounsgaard J, **Hultborn H**, **Jespersen B**, **Kiehn O**. Bistability of alpha-motoneurones in the decerebrate cat and in the acute spinal cat after intravenous 5-hydroxytryptophan. *J Physiol* 405: 345–367, 1988.

https://metlin.scripps.edu/index.php. Scripps Center For Metabolomics and Mass Spectrometry - METLIN [Online]. *METLIN* date unknown. https://metlin.scripps.edu/index.php [4 Jan. 2016].

Huber R, **Smith K**, **Delago A**, **Isaksson K**, **Kravitz EA**. Serotonin and aggressive motivation in crustaceans: Altering the decision to retreat. *Proc Natl Acad Sci* 94: 5939–5942, 1997.

Hughes GM, **Wiersma CAG**. The Coordination of Swimmeret Movements in the Crayfish, *Procambarus clarkii* (Girard). *J Exp Biol* 37: 657–670, 1960.

Huxley TH. *The Crayfish : An Introduction to the Study of Zoology*. 1st ed. London: C. Kegan Paul & Co., 1880.

Ikeda K, **Wiersma CAG**. Autogenic rhythmicity in the abdominal ganglia of the crayfish: The control of swimmeret movements. *Comp Biochem Physiol* 12: 107–115, 1964.

Ivanov AI, **Calabrese RL**. Intracellular Ca^{2+} Dynamics During Spontaneous and Evoked Activity of Leech Heart Interneurons: Low-Threshold Ca Currents and Graded Synaptic Transmission. *J Neurosci* 20: 4930–4943, 2000.

Iwasaki T, **Chen J**, **Friesen WO**. Biological clockwork underlying adaptive rhythmic movements. *Proc Natl Acad Sci* 111: 978–983, 2014.

Jahnsen H, **Llinás R**. Ionic basis for the electro-responsiveness and oscillatory properties of guinea-pig thalamic neurones in vitro. *J Physiol* 349: 227–247, 1984.

Johnson BR, **Harris-Warrick RM**. Aminergic modulation of graded synaptic transmission in the lobster stomatogastric ganglion. *J Neurosci* 10: 2066–2076, 1990.

Johnston RM, **Levine RB**. Thoracic leg motoneurons in the isolated CNS of adult *Manduca* produce patterned activity in response to pilocarpine, which is distinct from that produced in larvae. *Invert Neurosci* 4: 175–192, 2002.

Jones SR, **Mulloney B**, **Kaper TJ**, **Kopell N**. Coordination of Cellular Pattern-Generating Circuits that Control Limb Movements: The Sources of Stable Differences in Intersegmental Phases. *J Neurosci* 23: 3457–3468, 2003.

Kahn JA. Patterns of synaptic inhibition in motoneurons and interneurons during fictive swimming in the lamprey, as revealed by Cl– injections. *J Comp Physiol* 147: 189–194, 1982.

Kehrmann J, **Wessel S**, **Murali R**, **Hampel A**, **Bange F-C**, **Buer J**, **Mosel F**. Principal component analysis of MALDI TOF MS mass spectra separates *M. abscessus (sensu stricto)* from *M. massiliense* isolates. *BMC Microbiol* 16, 2016.

Killian KA, **Page CH**. Mechanosensory afferents innervating the swimmerets of the lobster. I. Afferents activated by cuticular deformation. *J Comp Physiol [A]* 170: 491–500, 1992a.

Killian KA, **Page CH**. Mechanosensory afferents innervating the swimmerets of the lobster. II. Afferents activated by hair deflection. *J Comp Physiol [A]* 170: 501–508, 1992b.

Knox PC, **Neil DM**. The Coordinated Action of Abdominal Postural and Swimmeret Motor Systems in Relation to Body Tilt in the Pitch Plane in the Norway Lobster *Nephrops Norvegicus*. *J Exp Biol* 155: 605–627, 1991.

Kristan WB, **Calabrese RL**. Rhythmic swimming activity in neurones of the isolated nerve cord of the leech. *J Exp Biol* 65: 643–668, 1976.

Kristan WB, **Stent GS**, **Ort CA**. Neuronal control of swimming in the medicinal leech. *J Comp Physiol* 94: 97–119, 1974.

Laughlin S. A Simple Coding Procedure Enhances a Neuron's Information Capacity. *Z Für Naturforschung C* 36: 910–912, 1981.

Laurent G. Voltage-dependent nonlinearities in the membrane of locust nonspiking local interneurons, and their significance for synaptic integration. *J Neurosci* 10: 2268–2280, 1990.

Lennard PR, **Getting PA**, **Hume RI**. Central pattern generator mediating swimming in *Tritonia*. II. Initiation, maintenance, and termination. *J Neurophysiol* 44: 165–173, 1980.

Lewis DV, **Wilson WA**. Calcium influx and poststimulus current during early adaptation in *Aplysia* giant neurons. *J Neurophysiol* 48: 202–216, 1982.

Lioe H, **Barlow CK**, **O'Hair RAJ**. How does acetylcholine lose trimethylamine? A density functional theory study of four competing mechanisms. *J Am Soc Mass Spectrom* 20: 238–246, 2009.

Liu Y-B, **Guo J-Z**, **Chiappinelli VA**. Nicotinic receptor–mediated biphasic effect on neuronal excitability in chick lateral spiriform neurons. *Neuroscience* 148: 1004–1014, 2007.

Ludwar BC, **Göritz ML**, **Schmidt J**. Intersegmental Coordination of Walking Movements in Stick Insects. *J Neurophysiol* 93: 1255–1265, 2005a.

Ludwar BC, **Westmark S**, **Büschges A**, **Schmidt J**. Modulation of Membrane Potential in Mesothoracic Moto- and Interneurons During Stick Insect Front-Leg Walking. *J Neurophysiol* 94: 2772–2784, 2005b.

MacMillan DL, **Deller SR**. Sensory Systems in the Swimmerets of the Crayfish *Cherax Destructor* and their Effectiveness in Entraining the Swimmeret Rhythm. *J Exp Biol* 144: 279–301, 1989.

Maravall M, **Petersen RS**, **Fairhall AL**, **Arabzadeh E**, **Diamond ME**. Shifts in Coding Properties and Maintenance of Information Transmission during Adaptation in Barrel Cortex. *PLOS Biol* 5: e19, 2007.

McClellan AD. Locomotor recovery in spinal-transected lamprey: Regenerated spinal coordinating neurons and mechanosensory inputs couple locomotor activity across a spinal lesion. *Neuroscience* 35: 675–685, 1990.

McCormick DA, **Huguenard JR**. A model of the electrophysiological properties of thalamocortical relay neurons. *J Neurophysiol* 68: 1384–1400, 1992.

McCormick DA, **Prince DA**. Actions of acetylcholine in the guinea-pig and cat medial and lateral geniculate nuclei, in vitro. *J Physiol* 392: 147–165, 1987.

Meng W, **Wang S-H**, **Li D-F**. Carbachol-Induced Reduction in the Activity of Adult Male Zebra Finch RA Projection Neurons. *Neural Plast* 2016: e7246827, 2016.

Miller EW, **Lin JY**, **Frady EP**, **Steinbach PA**, **Kristan WB**, **Tsien RY**. Optically monitoring voltage in neurons by photo-induced electron transfer through molecular wires. *Proc Natl Acad Sci* 109: 2114–2119, 2012.

Miller JP, **Selverston AI**. Mechanisms underlying pattern generation in lobster stomatogastric ganglion as determined by selective inactivation of identified neurons. II. Oscillatory properties of pyloric neurons. *J Neurophysiol* 48: 1378–1391, 1982.

Miller WL, **Sigvardt KA**. Extent and Role of Multisegmental Coupling in the Lamprey Spinal Locomotor Pattern Generator. *J Neurophysiol* 83: 465–476, 2000.

Mullins OJ, **Hackett JT**, **Buchanan JT**, **Friesen WO**. Neuronal control of swimming behavior: Comparison of vertebrate and invertebrate model systems. *Prog Neurobiol* 93: 244–269, 2011.

Mulloney B. A Test of the Excitability-Gradient Hypothesis in the Swimmeret System of Crayfish. *J Neurosci* 17: 1860–1868, 1997.

Mulloney B. During fictive locomotion, graded synaptic currents drive bursts of impulses in swimmeret motor neurons. *J Neurosci* 23: 5953–5962, 2003.

Mulloney B. A method to measure the strength of multi-unit bursts of action potentials. *J Neurosci Methods* 146: 98–105, 2005.

Mulloney B, **Acevedo LD**, **Bradbury AG**. Modulation of the crayfish swimmeret rhythm by octopamine and the neuropeptide proctolin. *J Neurophysiol* 58: 584–597, 1987.

Mulloney B, **Hall WM**. GABA-ergic neurons in the crayfish nervous system: An immunocytochemical census of the segmental ganglia and stomatogastric system. *J Comp Neurol* 291: 383–394, 1990.

Mulloney B, **Hall WM**. Functional organization of crayfish abdominal ganglia. III. Swimmeret motor neurons. *J Comp Neurol* 419: 233–243, 2000.

Mulloney B, **Hall WM**. Local commissural interneurons integrate information from intersegmental coordinating interneurons. *J Comp Neurol* 466: 366–376, 2003.

Mulloney B, **Hall WM**. Local and intersegmental interactions of coordinating neurons and local circuits in the swimmeret system. *J Neurophysiol* 98: 405–413, 2007a.

Mulloney B, **Hall WM**. Not by spikes alone: Responses of coordinating neurons and the swimmeret system to local differences in excitation. *J Neurophysiol* 97: 436–450, 2007b.

Mulloney B, **Harness PI**, **Hall WM**. Bursts of Information: Coordinating Interneurons Encode Multiple Parameters of a Periodic Motor Pattern. *J Neurophysiol* 95: 850–861, 2006.

Mulloney B, **Namba H**, **Agricola HJ**, **Hall WM**. Modulation of force during locomotion: differential action of crustacean cardioactive peptide on power-stroke and return- stroke motor neurons. *J Neurosci* 17: 6872–6883, 1997.

Mulloney B, **Smarandache-Wellmann C**, **Weller C**, **Hall WM**, **DiCaprio RA**. Proprioceptive feedback modulates coordinating information in a system of segmentally distributed microcircuits. *J Neurophysiol* 112: 2799–2809, 2014.

Mulloney B, **Smarandache-Wellmann CR**. Neurobiology of the crustacean swimmeret system. *Prog Neurobiol* 96: 242–267, 2012.

Murchison D, **Chrachri A**, **Mulloney B**. A separate local pattern-generating circuit controls the movements of each swimmeret in crayfish. *J Neurophysiol* 70: 2620–2631, 1993.

Namba H, **Mulloney B**. Coordination of Limb Movements: Three Types of Intersegmental Interneurons in the Swimmeret System and Their Responses to Changes in Excitation. *J Neurophysiol* 81: 2437–2450, 1999.

Neil DM, **Miyan JA**. Phase-Dependent Modulation of Auxiliary Swimmeret Muscle Activity in the Equilibrium Reactions of the Norway Lobster, *Nephrops Norvegicus* L. *J Exp Biol* 126: 157–179, 1986.

Ohkuma M, **Kawai F**, **Miyachi E**. Acetylcholine enhances excitability by lowering the threshold of spike generation in olfactory receptor cells. *J Neurophysiol* 110: 2082–2089, 2013.

Pape HC. Queer Current and Pacemaker: The Hyperpolarization-Activated Cation Current in Neurons. *Annu Rev Physiol* 58: 299–327, 1996.

Park Y, **Kim Y-J**, **Adams ME**. Identification of G protein-coupled receptors for *Drosophila* PRXamide peptides, CCAP, corazonin, and AKH supports a theory of ligand-receptor coevolution. *Proc Natl Acad Sci U S A* 99: 11423–11428, 2002.

Paul DH. Nonspiking Stretch Receptors of the Crayfish Swimmeret Receive an Efference Copy of the Central Motor Pattern for the Swtmmeret. *J Exp Biol* 141: 257–264, 1989.

Paul DH, **Mulloney B**. Nonspiking local interneuron in the motor pattern generator for the crayfish swimmeret. *J Neurophysiol* 54: 28–39, 1985a.

Paul DH, **Mulloney B**. Local interneurons in the swimmeret system of the crayfish. *J Comp Physiol A* 156: 489–502, 1985b.

Paul DH, **Mulloney B**. Intersegmental coordination of swimmeret rhythms in isolated nerve cords of crayfish. *J Comp Physiol A* 158: 215–224, 1986.

Pearce RA, **Friesen WO**. Intersegmental coordination of leech swimming: comparison of in situ and isolated nerve cord activity with body wall movement. *Brain Res* 299: 363–366, 1984.

Pearce RA, **Friesen WO**. Intersegmental coordination of the leech swimming rhythm. II. Comparison of long and short chains of ganglia. *J Neurophysiol* 54: 1460–1472, 1985.

Pearson KG, **Iles JF**. Discharge Patterns of Coxal Levator and Depressor Motoneurones of the Cockroach, *Periplaneta americana*. *J Exp Biol* 52: 139–165, 1970.

Platkiewicz J, **Brette R**. A Threshold Equation for Action Potential Initiation. *PLOS Comput Biol* 6: e1000850, 2010.

Platkiewicz J, **Brette R**. Impact of Fast Sodium Channel Inactivation on Spike Threshold Dynamics and Synaptic Integration. *PLOS Comput Biol* 7: e1001129, 2011.

Poon M, **Friesen WO**, **Stent GS**. Neuronal control of swimming in the medicinal leech. V. Connexions between the oscillatory interneurones and the motor neurones. *J Exp Biol* 75: 45–63, 1978.

Robinson RB, **Siegelbaum SA**. Hyperpolarization-activated cation currents: from molecules to physiological function. *Annu Rev Physiol* 65: 453–480, 2003.

Rosenbaum P, **Schmitz J**, **Schmidt J**, **Büschges A**. Task-dependent modification of leg motor neuron synaptic input underlying changes in walking direction and walking speed. *J Neurophysiol* 114: 1090–1101, 2015.

Rossow M. mollymolly/Dot-Density-Plot - File Exchange - MATLAB Central [Online]. 2013. http://www.mathworks.com/matlabcentral/fileexchange/file_infos/42893-mollymolly-dot-density-plot.html [25 Mar. 2015].

Russell DF, **Wallén P**. On the control of myotomal motoneurones during "fictive swimming" in the lamprey spinal cord in vitro. *Acta Physiol Scand* 117: 161–170, 1983.

Russo RE, **Hounsgaard J**. Short-term plasticity in turtle dorsal horn neurons mediated by L-type Ca^{2+} channels. *Neuroscience* 61: 191–197, 1994.

Seichter HA, **Blumenthal F**, **Smarandache-Wellmann CR**. The Swimmeret System of Crayfish: A Practical Guide for the Dissection of the Nerve Cord and Extracellular Recordings of the Motor Pattern. *J Vis Exp* 93: e52109, 2014.

Sherff CM, **Mulloney B**. Tests of the motor neuron model of the local pattern-generating circuits in the swimmeret system. *J Neurosci* 16: 2839–2859, 1996.

Sherff CM, **Mulloney B**. Passive properties of swimmeret motor neurons. *J Neurophysiol* 78: 92–102, 1997.

Sherman SM. Tonic and burst firing: dual modes of thalamocortical relay. *Trends Neurosci* 24: 122–126, 2001.

Siegler MV. Postural changes alter synaptic interactions between nonspiking interneurons and motor neurons of the locust. *J Neurophysiol* 46: 310–323, 1981a.

Siegler MV. Posture and history of movement determine membrane potential and synaptic events in nonspiking interneurons and motor neurons of the locust. *J Neurophysiol* 46: 296–309, 1981b.

Simmons P. The neuronal control of dragonfly flight. II. Physiology. *J Exp Biol* 71: 141–155, 1977.

Simmons PJ, **van Steveninck R de R**. Reliability of Signal Transfer at a Tonically Transmitting, Graded Potential Synapse of the Locust Ocellar Pathway. *J Neurosci* 25: 7529–7537, 2005.

Skinner FK, **Kopell N**, **Mulloney B**. How Does the Crayfish Swimmeret System Work? Insights from Nearest-Neighbor Coupled Oscillator Models. *J Comput Neurosci* 4: 151–160, 1997.

Skinner FK, **Mulloney B**. Intersegmental coordination of limb movements during locomotion: mathematical models predict circuits that drive swimmeret beating. *J Neurosci* 18: 3831–3842, 1998.

Smarandache CR, **Hall WM**, **Mulloney B**. Coordination of Rhythmic Motor Activity by Gradients of Synaptic Strength in a Neural Circuit That Couples Modular Neural Oscillators. *J Neurosci* 29: 9351–9360, 2009.

Smarandache-Wellmann C, **Grätsch S**. Mechanisms of Coordination in Distributed Neural Circuits: Encoding Coordinating Information. *J Neurosci* 34: 5627–5639, 2014.

Smarandache-Wellmann C, **Weller C**, **Mulloney B**. Mechanisms of Coordination in Distributed Neural Circuits: Decoding and Integration of Coordinating Information. *J Neurosci* 34: 793–803, 2014.

Smarandache-Wellmann C, **Weller C**, **Wright TM**, **Mulloney B**. Five types of nonspiking interneurons in local pattern-generating circuits of the crayfish swimmeret system. *J Neurophysiol* 110: 344–357, 2013.

Smith JC, **Ellenberger HH**, **Ballanyi K**, **Richter DW**, **Feldman JL**. Pre-Bötzinger complex: a brainstem region that may generate respiratory rhythm in mammals. *Science* 254: 726–729, 1991.

Smith JC, **Feldman JL**. In vitro brainstem-spinal cord preparations for study of motor systems for mammalian respiration and locomotion. *J Neurosci Methods* 21: 321–333, 1987.

Städele C, **Heigele S**, **Stein W**. Neuromodulation to the Rescue: Compensation of Temperature-Induced Breakdown of Rhythmic Motor Patterns via Extrinsic Neuromodulatory Input. *PLOS Biol* 13: e1002265, 2015.

Stafstrom CE, **Schwindt PC**, **Crill WE**. Negative slope conductance due to a persistent subthreshold sodium current in cat neocortical neurons in vitro. *Brain Res* 236: 221–226, 1982.

Stein PSG. Intersegmental coordination of swimmeret motoneuron activity in crayfish. *J Neurophysiol* 34: 310–318, 1971.

Stein W, **Büschges A**, **Bässler U**. Intersegmental transfer of sensory signals in the stick insect leg muscle control system. *J Neurobiol* 66: 1253–1269, 2006.

Stopfer M, **Bhagavan S**, **Smith BH**, **Laurent G**. Impaired odour discrimination on desynchronization of odour-encoding neural assemblies. *Nature* 390: 70–74, 1997.

Südhof TC. Calcium Control of Neurotransmitter Release. *Cold Spring Harb Perspect Biol* 4: a011353, 2012.

Swensen AM, **Marder E**. Multiple Peptides Converge to Activate the Same Voltage-Dependent Current in a Central Pattern-Generating Circuit. *J Neurosci* 20: 6752–6759, 2000.

Szczupak L, **Edgar J**, **Peralta ML**, **Kristan WB**. Long-lasting depolarization of leech neurons mediated by receptors with a nicotinic binding site. *J Exp Biol* 201: 1895–1906, 1998.

Takeuchi A, **Takeuchi N**. The effect on crayfish muscle of iontophoretically applied glutamate. *J Physiol* 170: 296–317, 1964.

Takeuchi A, **Takeuchi N**. Localized action of gamma-aminobutyric acid on the crayfish muscle. *J Physiol* 177: 225–238, 1965.

Teshiba T, **Shamsian A**, **Yashar B**, **Yeh S-R**, **Edwards DH**, **Krasne FB**. Dual and Opposing Modulatory Effects of Serotonin on Crayfish Lateral Giant Escape Command Neurons. *J Neurosci* 21: 4523–4529, 2001.

Thompson WJ, **Stent GS**. Neuronal control of heartbeat in the medicinal leech I. Generation of the vascular constriction rhythm by heart motor neurons. *J Comp Physiol* 111: 261–279, 1976a.

Thompson WJ, **Stent GS**. Neuronal control of heartbeat in the medicinal leech II. Intersegmental coordination of heart motor neuron activity by heart interneurons. *J Comp Physiol* 111: 281–307, 1976b.

Tóth TI, **Daun-Gruhn S**. A three-leg model producing tetrapod and tripod coordination patterns of ipsilateral legs in the stick insect. *J Neurophysiol* 115: 887–906, 2016.

Trimmer BA. Characterization of a muscarinic current that regulates excitability of an identified insect motoneuron. *J Neurophysiol* 72: 1862–1873, 1994.

Trimmer BA, **Weeks JC**. Muscarinic acetylcholine receptors modulate the excitability of an identified insect motoneuron. *J Neurophysiol* 69: 1821–1836, 1993.

Trube A, **Audehm U**, **Dircksen H**. Crustacean cardioactive peptide - immunoreactive neurons in the ventral nervous system of crayfish. *J Comp Neurol* 348: 80–93, 1994.

Tschuluun N, **Hall WM**, **Mulloney B**. Limb Movements during Locomotion: Tests of a Model of an Intersegmental Coordinating Circuit. *J Neurosci* 21: 7859–7869, 2001.

Tschuluun N, **Hall WM**, **Mulloney B**. State-changes in the swimmeret system: a neural circuit that drives locomotion. *J Exp Biol* 212: 3605–3611, 2009.

Wang H-S, **Pan Z**, **Shi W**, **Brown BS**, **Wymore RS**, **Cohen IS**, **Dixon JE**, **McKinnon D**. KCNQ2 and KCNQ3 Potassium Channel Subunits: Molecular Correlates of the M-Channel. *Science* 282: 1890–1893, 1998.

Wark B, **Lundstrom BN**, **Fairhall A**. Sensory adaptation. *Curr Opin Neurobiol* 17: 423–429, 2007.

Weeks JC. Synaptic basis of swim initiation in the leech - II. A pattern-generating neuron (cell 208) which mediates motor effects of swim-initiating neurons. *J Comp Physiol* 148: 265–279, 1982.

Wei AD, **Butler A**, **Salkoff L**. KCNQ-like Potassium Channels in Caenorhabditis elegans CONSERVED PROPERTIES AND MODULATION. *J Biol Chem* 280: 21337–21345, 2005.

Weimann JM, **Skiebe P**, **Heinzel H-G**, **Soto C**, **Kopell N**, **Jorge-Rivera JC**, **Marder E**. Modulation of Oscillator Interactions in the Crab Stomatogastric Ganglion by Crustacean Cardioactive Peptide. *J Neurosci* 17: 1748–1760, 1997.

Wiersma CAG, **Ikeda K**. Interneurons commanding swimmeret movements in the crayfish, Procambarus clarki (girard). *Comp Biochem Physiol* 12: 509–525, 1964.

Willadt S, **Canepari M**, **Yan P**, **Loew LM**, **Vogt KE**. Combined optogenetics and voltage sensitive dye imaging at single cell resolution. *Front Cell Neurosci* 8, 2014.

Wilson DM. The Central Nervous Control of Flight in a Locust. *J Exp Biol* 38: 471–490, 1961.

Yu X, **Nguyen B**, **Friesen WO**. Sensory Feedback Can Coordinate the Swimming Activity of the Leech. *J Neurosci* 19: 4634–4643, 1999.

Yus-nájera E, **Muñoz A**, **Salvador N**, **Jensen BS**, **Rasmussen HB**, **Defelipe J**, **Villarroel A**. Localization of KCNQ5 in the normal and epileptic human temporal neocortex and hippocampal formation. *Neuroscience* 120: 353–364, 2003.

Zelano C, **Jiang H**, **Zhou G**, **Arora N**, **Schuele S**, **Rosenow J**, **Gottfried JA**. Nasal Respiration Entrains Human Limbic Oscillations and Modulates Cognitive Function. *J Neurosci* 36: 12448–12467, 2016.

Zhang C, **Guy RD**, **Mulloney B**, **Zhang Q**, **Lewis TJ**. Neural mechanism of optimal limb coordination in crustacean swimming. *Proc Natl Acad Sci* 111: 13840–13845, 2014.

Zill SN. Plasticity and proprioception in insects. I. Responses and cellular properties of individual receptors of the locust metathoracic femoral chordotonal organ. *J Exp Biol* 116: 435–461, 1985.

Zill SN, **Jepson-Innes K**. Evolutionary adaptation of a reflex system: sensory hysteresis counters muscle “catch” tension. *J Comp Physiol A* 164: 43–48, 1988.

Zucker RS. Calcium and transmitter release. *J Physiol-Paris* 87: 25–36, 1993.

Abbreviations

5-HT	Serotonin
4-AP	4-aminopyridine
A1, A2, A3, A4, A5, A6	Abdominal ganglion 1, 2, 3, 4, 5, 6
ACh	Acetylcholine
ASC_E	Ascending Coordinating Neuron (early)
ASC_L	Ascending Coordinating Neuron (late)
CCAP	Crustacean Cardioactive Peptide
CL	Confidence limit
CNS	Central nervous system
ComInt 1 / C1	Commissural Interneuron 1
CPG	Central Pattern Generator
DSC	Descending Coordinating Neuron
EdCl	Edrophonium chloride
EPSP	Excitatory postsynaptic potential
GABA	ɣ-Aminobutyric acid
HN	Heart Interneuron
IPS	Inhibitors of Power-Stroke
IPSP	Inhibitory postsynaptic potential
IRS	Inhibitors of Return-Stroke
LFB	Lateral fiber bundle
LG	Lateral Giant Axon
LN	Lateral Neuropil
LowCa^{2+} saline	Low Ca^{2+} / High Mg^{2+} Saline
MALDI-TOF MS	Matrix-Assisted Laser Desorption/Ionization – Time of Flight Mass Spectrometry
MFB	Medial fiber bundle
MN	Motor neuron
MnT	Minuscule Tract
MS	Mass spectrometry
NSSR	Non-spiking Stretch Receptor
PCA	Principal Component Analysis
PS	Power-Stroke
PSE	Power-Stroke Exciter
PSI	Power-Stroke Inhibitor
PSP	Postsynaptic potential
R_{in}	Input resistance
RS	Return-Stroke
RSE	Return-Stroke Exciter
RSI	Return-Stroke Inhibitor
SD	Standard deviation
T3, T4, T5	Thoracic ganglion 3, 4, 5
TEA	Tetraethylammonium
TTX	Tetrodotoxin
V_m	Membrane potential
VSD	Voltage-sensitive dye

Appendix

These are data for the individual experiments. A unique identifier (BXXpYY) for individual experiments labels each plot. The same identifier in different plots means that the results come from the same experiment.

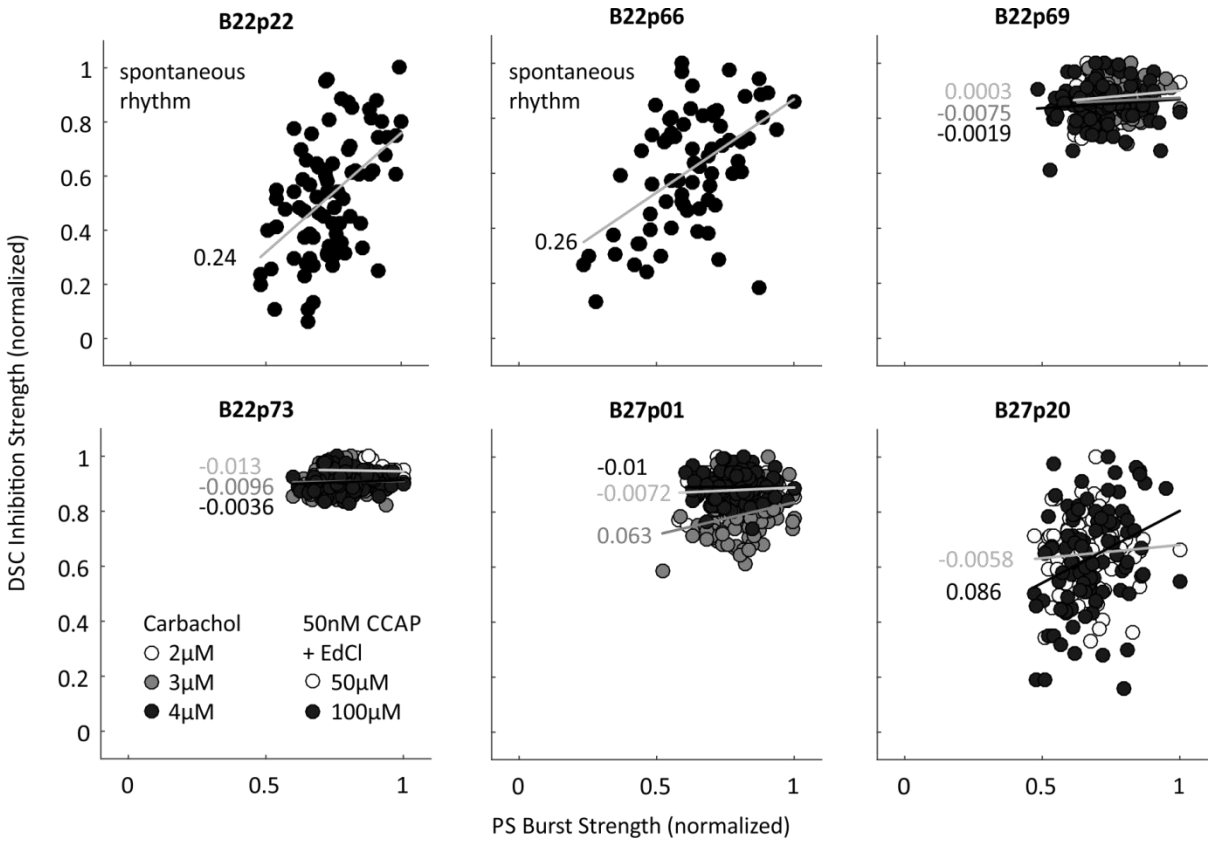

Supplementary Figure 1: Correlation between DSC inhibition and PS burst strength in six different experiments. Burst strength varied spontaneously in B22p22 and B22p66. B22p69, B22p73, and B27p01 were treated with different carbachol concentrations, B27p20 with 50nM CCAP + different EdCl concentrations. Concentrations are color-coded. Numbers denominate adjusted R^2 for the regression lines. Burst strengths were normalized to the maximum burst strength at each concentration.

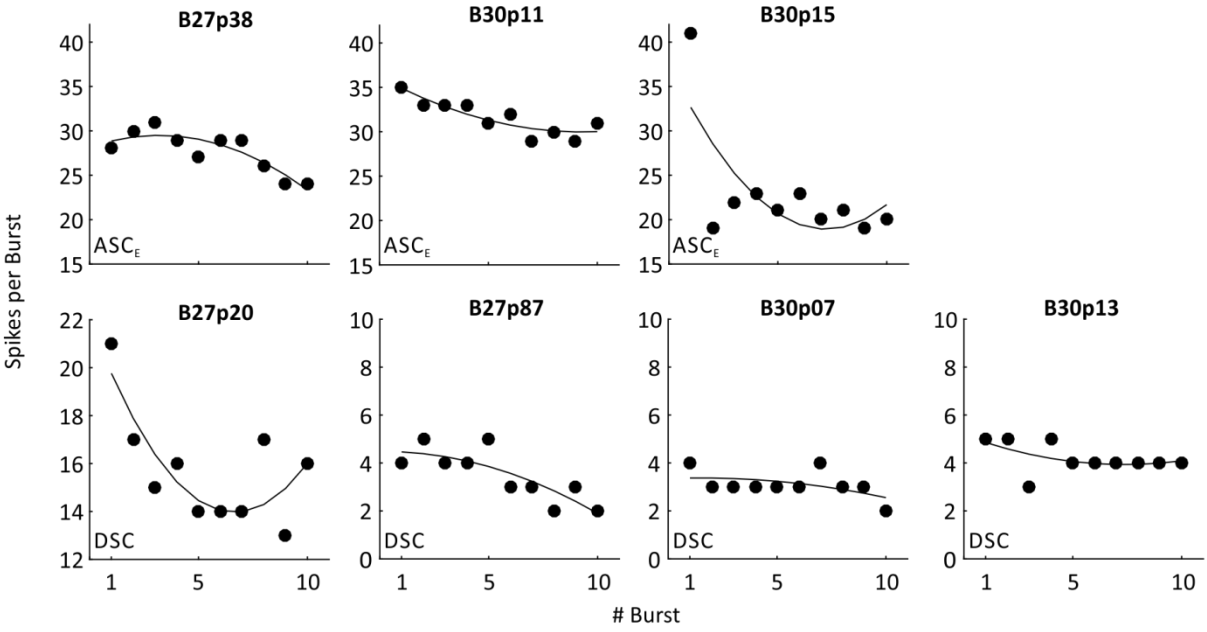

Supplementary Figure 2: Adaptation of ASC_E and DSC in response to constant current injection (+0.5nA) in 2µM carbachol. Spikes per burst were counted in ten consecutive bursts after depolarization. All experiments were in 50nM CCAP + 50µM EdCl. Data were fitted with second order polynomials (lines).

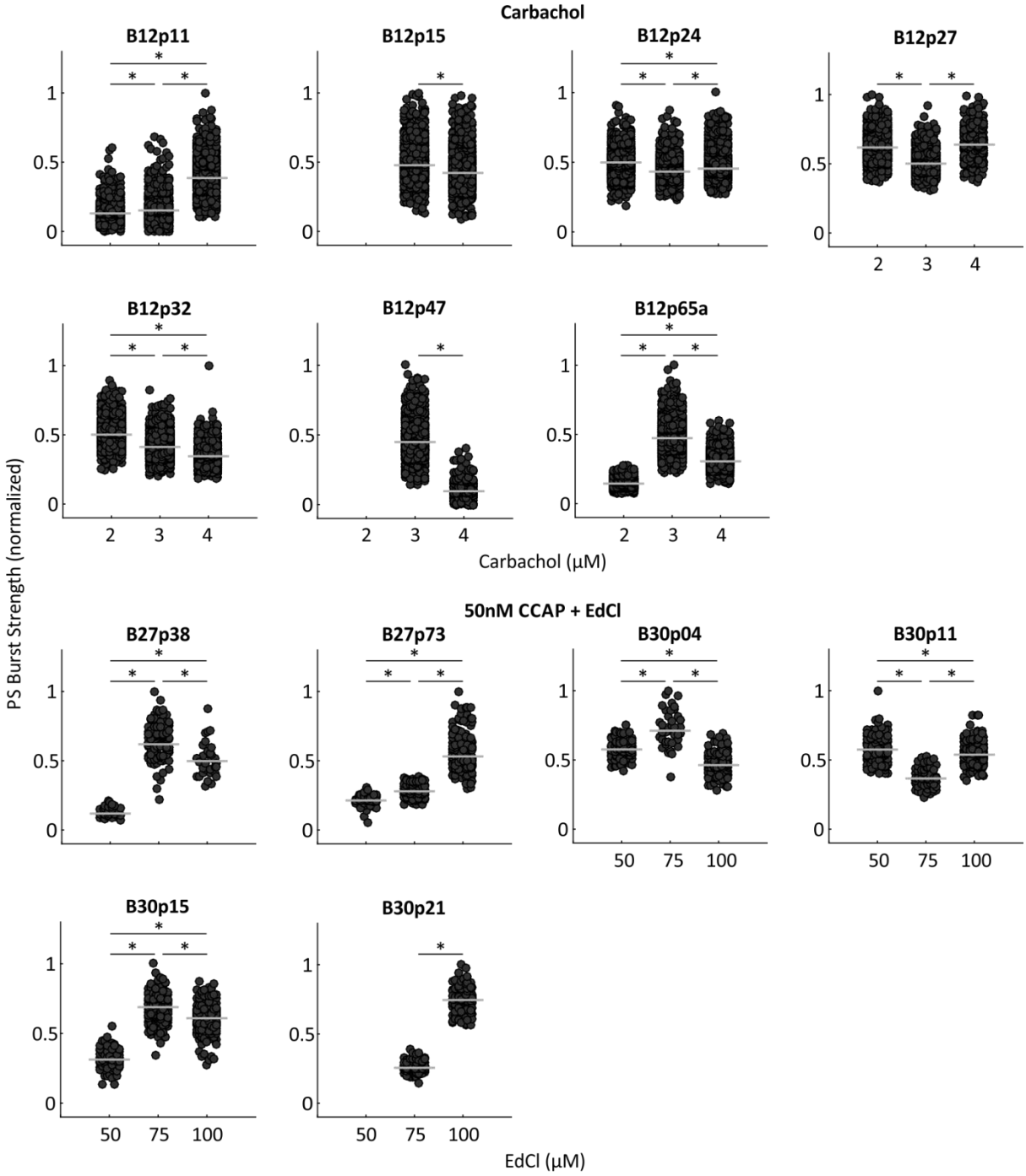

Supplementary Figure 3: PS burst strength at different carbachol or EdCl concentrations while recording intracellularly from ASC_E. Each dot represents a single burst strength value. Grey bars indicate median. * $p < 0.05$.

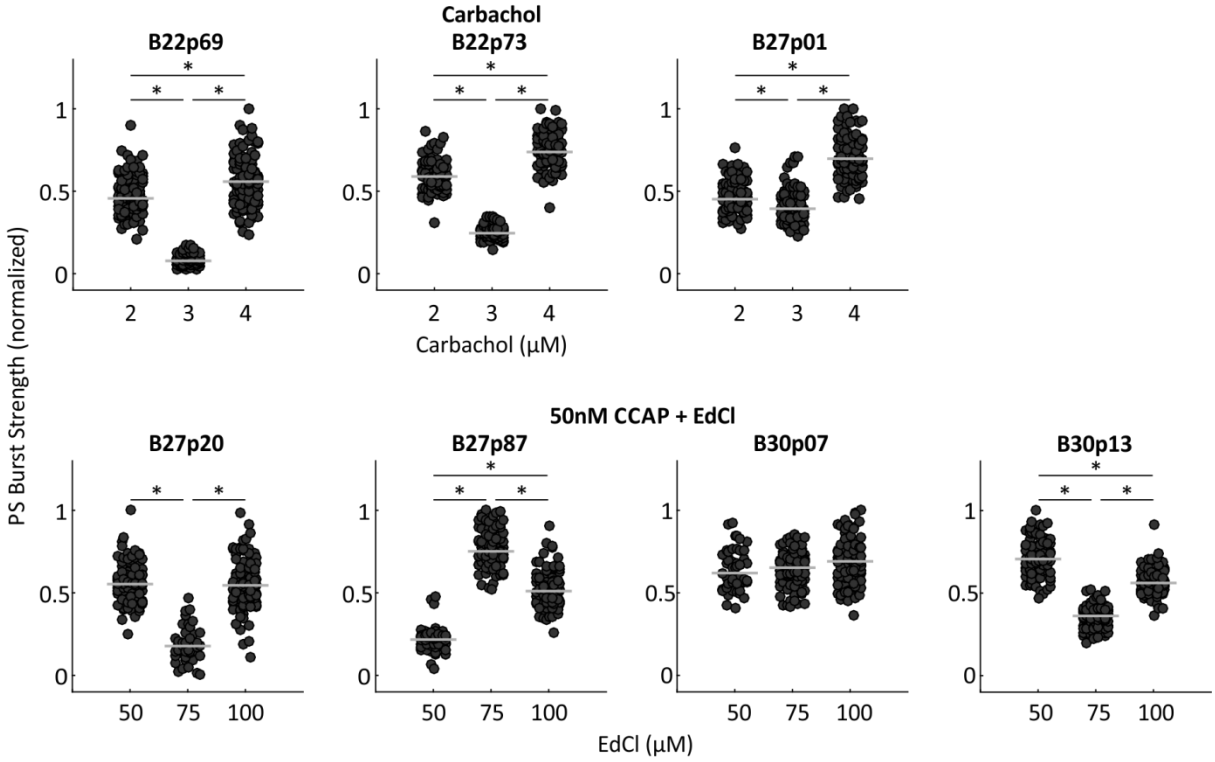

Supplementary Figure 4: PS burst strength at different carbachol or EdCl concentrations while recording intracellularly from DSC. Each dot represents a single burst strength value. Grey bars indicate median. * p < 0.05.

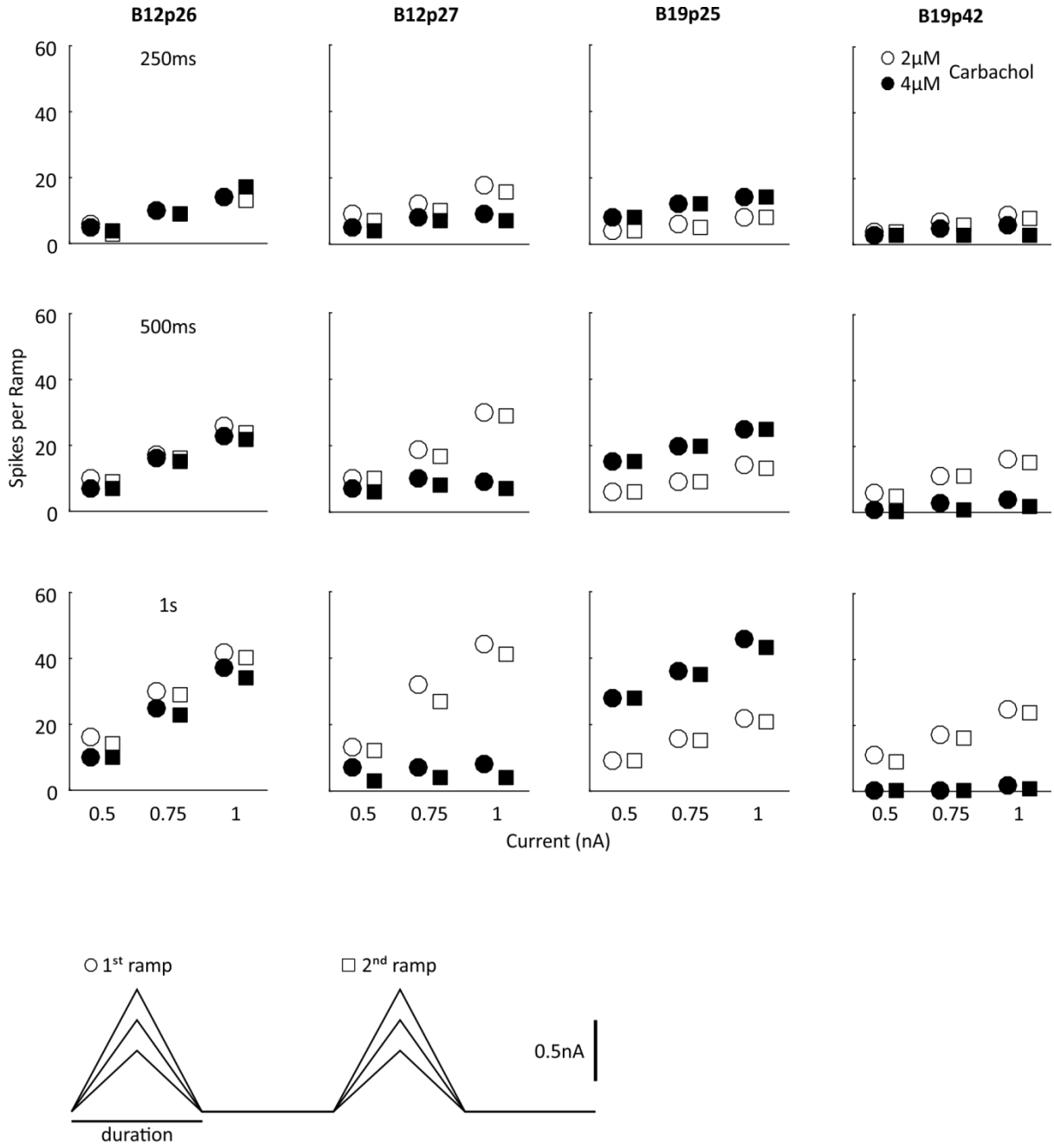

Supplementary Figure 5: Number of spikes elicited in isolated ASC_E held at -55mV by paired ramp stimuli with different current amplitudes. Data in each column belong to the same experiment. Data in each row belong to the same ramp duration. Times in the first column denote ramp duration. Carbachol concentration is color-coded. Data for the first ramp are plotted as circles, data for the second ramp as squares. The neuron in B19p25 was still tonically active when hyperpolarized to -55mV. Bottom panel depicts schematic of paired ramp stimulations.

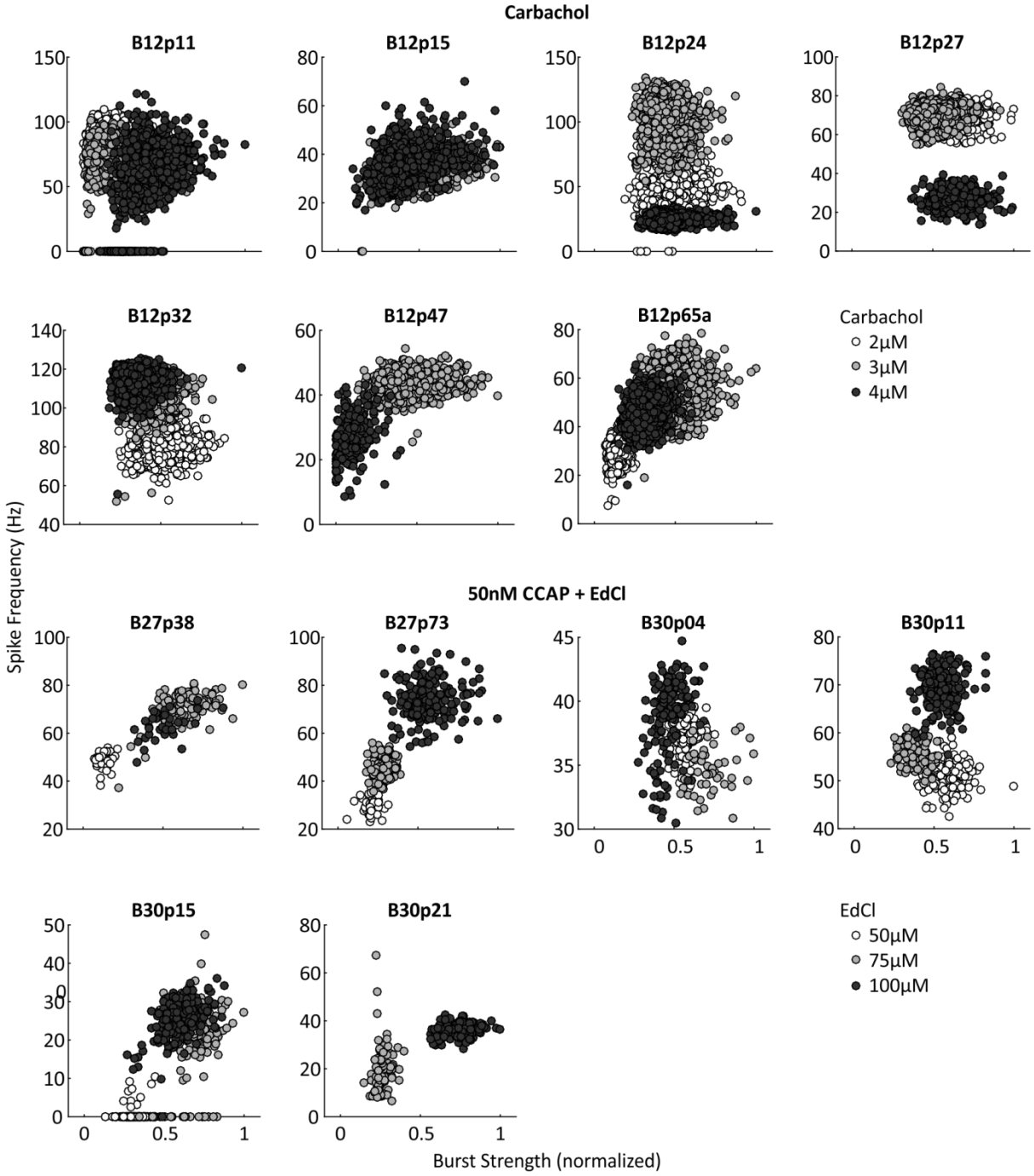

Supplementary Figure 6: Frequency of ASC_E's spikes per burst vs. different PS burst strength in different carbachol and EdCl concentrations. Each dot represents a single measurement.

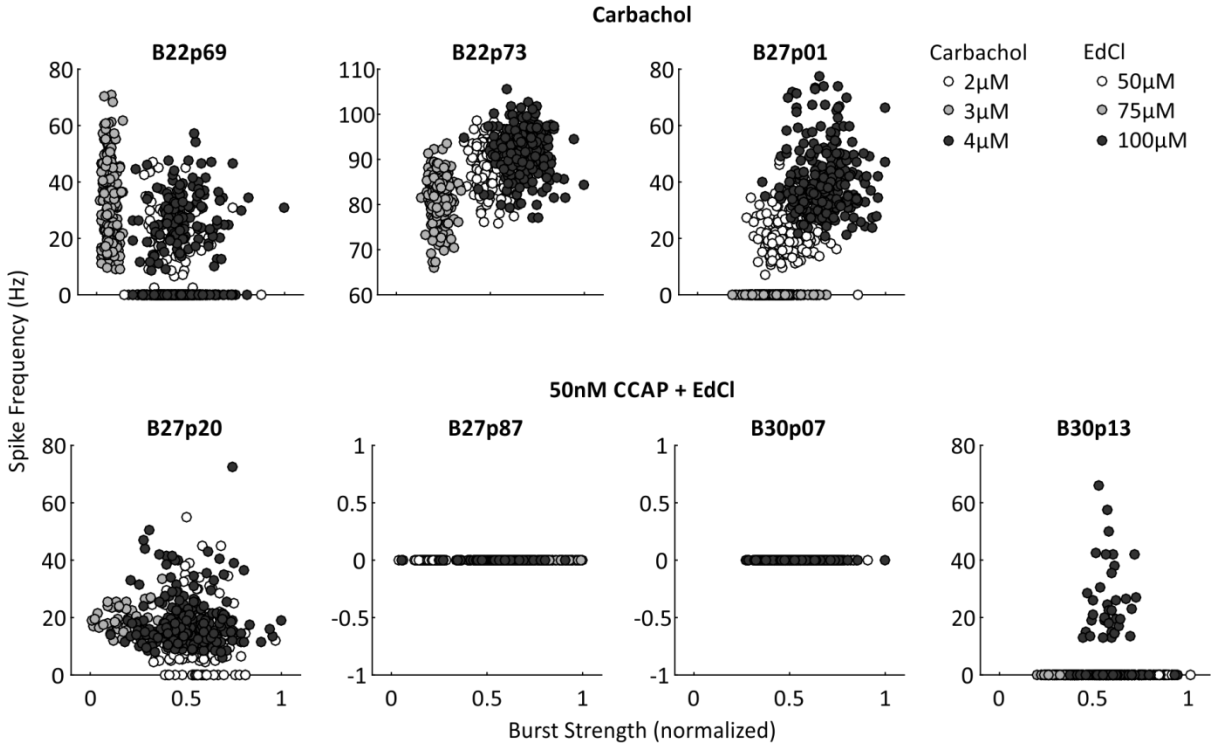

Supplementary Figure 7: Frequency of DSC's spikes per burst vs. different PS burst strength in different carbachol and EdCl concentrations. Each dot represents a single measurement.

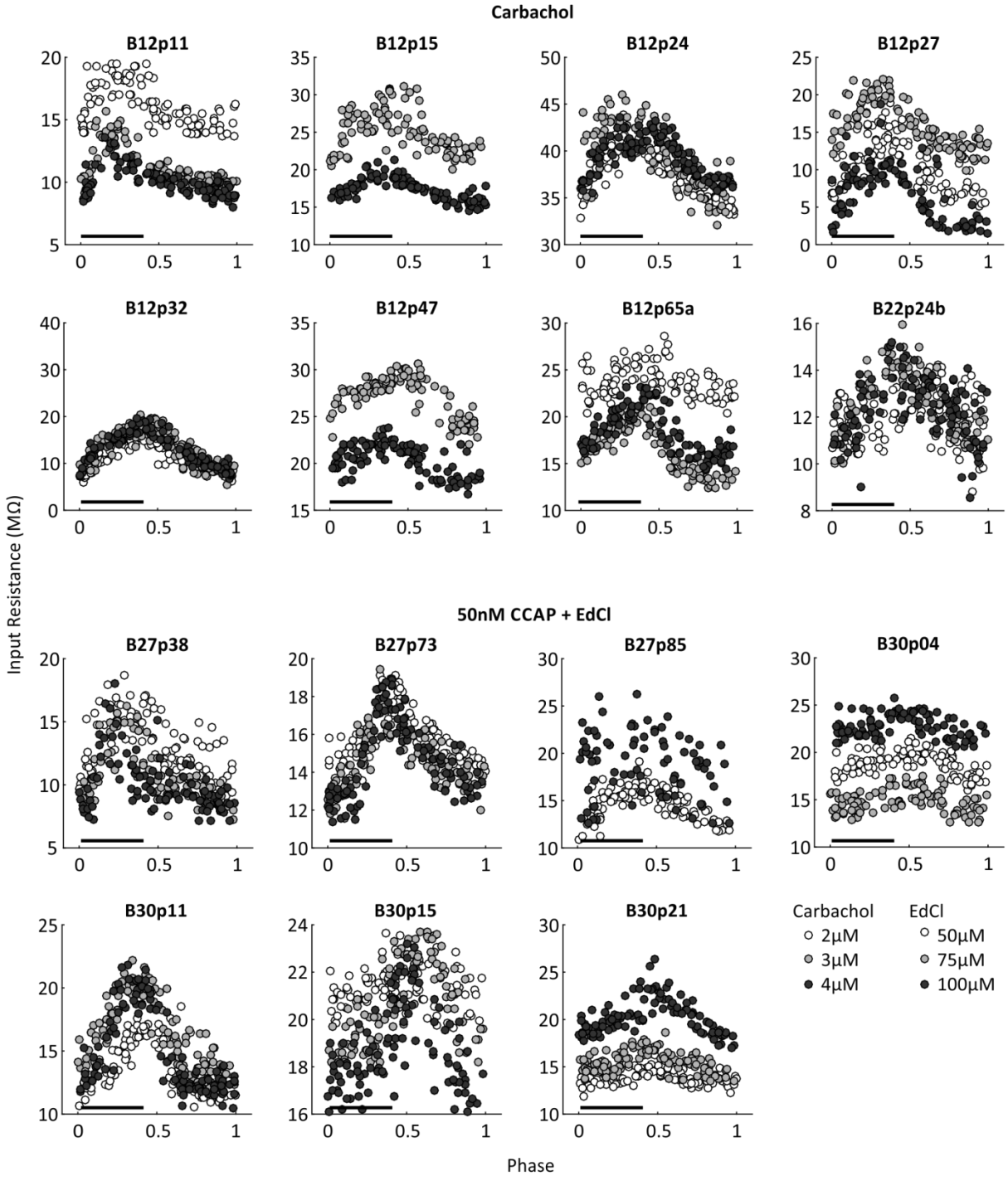

Supplementary Figure 8: ASC_E's R_{in} vs. phase in different carbachol and EdCl concentrations. Each dot represents a single R_{in} value. Black bars indicate approximate phase of PS activity. Burst strength could not be calculated for B22p24b; therefore, it was excluded from further analyses.

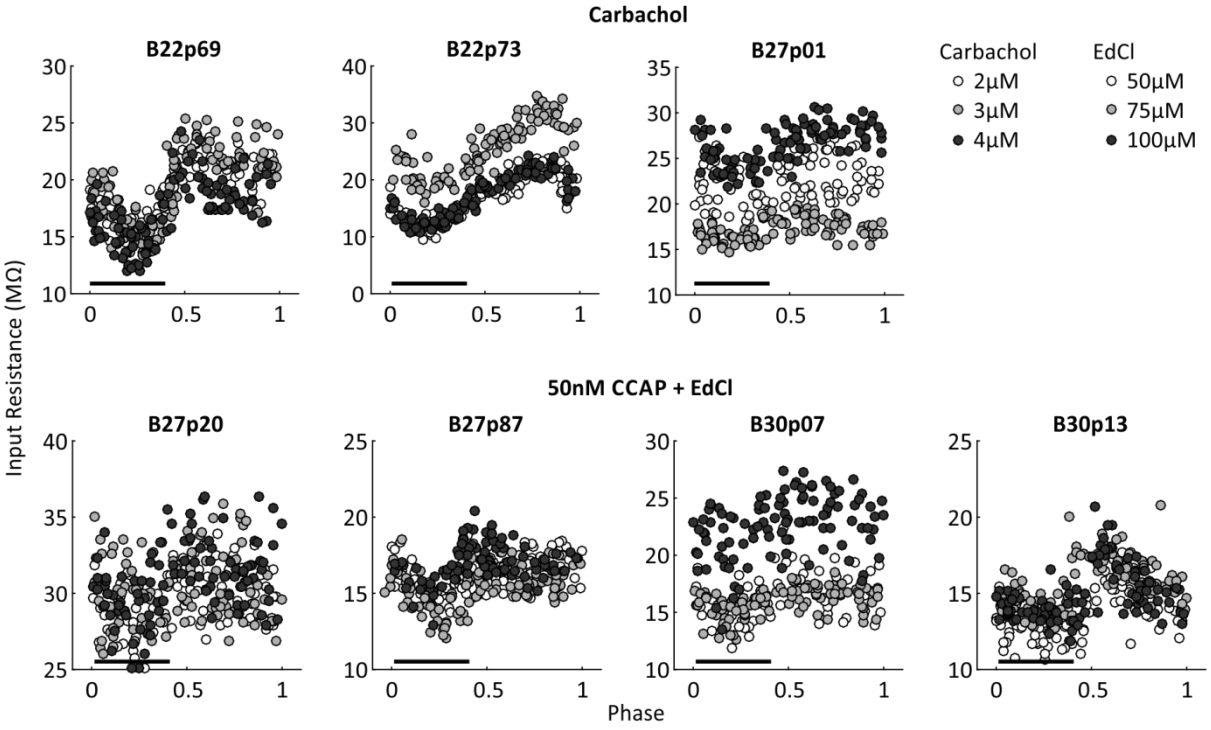

Supplementary Figure 9: DSC's R_{in} vs. phase in different carbachol and EdCl concentrations. Each dot represents a single R_{in} value. Black bars indicate approximate phase of PS activity.

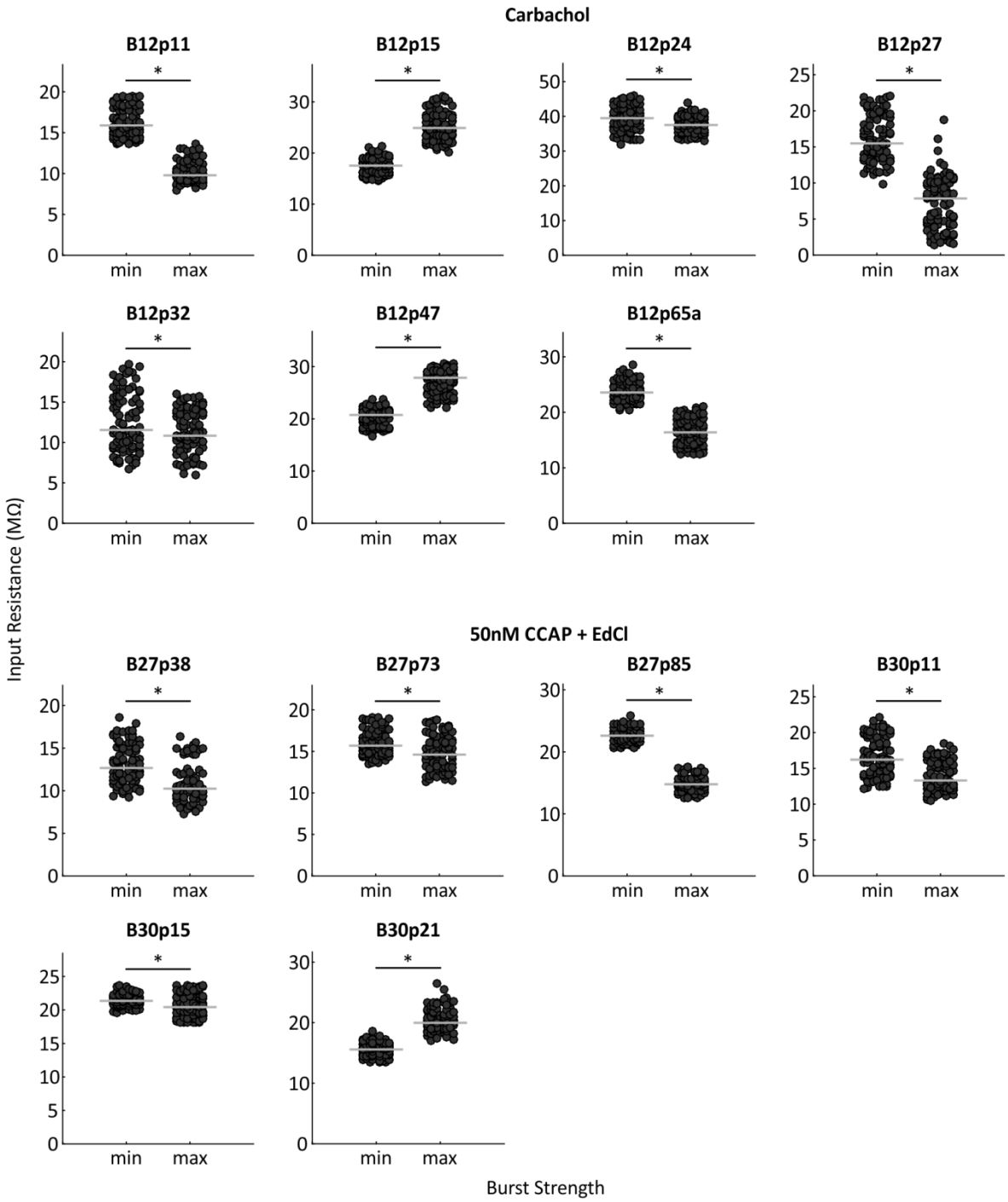

Supplementary Figure 10: Differences in ASC_E's R_{in} at minimum and maximum excitation level with the network intact. Each dot represents a single R_{in} value. Grey bars indicate median. * $p < 0.05$.

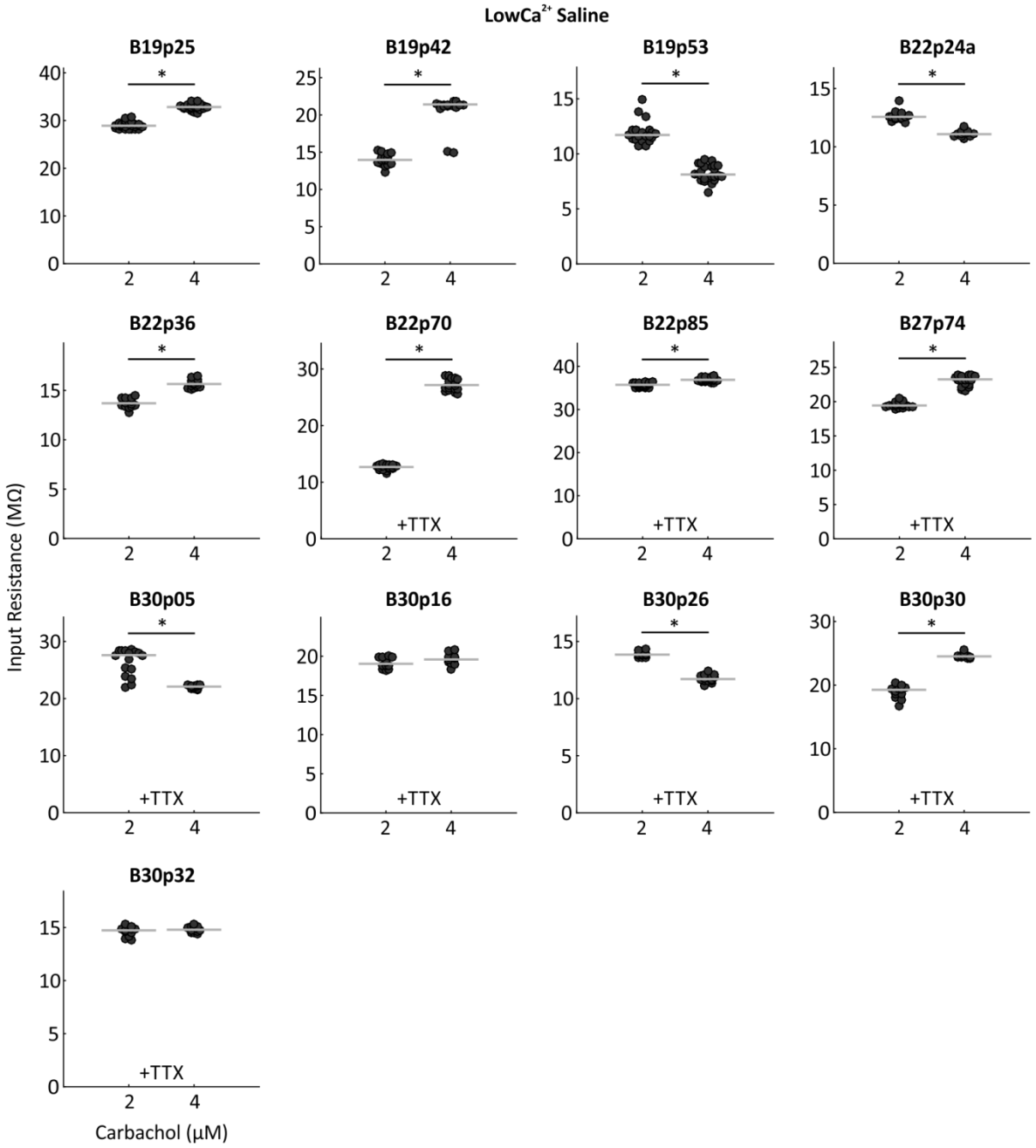

Supplementary Figure 11: Differences in the isolated ASC_E's R_{in} at minimum and maximum carbachol concentration. Each dot represents a single R_{in} value. Grey bars indicate median. * $p < 0.05$.

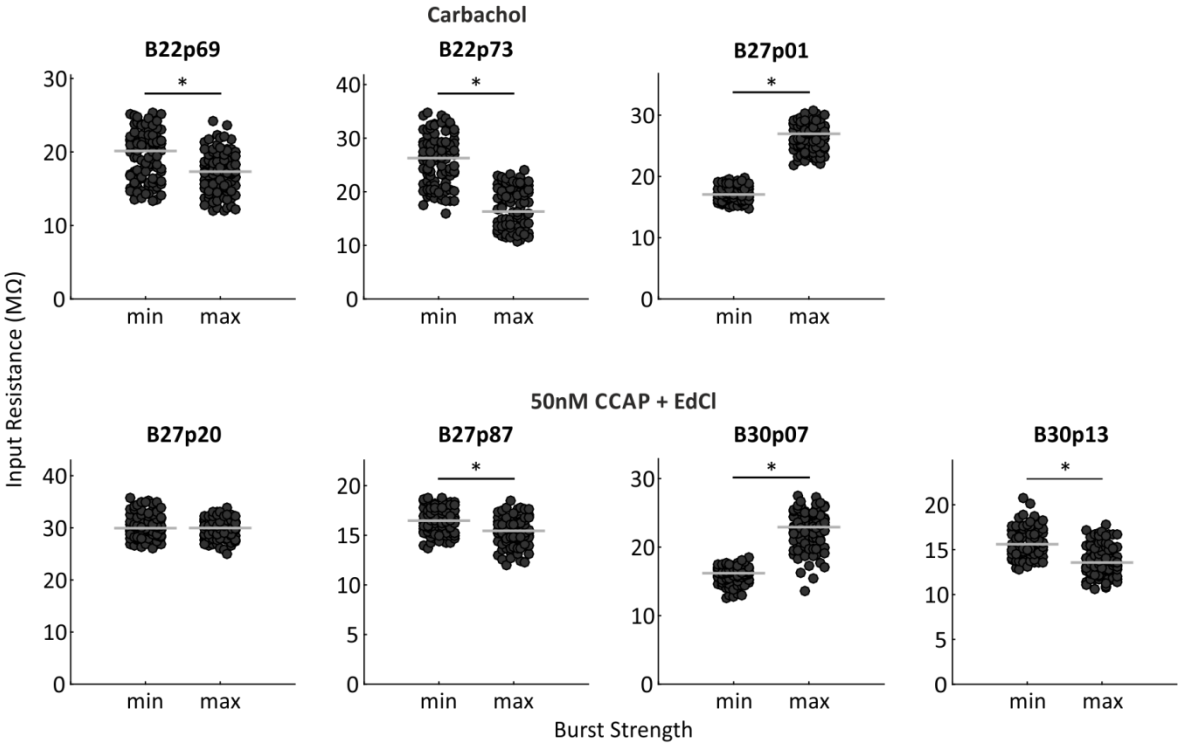

Supplementary Figure 12: Differences in DSC's R_{in} at minimum and maximum excitation level with the network intact. Each dot represents a single R_{in} value. Grey bars indicate median. * p < 0.05.

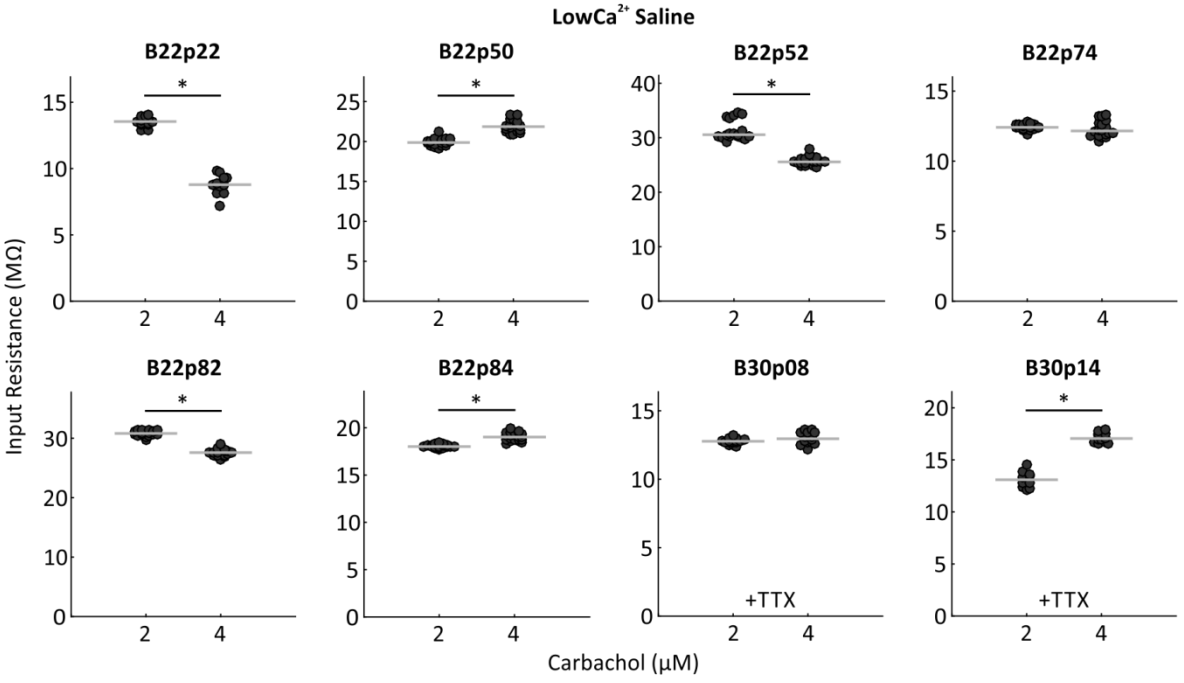

Supplementary Figure 13: Differences in the isolated DSC's R_{in} at minimum and maximum carbachol concentration. Each dot represents a single R_{in} value. Grey bars indicate median. * p < 0.05.

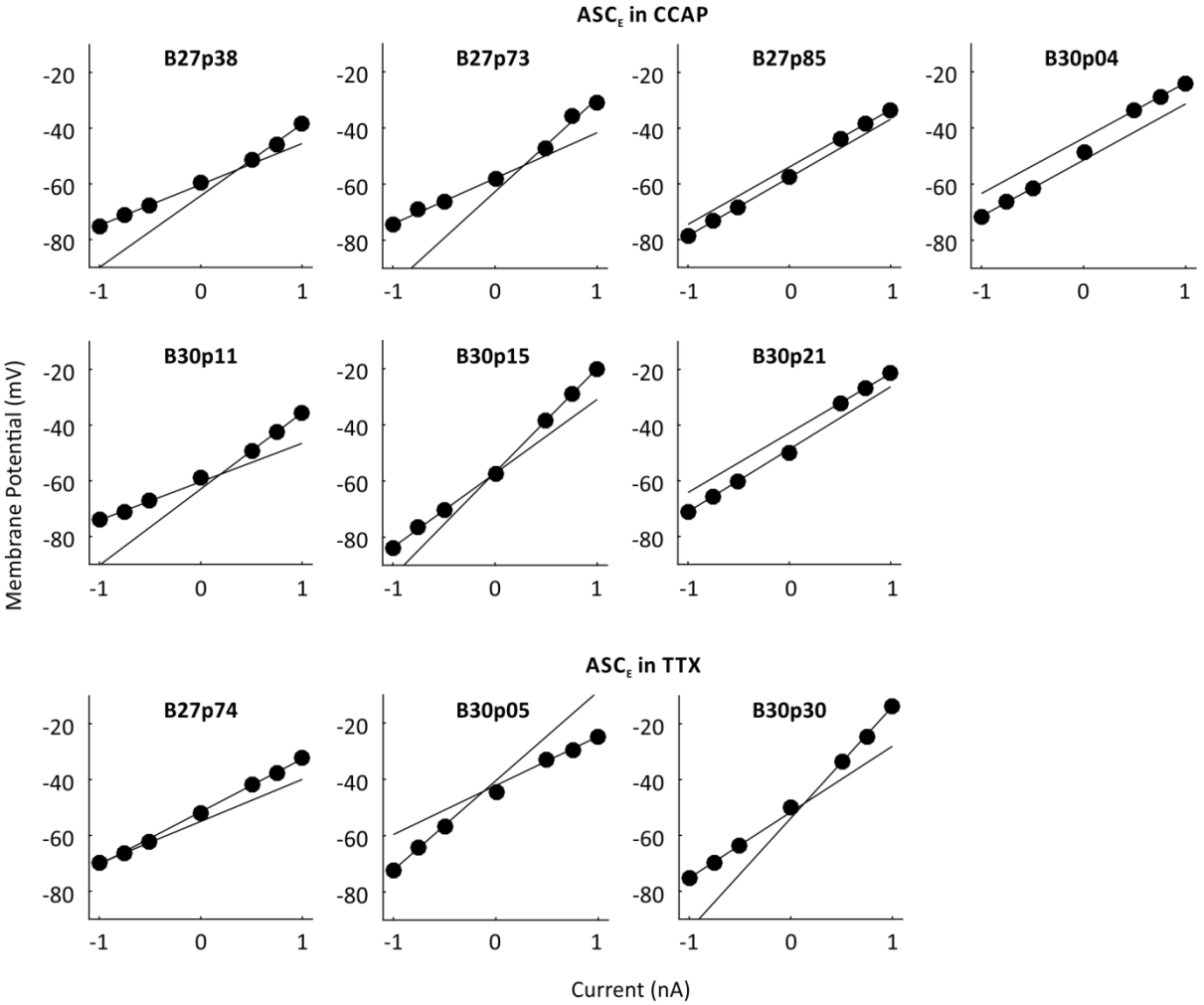

Supplementary Figure 14: V-I curves for ASC$_E$ with the network intact (CCAP) and in isolation (TTX). The neurons were de- and hyperpolarized with three different current amplitudes, respectively. The V-I relationships were fitted with linear regression lines. Regression lines were calculated separately for positive and negative current injections, and extrapolated across the whole range of injected currents.

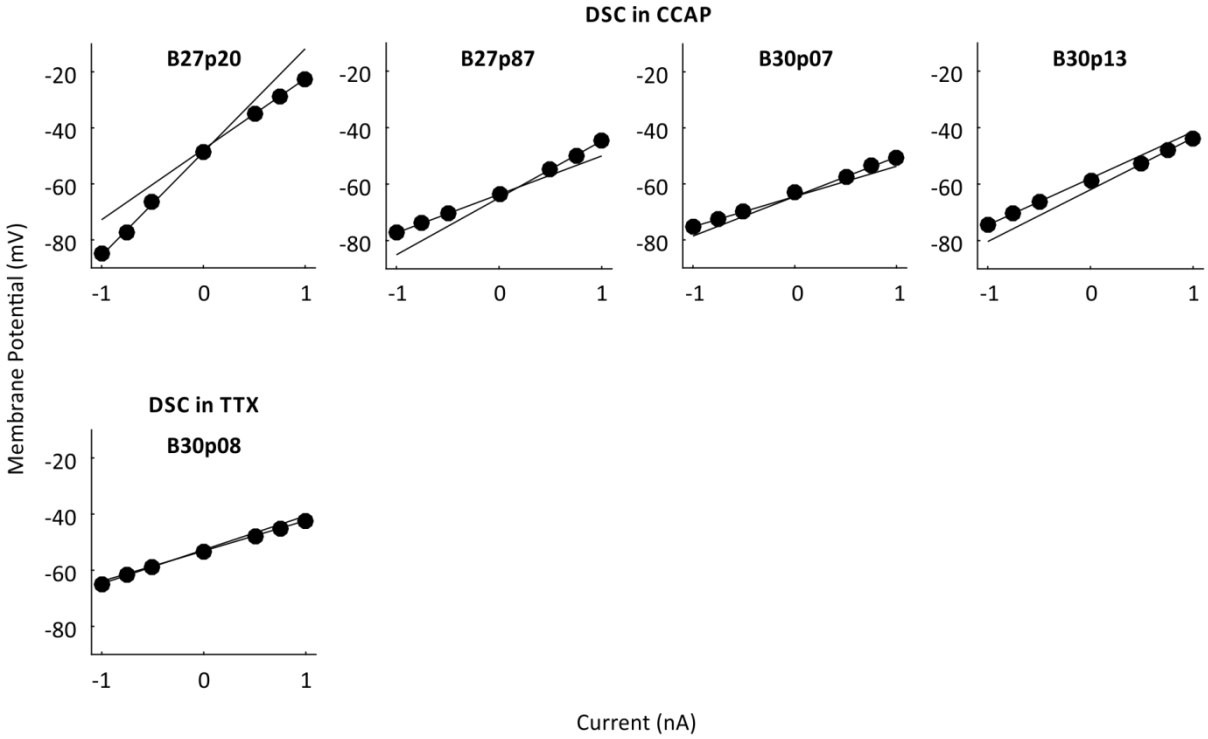

Supplementary Figure 15: V-I curves for DSC with the network intact (CCAP) and in isolation (TTX). The neurons were de- and hyperpolarized with three different current amplitudes, respectively. The V-I relationships were fitted with linear regression lines. Regression lines were calculated separately for positive and negative current injections, and extrapolated across the whole range of injected currents.

Acknowledgements

My sincere gratitude goes to my supervisor, Carmen Wellmann, for her constant support during my PhD studies, immense knowledge, and lively discussions. My thanks also go to the other members of my thesis committee, Ansgar Büschges and Wolfgang Walkowiak, for their guidance in research and writing. Furthermore, I wish to express my heartfelt thankfulness to Ansgar Büschges for being second assessor of this thesis, and for our research discussions over a cup of tea.

I appreciate the help of my fellow lab members Heike Greis, Felix Blumenthal, Felix Clotten, and Laura Schläger during experiments, and their helpful comments on manuscripts. Furthermore, I am grateful for the thorough technical support of Michael Dübbert and Jan Sydow from the electronics lab for experimental setup and rigging.

I want to thank T. Michael Wright and Susanne Neupert for fruitful collaborations. Further, I thank T. Michael Wright and Till Bockemühl for help with MATLAB and statistics. I am also grateful to all members of the Wellmann, Büschges, and Daun lab for their support.

Finally, I would like to thank my family.

This work was funded by the DFG's Emmy Noether-Programm SM 206/3-1 and University of Cologne Advanced Researcher Grant ZuK 81/1.

Eigentständigkeitserklärung

Ich versichere, dass ich die von mir vorgelegte Dissertation selbständig angefertigt, die benutzten Quellen und Hilfsmittel vollständig angegeben und die Stellen der Arbeit – einschließlich Tabellen, Karten und Abbildungen –, die anderen Werken im Wortlaut oder dem Sinn nach entnommen sind, in jedem Einzelfall als Entlehnung kenntlich gemacht habe; dass diese Dissertation noch keiner anderen Fakultät oder Universität zur Prüfung vorgelegen hat; dass sie – abgesehen von unten angegebenen Teilpublikationen – noch nicht veröffentlicht worden ist, sowie, dass ich eine solche Veröffentlichung vor Abschluss des Promotionsverfahrens nicht vornehmen werde. Die Bestimmungen der Promotionsordnung sind mir bekannt. Die von mir vorgelegte Dissertation ist von Dr. Carmen Wellmann betreut worden.